Analysis of Differential Protection Applied to Lines Interconnecting Inverter-Based Resources

DAVI MOGROVEJO BRASIL

MSC DISSERTATION
ON ELECTRICAL ENGINEERING

ELECTRICAL ENGINEERING DEPARTMENT

TECHNOLOGY FACULTY

UNIVERSITY OF BRASILIA

University of Brasilia
Technology Faculty
Electrical Engineering Department

Analysis of Differential Protection Applied to Lines Interconnecting Inverter-Based Resources

Davi Mogrovejo Brasil

MSc dissertation submitted to the Graduate Program in Electrical Engineering at the University of Brasilia, as part of the necessary requirements to obtain the degree of MSc in Electrical Engineering.

APPROVED BY:

Prof. Kleber Melo e Silva, D.Sc. (ENE - UnB)
(Advisor)

Maria Leonor Silva de Almeida, D.Sc. (UFG)
(External Examiner)

Raphael Leite de Andrade Reis, D.Sc. (UFPB)
(External Examiner)

Brasilia/DF, May 28st 2026.

FICHA CATALOGRÁFICA

BRASIL, DAVI MOGROVEJO

Analysis of Differential Protection Applied to Lines Interconnecting Inverter-Based Resources.

[Brasília/Distrito Federal] 2026.

xi, 117p., 210 x 297 mm (ENE/FT/UnB, Mestre, Dissertação de Mestrado, 2026).

Universidade de Brasília, Faculdade de Tecnologia, Departamento de Engenharia Elétrica.

Departamento de Engenharia Elétrica

1. Alpha plane 2. IBRs
3. current mapping strategy 4. differential protection
5. renewable resources

I. ENE/FT/UnB II. Título (série)

REFERÊNCIA BIBLIOGRÁFICA

BRASIL, D. M. (2026). Analysis of Differential Protection Applied to Lines Interconnecting Inverter-Based Resources. Dissertação de Mestrado em Engenharia Elétrica, Publicação PPGEE 840/26, Departamento de Engenharia Elétrica, Universidade de Brasília, Brasília, DF, 117p.

CESSÃO DE DIREITOS

Davi Mogrovejo Brasil

Departamento de Eng. Elétrica (ENE)

Faculdade de Tecnologia (FT)

Universidade de Brasília (UnB)

Campus Darcy Ribeiro

Brasília - DF CEP 70919-970

ACKNOWLEDGMENTS

I would like to express my deepest gratitude to my advisor, Dr. Professor Kleber de Melo Silva, for his invaluable guidance, encouragement, and patience throughout the development of this work. His insights and expertise have been fundamental to my academic growth and the completion of this dissertation.

I am also immensely grateful to Neoenergia/Elektro for the support given by the company, which provided me with the resources to dedicate myself to my studies and research. The opportunity to collaborate with a multinational company so committed to the advancement of renewable energy systems has been an enriching experience.

ABSTRACT

Renewable energy sources connected through power electronic converters, such as Type IV wind turbines and photovoltaic plants, present fault-current behavior that differs significantly from that of synchronous generators. Their transient response is shaped by converter controls, current limiters, synchronization algorithms, semiconductor protection, and grid-code requirements. These characteristics may affect conventional transmission-line protection functions, especially when the protected line is connected to an inverter-based resource (IBR).

This dissertation evaluates the application of alpha-plane differential protection and a previously proposed Current Mapping Strategy (CMS) to transmission lines connected to Type IV wind turbine-based IBRs. The CMS is not proposed as an original protection logic in this work; instead, it is adopted from previous literature and analyzed in a new application involving converter-limited fault currents and zero-sequence current circulation through a grounded transformer connection. Electromagnetic transient simulations were performed in EMTP software for different fault types, fault resistances, and fault locations. The results show that IBR-side zero-sequence current associated with the transformer connection can affect phase selection in phase-segregated protection elements. The removal of this zero-sequence component from the IBR-side phase currents improves the identification of the faulted phases, while CMS-based protection provides a useful alternative representation of the differential quantities in the alpha plane.

Keywords: Alpha plane, inverter-based resources, current mapping strategy, differential protection, Type IV wind turbine, zero-sequence current.

RESUMO

Análise da Proteção Diferencial Aplicada a Linhas que Interligam Recursos Baseados em Inversores.

Fontes de energia renovável conectadas por conversores eletrônicos, como turbinas eólicas Tipo IV e plantas fotovoltaicas, apresentam comportamento de corrente de falta significativamente diferente daquele observado em geradores síncronos. A resposta transitória dessas fontes às faltas depende dos controles do conversor, dos limitadores de corrente, dos algoritmos de sincronização, da proteção dos semicondutores e dos requisitos de código de rede. Essas características podem afetar funções tradicionais de proteção de linhas de transmissão, especialmente quando a linha protegida está conectada a um recurso baseado em inversor (IBR).

Esta dissertação avalia a aplicação da proteção diferencial no plano alfa e de uma Estratégia de Mapeamento de Corrente (CMS), previamente proposta na literatura, a linhas de transmissão conectadas a turbinas eólicas Tipo IV. A CMS não è proposta como uma lógica original neste trabalho; ela è adotada de estudos anteriores e analisada em um novo contexto de aplicação, envolvendo correntes de falta limitadas pelo conversor e circulação de corrente de sequência zero pela conexão aterrada do transformador. Simulações de transientes eletromagnéticos foram realizadas no EMTP para diferentes tipos de falta, resistências de falta e localizações ao longo da linha. Os resultados mostram que a corrente de sequência zero associada ao transformador do lado do IBR pode afetar a seleção de fases nos elementos segregados de proteção. A remoção dessa componente das correntes de fase do lado do IBR melhora a identificação das fases faltosas, enquanto a proteção baseada em CMS fornece uma representação alternativa das grandezas diferenciais no plano alfa.

Palavras-chave: Plano alfa, recursos baseados em inversores, estratégia de mapeamento de corrente, proteção diferencial, turbina eólica Tipo IV, corrente de sequência zero.

CONTENTS

LIST OF FIGURES

LIST OF TABLES

LIST OF SYMBOLS

Symbol	Description
$\bar{I}_L$	Current phasor measured at the local terminal of the protected line.
$\bar{I}_R$	Current phasor measured at the remote terminal of the protected line.
I_{op}	Operating current of the differential protection.
I_{res}	Restraint current of the differential protection.
Γ_α	Alpha-plane complex variable.
Γ_{CMS}	CMS complex variable plotted in the alpha plane.
$\bar{I}_{dif}$	Differential current used in the CMS formulation.
$\bar{I}_M$, $\bar{I}_N$	Mapped currents used in the CMS formulation.
Γ_f	CMS parameter associated with the fault settlement region.
k_Δ	CMS parameter associated with the distance between the pre-fault point and the fault settlement region.
Ψ	CMS parameter used to define the operation characteristic radius.
$\bar{I}_0$	Zero-sequence current phasor.
$\bar{I}_1$	Positive-sequence current phasor.
$\bar{I}_2$	Negative-sequence current phasor.
a	Symmetrical-component operator equal to $1\angle 120°$.
P_w	Mechanical power extracted from the wind.
C_p	Wind turbine power coefficient.
λ	Tip-speed ratio.
λ'	Auxiliary variable used in the C_p expression.
R_{blade}	Wind turbine blade radius.
v_w	Wind speed.
β	Blade pitch angle.
ω_m	Mechanical angular speed.
V_{dc}	DC-link voltage.
C_{dc}	DC-link capacitance.
I_{max}	Maximum converter current limit.
K_p, K_i	Proportional and integral gains of PI controllers.

GLOSSARY

Term	Definition
IBR	Inverter-Based Resource. A generation resource connected to the power system through a power electronic converter.
Type IV wind turbine	Full-converter wind turbine topology in which the generator is fully decoupled from the grid by a back-to-back converter.
MSC	Machine-Side Converter. Converter connected to the generator side of the Type IV wind turbine.
GSC	Grid-Side Converter. Converter connected to the grid side of the Type IV wind turbine.
PLL	Phase-Locked Loop. Synchronization algorithm used by grid-following converters to estimate the grid voltage angle.
CMS	Current Mapping Strategy. Protection formulation that maps the original differential quantities into equivalent currents before plotting the operating point in the alpha plane.
FSR	Fault Settlement Region. Region in the alpha plane where the CMS operating point is expected to settle during an internal fault.
OC	Operation Characteristic. Tripping region associated with the CMS formulation.
87L	ANSI function number for line differential protection.
87LQ	Negative-sequence line differential element.
87LG	Zero-sequence line differential element.
AG fault	Phase-A-to-ground fault.
ABG fault	Phase-A-and-B-to-ground fault.
ABC fault	Three-phase fault.
EMTP	Electromagnetic Transients Program. Simulation environment used for time-domain electromagnetic transient studies.

CHAPTER 1

INTRODUCTION

1.1 BACKGROUND

Electric power systems have traditionally been planned, operated, and protected considering the behavior of synchronous generators. In conventional systems, the short-circuit response is mainly determined by the internal voltage of rotating machines, their subtransient and transient reactances, and the equivalent impedance between the source and the fault point. As a result, classical protection schemes were developed under the assumption that faults produce relatively high currents, with phase and sequence components that can be interpreted using well-established short-circuit theory.

This assumption is no longer sufficient for many modern transmission systems. The increasing integration of renewable energy sources has introduced a large number of generating units connected to the grid through power electronic converters. These sources are commonly referred to as Inverter-Based Resources (IBRs), since the interface between the primary energy source and the electrical network is performed through controlled semiconductor devices rather than through a direct electromechanical connection. Unlike synchronous generators, IBRs do not contribute fault current according to the natural electromagnetic response of a rotating machine. Their response is imposed by converter controls, current limiters, synchronization algorithms, semiconductor protection, grid-code requirements, and the topology of the connection between the generation plant and the power system.

The growth of renewable generation is motivated by several environmental, economic, and technical factors. From an environmental perspective, the use of renewable sources contributes to reducing the dependence on fossil fuels and the emission of pollutant gases. Conventional generation based on coal, oil, and natural gas has historically been associated with greenhouse gas emissions and air pollution. Therefore, increasing the share of renewable sources is an important step toward a more sustainable energy sector. From an economic and strategic perspective, the diversification of the energy matrix also improves energy security, reduces exposure to fuel price variations, and stimulates investments in new technologies, transmission infrastructure, and power electronic equipment.

In Brazil, the integration of renewable sources is particularly relevant because the National Interconnected System, known as Sistema Interligado Nacional (SIN), is geographically extensive and includes different generation technologies distributed across large distances. The expansion of wind and solar generation has increased the importance of studying the technical impacts of these sources on transmission systems. Wind generation, in particular, has become an important component of the Brazilian energy matrix due to favorable wind conditions in several regions of the country. As new wind power plants are connected to the grid, the protection of the transmission lines that interconnect these plants to the SIN becomes a fundamental requirement for reliable operation.

Wind power plants convert the kinetic energy of the wind into electrical energy. The wind transfers mechanical power to the turbine blades, causing the rotor to rotate. This mechanical rotation is then converted into electrical power by the generator. In modern wind turbines, variable-speed operation is often used to improve energy extraction from the wind. Nevertheless, the variable mechanical speed of the turbine implies that the electrical frequency produced by the generator may not be directly compatible with the grid frequency. For this reason, modern wind turbines frequently require power electronic converters to adapt the generated electrical power to the voltage, frequency, and power quality requirements of the power system.

Among the different wind turbine technologies, Type IV wind turbines, also known as full-converter wind turbines, are of special interest in this dissertation. In this topology, the generator is fully decoupled from the grid by a power electronic interface. The generator-side converter rectifies the variable-frequency voltage produced by the generator, the DC-link maintains the energy balance between the generator and the grid, and the grid-side converter injects controlled AC currents into the power system. This structure provides operational flexibility, allows active and reactive power control, and makes variable-speed wind generation possible. However, it also changes the electrical behavior of the source during faults.

The Type IV topology was selected in this dissertation because the full-converter interface makes the grid-side current mainly dependent on the converter control strategy. Since the generator is not directly connected to the grid, the current observed by the protection system during a fault does not correspond to the natural response of a synchronous generator. Instead, the converter acts as a controlled interface between the wind turbine and the network. This characteristic makes the Type IV wind turbine a suitable case for evaluating the impact of IBR behavior on transmission line protection.

During short-circuit conditions, the converter cannot be treated as a conventional voltage source behind an impedance. Semiconductor devices such as IGBTs have limited overcurrent capability and must be protected by current limiters, DC-link protection, and control actions. For this reason, the fault current contribution of a Type IV wind turbine is usually limited to values close to its rated current. In addition, the current angle and sequence content are not determined only by the network impedance, but also by the adopted control strategy. The IBR may prioritize positive-sequence current, reactive current support, active current, or current limitation depending on the implemented control logic.

This behavior creates important challenges for transmission line protection. Overcurrent protection may lose sensitivity because the current supplied by the IBR may not increase significantly during faults. Distance protection may estimate an incorrect apparent impedance because the measured current angle is influenced by the converter controller. Directional and sequence-based elements may also be affected, especially when the negative-sequence current is limited or not intentionally injected by the converter. Therefore, protection schemes developed for systems dominated by synchronous generation must be reevaluated when applied to lines connected to IBRs.

Line differential protection is one of the most selective protection principles used in power systems. It compares the currents measured at the terminals of a protected line. Under normal operating conditions and external faults, the currents entering and leaving the protected zone should be balanced, considering current transformer errors, communication delays, current transformer errors, communication delays, and compensation procedures. During an internal fault, the current balance is lost and the relay should operate. This principle is attractive for IBR-connected lines because it does not depend only on the magnitude of the current measured at one terminal.

However, the application of differential protection to lines connected to IBRs is not straightforward. The current measured at the IBR terminal may have low magnitude, controlled phase angle, low negative-sequence content, and transient components associated with converter control and switching. In addition, the transformer connection used to interface the wind plant with the transmission network may create or block zero-sequence current paths. These aspects can modify the phase currents used by the protection algorithm and may affect both fault detection and faulted-phase selection.

In this dissertation, the protected element is a transmission line connected to a Type IV wind turbine model. The faults analyzed in this work are not faults inside the turbine itself; they are faults applied on the transmission line that interconnects the IBR-based source to the remaining system. This distinction is important because the objective is to evaluate how the protection of the line behaves when one terminal is connected to a conventional network and the other terminal is connected to a converter-interfaced wind generation system.

The protection methods evaluated in this dissertation include conventional alpha-plane differential protection and the Current Mapping Strategy (CMS). The CMS was previously proposed in the literature as an alternative current representation for differential protection Bainy *et al.* (2021). In this work, the CMS is not presented as an original protection logic proposed by the author. Instead, it is selected, implemented, and evaluated in a new application context: a transmission line connected to a Type IV wind turbine. The contribution of this dissertation is therefore associated with the analysis of this method under IBR-related fault conditions and with the investigation of how zero-sequence components and converter-limited currents affect the protection response.

A specific issue addressed in this dissertation is the influence of zero-sequence current during ground faults. In the analyzed system, the transformer is connected as delta–grounded-wye in the direction from the IBR to the remaining system. The IBR, represented at the local terminal, is connected to the delta side, while the protected transmission line is connected to the grounded-wye side. This grounded-wye connection provides a zero-sequence current path during ground faults. During single-line-to-ground and double-line-to-ground faults, this zero-sequence current may appear in the phase currents measured at the local terminal of the protected line. Since the Type IV wind turbine itself does not behave as a conventional zero-sequence source, the measured zero-sequence component at the local terminal is associated with the grounded transformer path rather than with the native contribution of the converter. If this component is directly used in the phase-segregated differential protection, the relay may identify non-faulted phases as involved in the fault.

For this reason, this work evaluates the removal of the zero-sequence component from the phase currents measured at the IBR-side terminal before applying the phase differential protection logic. This procedure is not intended to remove ground-fault information from the complete protection system. Instead, it is used to improve phase selection by preventing the zero-sequence current returning through the grounded transformer from contaminating the phase quantities used by the phase-segregated elements. The zero-sequence element itself remains relevant for identifying ground faults, but the phase elements require a more careful treatment when the IBR-side current contains a zero-sequence component that does not represent a direct phase contribution from the converter.

The study of this topic is relevant because the reliable integration of renewable generation depends not only on the ability to generate power, but also on the ability to protect the interconnection system properly. As IBRs become more common, protection engineers must understand how converter controls, transformer connections, sequence components, and current limitation affect relay operation. This dissertation contributes to this discussion by evaluating the behavior of differential protection algorithms in a line connected to a Type IV wind turbine under different fault types, fault resistances, and fault locations.

1.2 MOTIVATION

The motivation for this dissertation is not limited to the general expansion of renewable energy. Although the growth of wind and solar generation is an important background factor, the central motivation is the practical protection problem created by the replacement of synchronous-machine fault behavior with converter-controlled fault behavior. Modern transmission systems increasingly include lines whose terminals are connected to IBR-based plants. These lines must be protected with the same dependability and security expected in conventional systems, but the electrical quantities available to the relays may be significantly different.

In Brazil, the expansion of renewable generation has become increasingly relevant in the planning and operation of the SIN. Wind and solar power plants have been connected to the grid in different regions of the country, requiring new transmission infrastructure and new protection studies. This growth reinforces the need to evaluate whether traditional protection functions remain adequate when applied to systems with high participation of IBRs.

Figure 1.1 illustrates the expansion of the Brazilian electricity matrix by source type, highlighting the participation of different generation technologies. The figure supports the motivation of this work because it shows the increasing relevance of renewable sources in the Brazilian power system. As these sources become more representative, the protection of lines connected to converter-interfaced generation becomes a practical and necessary engineering problem.

In a conventional transmission system, an internal fault usually produces a high current contribution from the connected sources. This current increase supports the operation of overcurrent, distance, directional, and differential elements. In a system connected to a Type IV wind turbine, the converter limits the current in order to protect its semiconductor devices and DC-link. As a result, the current contribution from the wind plant may be low, controlled, and not directly proportional to the fault severity. This may reduce the sensitivity of protection functions or produce trajectories in the alpha plane that differ from those expected in conventional systems.

The motivation is also related to the need for correct phase selection. In many protection applications, it is not sufficient to detect that a fault occurred; it is also important to identify which phases are involved. This becomes relevant for fault classification, event analysis, protection coordination, and possible single-pole tripping or reclosing studies. When zero-sequence current appears in the local terminal due to the grounded transformer connection, the phase currents used by the relay may suggest that more phases are involved in the fault than actually are. This can reduce the selectivity of the protection and lead to incorrect interpretation of the event.

Another motivation is the limited use of differential protection studies in the specific context of IBR-connected lines. Several studies in the literature discuss the behavior of IBRs, the impact of converter-based generation on distance protection, and the challenges associated with negative-sequence quantities Nagpal *et al.* (2020), Chowdhury & Fischer (2020a), Chowdhury

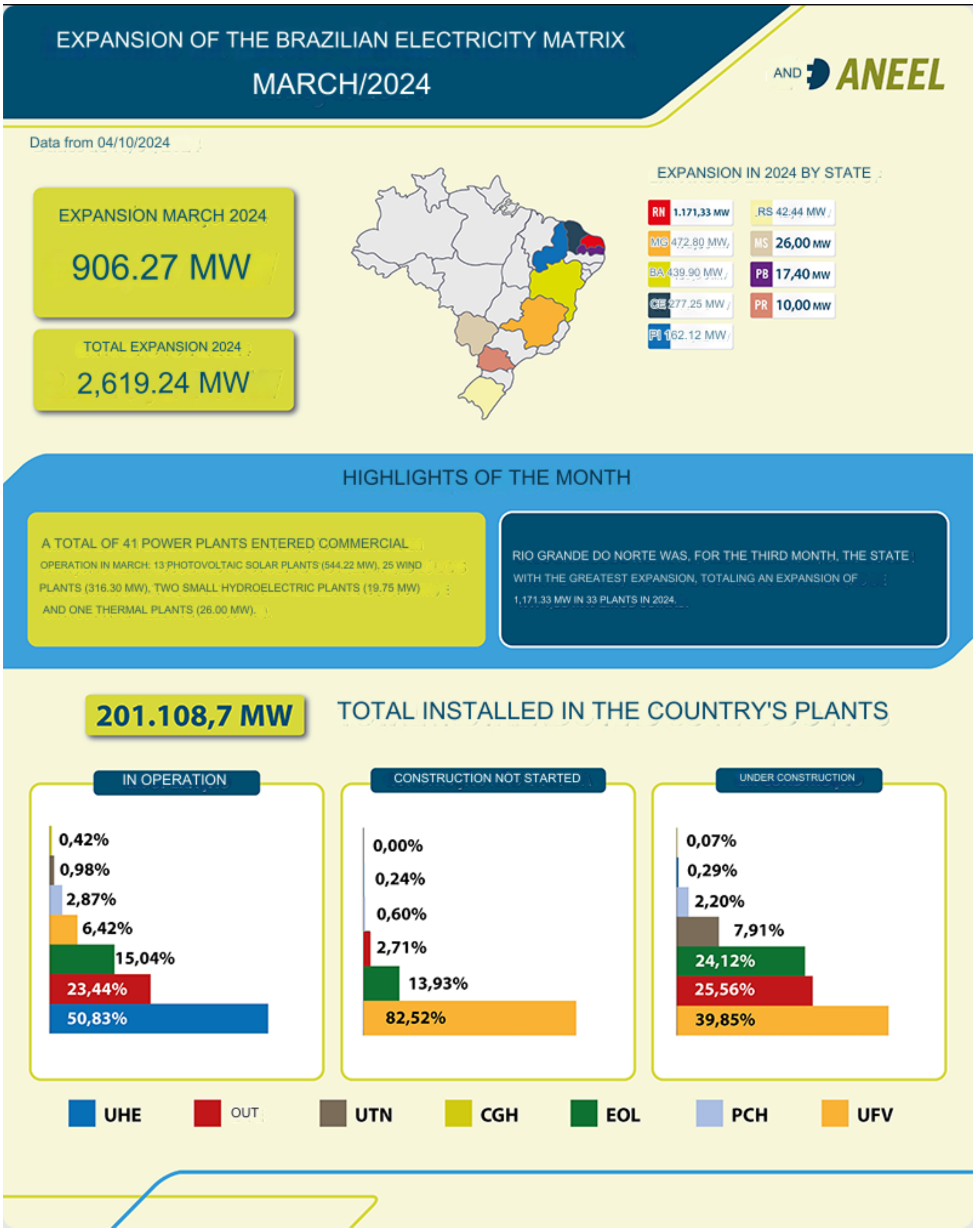

Figure 1.1. ANEEL's total power divided by type.

& Fischer (2020b), Bini *et al.* (2021), Chen *et al.* (2015). Other works propose advanced differential protection strategies, including current mapping methods, for applications such as transmission lines and compensated lines Bainy *et al.* (2021). However, there is still a need to connect these two topics more directly: the evaluation of differential protection based on alpha-plane and CMS logic when the protected line is connected to a Type IV wind turbine with converter-limited fault current.

Therefore, this dissertation aims to contribute to this gap by using a Type IV wind turbine model and applying different internal faults on the interconnection line. The analysis includes phase A-to-ground faults, phases A and B-to-ground faults, and three-phase-to-ground faults. The cases also consider different fault resistances and fault locations. This selection of cases allows the study of balanced and unbalanced disturbances, the influence of ground return paths, and the effect of fault severity on the protection response.

The choice of a Type IV wind turbine is motivated by the full decoupling between the generator and the grid. Since all the generated power passes through the converter, the grid-side response is strongly governed by the converter controls. This makes the Type IV turbine a suitable case for studying IBR behavior in protection applications. In addition, the full-converter topology allows the dissertation to analyze a scenario in which the current injected into the grid is not a natural short-circuit current from a rotating machine, but a controlled quantity limited by the converter.

The choice of the CMS is motivated by its ability to modify the representation of the terminal currents in the alpha plane. The classical alpha-plane method evaluates the complex ratio between local and remote currents. In systems with limited and controlled IBR currents, this ratio may not provide the expected separation between operating and restraining conditions. The CMS provides an alternative mapping of the currents, which can improve the movement of the operating point toward the tripping region during internal faults. For this reason, it is evaluated in this dissertation as a promising method for improving the behavior of differential protection in IBR-connected lines.

It is important to emphasize that this work does not claim the original proposal of the CMS. The method was previously developed and published by other authors. The contribution of this dissertation is its application, implementation, and evaluation in the specific context of a transmission line connected to a Type IV wind turbine. This distinction is important because it separates the methodological basis adopted from the original contribution of this research. The originality of the work lies in the analysis of the interaction between the Type IV wind turbine fault response, the transformer zero-sequence path, and the differential protection algorithms.

The dissertation is also motivated by the need to produce results that are useful for protection engineers. For this reason, the analysis is based on electromagnetic transient simulations and on the observation of currents, sequence components, alpha-plane trajectories, and CMS responses. The objective is not only to state whether a method operates or not, but to explain why it behaves in a certain way. The results are interpreted considering the action of converter controls, the fact that the positive-sequence current remains close to 1 pu in the analyzed post-fault interval, the low negative-sequence contribution, and the zero-sequence current path provided by the grounded transformer.

Thus, the motivation of this dissertation can be summarized in four main points. First, IBRs are increasingly present in transmission systems and their fault behavior differs from that of synchronous generators. Second, Type IV wind turbines inject limited and controlled fault currents, which may affect the behavior of line protection. Third, ground faults in systems with grounded-wye transformer connections can introduce zero-sequence components that affect phase-segregated protection. Fourth, the CMS provides a current mapping approach that may improve alpha-plane differential protection, but its behavior must be evaluated in the specific context of interconnecting IBRs.

1.3 PROBLEM STATEMENT

The main problem addressed in this dissertation is the performance of line differential protection when the protected line is connected to a Type IV wind turbine. In this condition, one terminal of the line receives current from a conventional network, while the other terminal is connected to an IBR whose fault current is limited and controlled by a full-converter interface. This asymmetry modifies the current relationship used by differential protection algorithms and may affect both fault detection and phase selection.

In the classical alpha-plane differential method, the protection decision is based on the relationship between currents measured at the local and remote terminals. For external faults and normal operating conditions, the current ratio should remain in the restraining region. For internal faults, the ratio should move toward the operating region. However, when the local terminal is connected to a Type IV wind turbine, the local current may have low magnitude, limited sequence content, and transient behavior caused by converter controls. Therefore, the alpha-plane trajectory may not behave as expected for a conventional source.

The problem becomes more complex in ground faults. In the analyzed system, the transformer connected to the IBR terminal has a grounded-wye connection that provides a zero-sequence current path. As a result, during single-line-to-ground and double-line-to-ground faults, the measured phase currents at the IBR-side terminal may include a zero-sequence component that is not a direct contribution from the converter itself. If this component is used without treatment in the phase differential elements, the protection may incorrectly indicate the involvement of healthy phases.

Therefore, the problem investigated in this dissertation can be stated as follows: how does differential protection behave when applied to a transmission line connected to a Type IV wind turbine, considering converter-limited fault currents, low or absent negative-sequence injection, zero-sequence current circulation through the grounded transformer, different fault types, different fault resistances, and different fault locations?

To answer this question, this dissertation evaluates conventional alpha-plane protection and CMS-based protection using electromagnetic transient simulations. The analysis considers faults applied on the line, not inside the turbine. The results are interpreted by correlating the currents injected by the Type IV wind turbine, the behavior of sequence components, and the response of each protection method.

1.4 OBJECTIVES AND CONTRIBUTIONS

The main objective of this dissertation is to evaluate the performance of differential protection applied to a transmission line connected to a Type IV wind turbine and to analyze whether a CMS can improve the behavior of alpha-plane-based protection under IBR fault conditions.

The specific objectives are:

- To evaluate the impact of converter current limitation on line differential protection;
- To study the behavior of phase, positive-sequence, negative-sequence, and zero-sequence currents during different fault scenarios;
- To evaluate conventional alpha-plane differential protection for faults applied on a line connected to an IBR;
- To apply the CMS previously proposed in the literature to the analyzed IBR-connected line;
- To investigate the effect of zero-sequence current returning through the grounded transformer on phase-segregated protection;
- To evaluate the removal of the zero-sequence component from the IBR-side phase currents as a strategy to improve phase selection;

The main contributions of this dissertation are:

- The application and analysis of a previously reported CMS in a new context involving a full-converter wind turbine;
- The comparison between conventional alpha-plane protection and CMS-based protection for line faults involving IBR-connected systems;
- The identification of the influence of zero-sequence current associated with the grounded transformer connection on phase-segregated protection;
- The evaluation of zero-sequence removal at the IBR-side terminal as a procedure to improve the identification of the correct faulted phases;

It must be emphasized that the CMS itself is not proposed as an original method in this dissertation. The method is adopted from previous work and evaluated here under a different application: a line connected to a Type IV wind turbine. The original contribution is the technical analysis of this method under IBR-related fault conditions, including transformer zero-sequence effects and converter-limited current injection.

1.5 DISSERTATION STRUCTURE

This dissertation is organized into six chapters.

Chapter 1 presents the general context, motivation, problem statement, objectives, contributions, scope, and structure of the dissertation. The chapter emphasizes the protection problem created by the connection of Type IV wind turbines to transmission lines and explains why differential protection must be reevaluated under IBR fault conditions.

Chapter 2 presents the bibliographic review. The chapter discusses previous studies related to IBR fault behavior, Type III and Type IV wind turbines, photovoltaic generation, distance protection, differential protection, and protection challenges associated with converter-interfaced resources. The review is used to identify the relation between previous works and the contribution of this dissertation. In particular, it highlights that several studies address IBR impacts on protection, while the present work focuses on the application of alpha-plane and CMS-based differential protection to a line connected to a Type IV wind turbine.

Chapter 3 presents the theoretical fundamentals required for the protection analysis. The chapter introduces the main objectives of power system protection, including sensitivity, dependability, security, selectivity, speed, coordination, simplicity, and maintainability. It then presents line differential protection, the calculation of operating and restraint currents, the alpha-plane method, sequence-based elements, and the Current Mapping Strategy. The chapter also explains the zero-sequence removal procedure applied to the IBR-side currents and justifies its use based on the grounded transformer connection.

Chapter 4 describes the Type IV wind turbine model used in the simulations. The chapter presents the full-converter structure, including the AC-DC converter, DC-link, DC chopper, DC-AC converter, filters, transformer, PLL, DQ0 transformations, MPPT logic, and PI control loops. The chapter also distinguishes the portions of the model obtained from previous EMTP-based implementations from the parts implemented or modified in this dissertation. The parameters and constants used in the model are described and referenced to support reproducibility.

Chapter 5 presents the simulation results and discussions. The chapter begins with the description of the simulated system, the transformer connection, the transmission line, the fault locations, and a table summarizing all fault cases. For each case, the chapter presents the behavior of local and remote sequence currents, the response of classical alpha-plane protection, and the performance of CMS. The results are interpreted quantitatively, including fault application time, current magnitudes before and after the fault. Special attention is given to the comparison between cases with and without zero-sequence removal.

Chapter 6 presents the conclusions of the dissertation. The chapter summarizes the main findings regarding the behavior of Type IV wind turbine fault currents, the limitations observed in conventional alpha-plane protection, the performance of CMS-based protection, and the importance of treating zero-sequence components for correct phase selection. The chapter also presents suggestions for future work, including the analysis of different transformer connections, grid-forming control, negative-sequence current injection, communication synchronization errors, and additional IBR control strategies.

CHAPTER 2

BIBLIOGRAPHIC REVIEW

According to Gevorgian *et al.* (2012), the expansion of wind power plants (WPPs) is accelerating, with a significant increase in their numbers in the U.S. over the last decade. Projections indicate that U.S. wind power generation will reach 330 GW by 2030. As WPPs become more critical, planning engineers must conduct impact studies to assess short-circuit current (SCC) contributions to the transmission network during various fault scenarios. This data is essential for sizing circuit breakers and ensuring effective system protection. However, protection engineers face challenges due to the diverse topologies of wind turbine generators (WTGs) compared to conventional units. This paper analyzes the short-circuit behavior of a WPP with different types of wind turbines, focusing on symmetrical and unsymmetrical faults, using time-domain simulations and steady-state calculations with three software tools.

Barsch *et al.* (2012) examines various design and performance aspects of wind turbine generators (WTGs) integrated into a power grid. It aims to assist engineers in understanding how the design of WTG plants influences short-circuit contributions and the resulting effects on protection systems. The discussion includes interconnection configurations, collector system design, generator selection, and protection system choices.

Sulla (2012) investigates the behavior of wind turbines, particularly those using Doubly-Fed Induction Generators, during grid faults. With the increasing share of wind power, these non-synchronous generators exhibit different fault behaviors compared to traditional synchronous generators. The research first focuses on calculating fault currents from DFIG turbines, proposing an analytical method that avoids detailed simulations. It also introduces a modeling technique for representing a DC link with chopper protection during symmetrical faults. The study finds that using an aggregate model can accurately simulate the total fault current of wind farms, simplifying the simulation process.

As noted in Hooshyar *et al.* (2014a), the expanding integration of wind farms (WFs) into high-voltage (HV) networks has established distance protection as the preferred solution. However, the paper identifies critical deficiencies in distance protection for lines connected to induction generator (IG)-based WFs during symmetrical faults. It reveals that squirrel cage induction generator (SCIG)-based WFs encounter security concerns with distance protection, whereas doubly fed induction generator (DFIG)-based WFs experience severe dependability problems due to operational conditions unique to these configurations, which remain unaddressed in current relaying practices. These issues may result in unnecessary WF disconnection, conflicting with modern grid code requirements mandating continuous operation during disturbances. To address these challenges, the authors propose an innovative modified permissive overreach transfer trip (POTT) scheme combined with a fault current classification technique. This approach aims to restore accurate, high-speed protection for distance relays across the entire line length. Comprehensive performance evaluations validate the findings and demonstrate the proposed solution's effectiveness under various operating scenarios, especially for DFIG-based WFs with nonzero crowbar resistance, which represent a common situation faced by distance relays.

In Hooshyar *et al.* (2014b), the fault ride-through (FRT) requirements established by modern grid codes create intricate interactions between full-scale converter-interfaced renewable energy power plants (CIREPPs) and the protection systems used in high-voltage transmission grids, which often depend on distance relays as primary or backup safeguards. These interactions, driven by the specific fault behaviors of CIREPPs, have largely been overlooked in existing relaying research. In Part I of this paper, it is introduced a CIREPP model specifically designed for relaying studies, emphasizing the critical characteristics that pose risks to the protection systems. Additionally, it is identified various operating scenarios that can lead to malfunctions in distance relays located at CIREPP substations. These scenarios include the relay's failure to detect in-zone short circuits and erroneous tripping for out-of-zone faults, which can ultimately weaken the FRT strategies implemented within CIREPPs. The findings of this research are also applicable to alternating current (AC) lines connected to voltage-sourced converter-based high-voltage direct current (HVDC) systems. Where in Hooshyar *et al.* (2014c), Part II examines why existing countermeasures used by commercial relays in conventional power systems do not work effectively in the presence of CIREPPs. It presents a novel formula for calculating impedance in the relay's phase element, aimed at preventing malfunctions during line-to-line-to-ground faults. Additionally, the paper suggests a communication-assisted approach that requires minimal bandwidth for addressing balanced and line-to-line faults. Considerations for single-line-to-ground faults are also discussed. The proposed solutions are designed to be straightforward and independent of the host system's grid code, making them suitable for industrial memory-polarized distance relays. A detailed performance assessment is provided to confirm the reliability of these proposed methods.

Chen *et al.* (2015) investigates the complex fault current behavior of variable-speed wind turbine generators (WTGs), emphasizing Type 3 (doubly fed induction) and Type 4 (full converter) systems. These generators are influenced by proprietary control strategies that lead to complex fault characteristics, where some manufacturers design them to produce balanced three-phase fault currents even under unbalanced fault conditions. Traditional short-circuit analysis methods commonly used by protection engineers are inadequate for capturing this behavior. The paper presents a detailed MATLAB and Simulink model that illustrates the fault current characteristics of Type 4 WTGs, incorporating pseudo-control logic. Additionally, it features a case study of the misoperation of directional overcurrent relays during a fault event in an actual wind power plant, offering valuable insights and recommendations for improving protection measures for wind farms that utilize these converter-based WTGs.

Vila *et al.* (2016) examines the Penonome wind power facility in Panama, designed for a total capacity of 337.5 MW, with the initial two phases currently producing 270 MW. This installation connects wind turbines from multiple manufacturers to a 34.5 kV electrical system, which interfaces with Panama's 230 kV transmission network through two transformers at the El Coco substation. Grounding for the 34.5 kV system is realized using zig-zag and grounded-wye/delta transformer configurations. This paper investigates the protective measures required for the 34.5 kV system and discusses the requirements for protection coordination, presenting the outcomes of the coordination study. Furthermore, it offers suggestions for future enhancements to the protection system and describes an actual incident involving two cross-country faults within the 34.5 kV network.

Nagpal & Henville (2017) explains that power-electronic sources, including Type 3 wind turbine generators and static synchronous compensators (STATCOM), interconnect via power converters employing fast switching to regulate output current during short circuits. The resulting short-circuit current profiles diverge markedly from those of conventional rotating machines. Consequently, standard transmission-line protection schemes may encounter reliability problems if these distinctions are not considered. This paper utilizes actual short-circuit current records to demonstrate risks to conventional protection schemes, particularly those relying on negative-sequence quantities for unbalanced fault detection. It also discusses the protection strategies employed by BC Hydro for transmission lines linked to Type 3 wind turbines and STATCOM sources, which effectively manage ground faults regardless of the converter control algorithm, as long as a transformer providing zero-sequence current is used.

According to Fang *et al.* (2018), inverter-interfaced renewable energy generators (IIREGs) exhibit fault characteristics differing from synchronous generators due to their distinct configurations and control strategies. This disparity renders conventional distance protection unsuitable for transmission lines connected to IIREGs. Through fault current analysis, the investigation reveals that distance relays on the IIREG side are susceptible to misoperation or failure. To resolve this, an improved protection scheme incorporating time delay and zero-sequence impedance is introduced. Simulation studies, supplemented by a field short-circuit test at a wind power plant, confirm the limitations of traditional protection methods and verify the reliability of the new approach.

According to Nagpal *et al.* (2020), the growing penetration of solar photovoltaic systems and Type III/IV wind energy conversion technologies into transmission networks introduces considerable difficulties for protection engineering. These systems rely on fully rated power electronic converters to interconnect with the grid, with their sizing determined by total power output. Type III topologies employ doubly fed asynchronous generators, where the stator links directly to the network and the rotor interfaces through a converter managing roughly 30% of the total capacity. IBRs exhibit fault responses that deviate substantially from conventional synchronous machines; whereas traditional sources deliver high, uncontrolled short-circuit currents, IBRs provide limited, regulated contributions governed by fast-switching power electronics. Such regulation restricts current magnitudes to comply with thermal constraints and interconnection requirements, resulting in distinctive fault characteristics. Established protection methodologies, which depend on elevated fault currents, may prove inadequate in IBR-dominated scenarios, leading to potential misoperations or failure to detect disturbances.

Additional variability from weather conditions further compromises line protection dependability. This document examines protection challenges associated with IBR interconnections, suggests remedial measures, and disseminates insights derived from operational experience, concentrating on transmission and sub-transmission protection at interconnection points while omitting distribution-level systems. The objective is to support protection specialists in successfully incorporating IBRs into power networks through advanced multifunctional relays.

Chowdhury & Fischer (2020a) present the first part of a two-paper study on transmission-line protection problems in systems with inverter-based resources. The work is based on a collaborative study led by Sandia National Laboratories and the North American Electric Reliability Corporation, using real-code electromagnetic transient models from four inverter manufacturers, including Type 3 wind, Type 4 wind, and photovoltaic resources. The simulated voltage and current records were reproduced in protective relay hardware with settings typical of conventional generation systems. The results show that IBR fault-current behavior can challenge several line-protection functions, especially those that depend on negative-sequence current, directional decisions, fault-type identification, weak-infeed logic, distance elements, and line current differential protection. This reference is important to the present dissertation because it demonstrates, using relay hardware and realistic inverter models, that line protection cannot be evaluated only from the viewpoint of conventional synchronous-generator fault theory when one terminal is connected to an IBR.

Chowdhury & Fischer (2020b) continue the same study and focus on practical solutions for transmission-line protection in systems with IBRs. Instead of requiring replacement of the relays or the inverter technology, the authors propose adjustments in protection settings and logic to improve reliability. The paper discusses the use of increased overcurrent supervision thresholds, enhanced directional-element security, fault-type identification based on weak-infeed undervoltage logic, blocking logic for three-phase faults, and dropout timers to improve Zone 2 distance protection dependability. The study also reports that Type 4 wind, Type 3 wind, and photovoltaic resources may require different protection considerations because their negative-sequence current contribution and phase-angle behavior are not identical. This work complements the present dissertation by showing that IBR-related protection problems can be mitigated by adapting protection logic and settings, while this dissertation evaluates the effect of IBR fault behavior on alpha-plane and CMS-based differential protection of a line connected to a Type IV wind turbine.

Rampokanyo *et al.* (2021) describes a Technical Brochure addressing issues arising from decreasing system inertia and outlining its objectives. It underscores inertia's fundamental role in power system operation and provides essential definitions concerning inertia and frequency stability. The publication elaborates on frequency containment reserves (FCR) and fast frequency response (FFR) services, supplemented by an overview of utility practices derived from surveys. Challenges linked to declining inertia are examined, along with an assessment of existing and emerging technologies capable of delivering FCR and FFR. Furthermore, it distinguishes between conventional grid-following control for IBRs and emerging grid-forming schemes. The brochure synthesizes findings from global research on frequency reserve adequacy and inertia requirements, describing products developed by system operators. Additionally, it serves as a reference for regulatory frameworks and operational practices regarding frequency containment reserves, concluding with a summary of key outcomes and recommendations.

Ali & Knight (2021) addresses the fact that as renewable energy capacity expands to meet both environmental and economic objectives, the variable nature of these sources necessitates increased transmission capacity. Dynamic thermal line rating offers a way to boost transmission capacity without infrastructure upgrades, but it may cause existing protection devices to malfunction. This study introduces an algorithm designed to enhance the performance of traditional protection relays, such as distance and overcurrent relays. The algorithm leverages dynamic thermal rating, the ratio of negative to positive sequence currents, and voltage criteria to reliably identify symmetrical and asymmetrical faults, as well as unsafe overloads, while preventing relay operation during safe overloads. Simulations in MATLAB/Simulink demonstrate the effectiveness of this method.

In Bini *et al.* (2021), it is discussed the impact of inverter-based resources (IBRs), such as photovoltaic (PV) power plants, on traditional digital protection systems in transmission lines connecting these sources to the bulk power grid. A key focus is on how fault currents behave differently in systems with IBRs compared to those with synchronous generators, particularly regarding negative-sequence components. The study also details advanced protective relay functions, time-domain analysis techniques, and adjustments needed in the settings of intelligent electronic devices (IEDs) for effective fault management. Data from real events involving a PV plant were used to validate the proposed solutions. These insights will be applied to a new wind farm currently being designed.

Bainy *et al.* (2021) presents the Current Mapping Strategy (CMS) as a particular formulation of the generalized alpha plane applied to two-terminal current differential protection of series-compensated transmission lines. The main contribution of this work is the definition of an adjustable Fault Settlement Region (FSR) and an Operation Characteristic (OC) in the alpha plane, allowing the protection engineer to tune the method according to the desired sensitivity or security. The authors validated the method using ATP simulations on a 400 km, 500 kV series-compensated transmission line and compared the CMS with the regular alpha-plane approach under transient and parametric conditions. The results showed that the CMS provided smoother trajectories toward the FSR and maintained reliable performance under challenging conditions such as subsynchronous oscillations and outfeed. Although the study was not focused on IBR-connected lines or Type IV wind turbines, it is directly relevant to this dissertation because the CMS formulation adopted in the protection analysis is based on this previous work. Therefore, the present dissertation does not propose the CMS as an original method; instead, it evaluates its application in a new context involving a transmission line connected to a Type IV wind turbine-based IBR.

Wang *et al.* (2022) explains that the electromagnetic transient (EMT) model of Type 4 wind turbine generators (WTGs) requires small simulation steps, which decreases efficiency for large-scale Type 4 WTG-based wind power plants (WPPs). To improve this, a streamlined model is proposed that substitutes power electronic switches and the DC link with a controlled voltage source, eliminating the need for small simulation steps. This new model is easier to implement and accurately reflects the EMT characteristics of Type 4 WTGs during faults, significantly reducing simulation time and enhancing efficiency for power grids connected to large-scale Type 4 WTG-based WPPs.

Kasztenny (2022b) introduces innovative distance elements specifically designed for protecting transmission lines located near inverter-based resources and wind turbine generators. The authors begin by identifying the shortcomings in the logic of existing distance elements, which often rely on memory polarization for directional and negative-sequence current for fault-loop selection and reactance comparator polarization. By using a framework based on worst-case scenarios from published studies and field data, the analysis intentionally avoids proprietary or uncertain source information and does not assume compliance with any current or forthcoming interconnection standards. To enhance performance, the paper proposes alternatives that address these challenges, introducing an offset distance characteristic to eliminate memory polarization. Additionally, it employs separate directional elements to effectively manage the offset distance elements, utilizing the fault current contribution from the system rather than that from the source.

Kasztenny (2022a) presents distance elements aimed at safeguarding transmission lines situated near wind turbine generators and inverter-based sources. It discusses the challenges faced by current distance elements that utilize memory polarization for directionality and negative-sequence current for selecting fault loops. The analysis is grounded in worst-case scenarios drawn from field data rather than relying on proprietary information or interconnection standards. The authors address the shortcomings of existing distance element logic and suggest alternative solutions, including an offset distance characteristic to bypass memory polarization and distinct directional elements that utilize the fault current from the system. Furthermore, a voltage-based approach for selecting faulted loops is introduced to eliminate the dependence on negative-sequence current. The paper concludes with practical recommendations for implementing various distance elements, including underreaching (Zone 1) and overreaching elements (Zone 2) in pilot protection schemes.

In order to analyze the subjects studied in each article, a table containing all the articles was introduced in table 2.1, explaining the subjects contained in all the articles and which articles discuss about them and which do not discuss about, such as the following topics: Inverter-Based Resources, Type III Wind Turbines, Type IV Wind Turbines, Photovoltaic power plants, Distance Protection and lastly Differential Protection.

Table 2.1. Summary of literature review topics of research.

Reference	Covered Contents					
	IBR	T3	T4	PV	21	87L
Gevorgian *et al.* (2012)	✓	✓	✓	–	–	–
Barsch *et al.* (2012)	✓	✓	✓	–	–	–
Sulla (2012)	✓	✓	–	–	–	–
Hooshyar *et al.* (2014a)	✓	✓	✓	–	–	✓
Hooshyar *et al.* (2014b)	✓	–	–	–	✓	–
Hooshyar *et al.* (2014c)	✓	–	–	–	✓	–
Chen *et al.* (2015)	✓	✓	✓	–	✓	✓
Vila *et al.* (2016)	✓	✓	✓	–	–	–
Nagpal & Henville (2017)	✓	✓	–	–	✓	–
Fang *et al.* (2018)	✓	–	–	–	✓	–
Nagpal *et al.* (2020)	✓	✓	✓	✓	–	–
Chowdhury & Fischer (2020a)	✓	✓	✓	✓	✓	✓
Chowdhury & Fischer (2020b)	✓	✓	✓	✓	✓	–
Rampokanyo *et al.* (2021)	✓	–	–	–	–	–
Ali & Knight (2021)	–	–	–	–	✓	–
Bini *et al.* (2021)	✓	–	–	–	✓	✓
Bainy *et al.* (2021)	–	–	–	–	–	✓
Wang *et al.* (2022)	✓	–	✓	–	–	–
Kasztenny (2022b)	✓	✓	✓	–	✓	–
Kasztenny (2022a)	✓	–	–	–	✓	–

Legend:
IBR: Inverter Based Renewable Resource
T3: Type III Wind Turbine
T4: Type IV Wind Turbine
PV: Photovoltaic
21: Distance Protection
87L: Differential Protection

Source: Own authorship.

CHAPTER 3

FUNDAMENTALS OF LINE DIFFERENTIAL PROTECTION, ALPHA PLANE, AND CURRENT MAPPING STRATEGY

3.1 INTRODUCTION

This chapter presents the theoretical background required for the protection analysis developed in this dissertation. The main objective is to describe the principles of line differential protection and to introduce the alpha-plane and Current Mapping Strategy (CMS) formulations used to evaluate faults in transmission lines connected to inverter-based resources (IBRs).

The chapter is organized according to the signal-processing sequence used in the protection algorithm. First, the general principle of differential protection is presented. Then, the calculation of operating and restraint currents is described. After that, the main aspects of line differential protection are discussed, including current measurement at the local and remote terminals, communication requirements, current normalization, phasor estimation, and sequence components. Finally, the alpha-plane method and the CMS formulation are presented.

Figure 3.1 shows the general structure adopted in this dissertation. The measured phase currents and voltages are obtained at both terminals of the protected line. These signals are processed to obtain synchronized phasors. The symmetrical components are calculated from the synchronized phasors. For ground faults involving the delta–grounded-wye transformer, the zero-sequence component can also be removed from the local-terminal phase currents before the phase-segregated protection is evaluated. Then, the differential quantities are used by the conventional alpha-plane and CMS-based protection methods.

The organization of the chapter follows this flow because line differential protection is not only a mathematical comparison between two currents. In practical applications, the relay decision depends on signal measurement, synchronization, communication, compensation, phasor

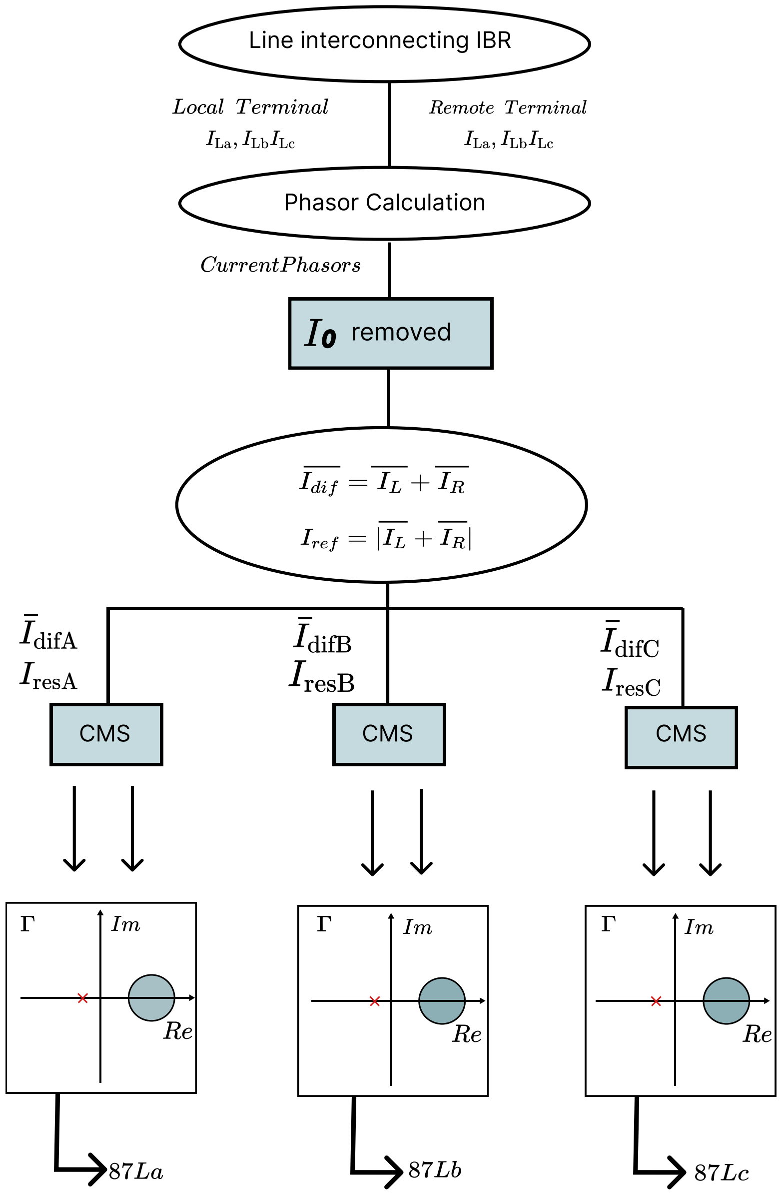

Figure 3.1. CMS-based protection logic considering IBR-side zero-sequence current removal.

estimation, and the final protection logic. This is particularly important in systems connected to IBRs because the currents measured during faults can be limited, controlled, and affected by transformer connections and converter control strategies.

3.2 PRINCIPLES OF POWER SYSTEM PROTECTION

Power system protection is responsible for detecting abnormal operating conditions and isolating the faulted portion of the system. A fault may expose conductors, transformers, converters, circuit breakers, and other equipment to high currents, abnormal voltages, and electromagnetic transients. Therefore, protection systems must act fast enough to avoid equipment damage and preserve system stability.

The main requirements of a protection system are sensitivity, dependability, security, selectivity, speed, coordination, simplicity, and economy. Sensitivity is the ability to detect faults even when the fault current is low or the fault resistance is high. Dependability is the ability to operate when operation is required. Security is the ability to avoid operation when the fault is outside the protected zone or when there is no fault. Selectivity means that only the faulted element must be disconnected. Speed is related to the time between fault inception and circuit breaker opening. Coordination ensures that primary and backup protection functions operate in a planned sequence.

In transmission line protection, these requirements are especially important because the line may connect different parts of the system over long distances. In the case of lines connected to IBRs, the problem becomes more complex because the current contribution from the converter-interfaced terminal may be limited and controlled. Therefore, the protection function must be evaluated not only according to classical short-circuit theory, but also considering the behavior of the IBR during faults.

3.3 BASIC PRINCIPLE OF DIFFERENTIAL PROTECTION

Differential protection is based on Kirchhoff's current law. In a protected zone, the algebraic sum of all currents entering and leaving the zone must be approximately zero during normal operation and external faults. If a fault occurs inside the protected zone, part of the current flows into the fault point and the balance between terminal currents is lost.

For a two-terminal transmission line, the current measured at the local terminal is represented by $\bar{I}_L$ and the current measured at the remote terminal is represented by $\bar{I}_R$. In this dissertation, both currents are defined as positive when they enter the protected line. Therefore, under load condition or external faults, the currents tend to be approximately opposite:

$$\bar{I}_L \approx -\bar{I}_R. \tag{3.1}$$

For an internal fault, both terminals may feed the fault inside the protected zone. In this case, the currents tend to enter the line from both terminals and the sum of currents is no longer close to zero:

$$\bar{I}_L + \bar{I}_R \neq 0. \tag{3.2}$$

The differential current, also called operating current, is defined as:

$$I_{\text{op}} = I_{\text{dif}} = \left|\bar{I}_L + \bar{I}_R\right|. \tag{3.3}$$

where I_{op} is the operating current and I_{dif} is the differential current. The bar symbol indicates a phasor quantity. The magnitude operator $|\cdot|$ indicates the absolute value of a phasor.

The restraint current is used to increase security during high through-current conditions, current transformer errors, external faults, and other non-ideal situations. In this dissertation, the restraint current is calculated as:

$$I_{\text{res}} = \left|\bar{I}_L\right| + \left|\bar{I}_R\right|. \tag{3.4}$$

where I_{res} is the restraint current. Other definitions of restraint current may be found in the literature, such as the maximum value between terminal currents or definitions based on the angular relationship between the phasors. However, the formulation in (3.4) is adopted in this dissertation unless otherwise stated.

The conventional percentage differential characteristic operates when two conditions are satisfied:

$$I_{\mathrm{op}} > SLP \cdot I_{\mathrm{res}}, \tag{3.5}$$

$$I_{\mathrm{op}} > I_{\mathrm{pk}}, \tag{3.6}$$

where SLP is the slope of the percentage differential characteristic and I_{pk} is the pickup current. The pickup current avoids relay operation for very small differential currents caused by noise, measurement errors, or normal system unbalances.

Figure 3.2 illustrates the percentage differential characteristic in the operating plane. The horizontal axis represents I_{res}, and the vertical axis represents I_{op}. The region above the characteristic corresponds to relay operation, while the region below the characteristic corresponds to restraint.

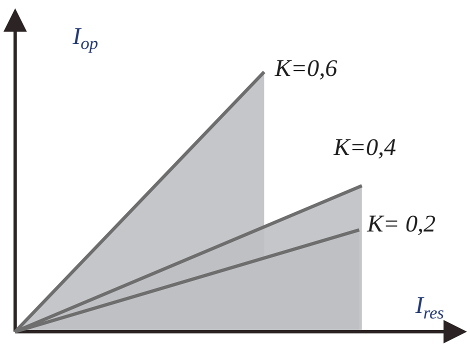

Figure 3.2. Operating and restraint regions of the percentage differential characteristic.

3.4 LINE DIFFERENTIAL PROTECTION

Line differential protection applies the differential principle to a transmission line. The protected zone is delimited by the current transformers installed at the line terminals. In a two-terminal line, the relay must compare the current measured at the local terminal with the current measured at the remote terminal. Therefore, a communication channel is required.

Figure 3.3 shows the basic line differential protection scheme. Current transformers measure the phase currents at the local and remote terminals. The phasors are exchanged through a communication channel and processed by the differential relay. If the algorithm detects an internal fault, a trip command is sent to the corresponding circuit breakers.

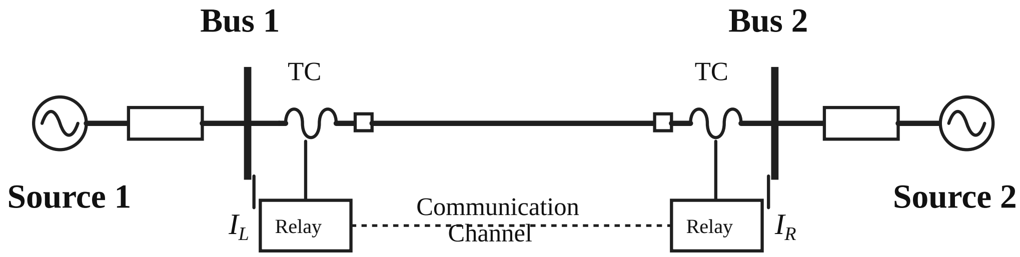

Figure 3.3. Basic structure of a two-terminal line differential protection scheme.

In practical applications, several aspects must be considered before the differential comparison is performed. The most important are current transformer ratios, synchronization of measurements, communication delay, phasor estimation, and the presence of sequence components during unbalanced faults.

3.4.1 Current Normalization

If the current transformers at both terminals have different ratios, their secondary currents must be normalized to a common base before the differential calculation. Let RTC_L and RTC_R be the current transformer ratios at the local and remote terminals, respectively. The primary currents can be obtained from the measured secondary currents as:

$$\bar{I}_{L,pri} = RTC_L \cdot \bar{I}_{L,sec}, \tag{3.7}$$

$$\bar{I}_{R,pri} = RTC_R \cdot \bar{I}_{R,sec}. \tag{3.8}$$

where $\bar{I}_{L,sec}$ and $\bar{I}_{R,sec}$ are the secondary currents, and $\bar{I}_{L,pri}$ and $\bar{I}_{R,pri}$ are the corresponding primary currents. After this conversion, both terminal currents can be expressed in the same base and used in (3.3) and (3.4).

3.5 SYMMETRICAL COMPONENTS AND SEQUENCE ELEMENTS

Unbalanced faults produce positive-, negative-, and zero-sequence components. These components are useful for protection because different fault types produce different sequence patterns. For example, single-line-to-ground faults involve positive-, negative-, and zero-sequence components, while three-phase faults are mainly associated with positive-sequence quantities.

The symmetrical component transformation is defined as:

$$\begin{bmatrix} \bar{I}_0 \\ \bar{I}_1 \\ \bar{I}_2 \end{bmatrix} = \frac{1}{3} \begin{bmatrix} 1 & 1 & 1 \\ 1 & a & a^2 \\ 1 & a^2 & a \end{bmatrix} \begin{bmatrix} \bar{I}_A \\ \bar{I}_B \\ \bar{I}_C \end{bmatrix}, \tag{3.9}$$

where $\bar{I}_0$ is the zero-sequence current, $\bar{I}_1$ is the positive-sequence current, $\bar{I}_2$ is the negative-sequence current, and:

$$a = 1\angle 120^\circ = e^{j\frac{2\pi}{3}}. \tag{3.10}$$

Line differential protection may use phase elements and sequence elements. The phase elements are usually identified as 87LA, 87LB, and 87LC. The negative-sequence element is identified as 87LQ, and the zero-sequence element is identified as 87LG. The sequence elements are particularly important for unbalanced faults, especially when the phase elements lose sensitivity due to high fault resistance, weak sources, or load current influence.

In systems connected to IBRs, the behavior of sequence components requires special attention. A Type IV wind turbine connected through a full converter may not inject negative-sequence current in the same way as a synchronous generator. The negative-sequence contribution may be limited or suppressed by the converter control. Therefore, the 87LQ element may present low sensitivity or unstable behavior if the IBR does not provide a significant negative-sequence current during faults.

The zero-sequence component also depends on transformer connection and grounding. In the system analyzed in this dissertation, the transformer is connected as delta–grounded-wye in the direction from the IBR to the remaining system. The IBR at the local terminal is connected to the delta side, while the protected transmission line is connected to the grounded-wye side. Therefore, during ground faults, zero-sequence current can circulate through the grounded-wye path and appear in the local-terminal measurements of the protected line. This behavior affects the phase currents used by the phase-segregated differential protection.

3.6 ZERO-SEQUENCE REMOVAL AT THE IBR-SIDE TERMINAL

The zero-sequence current measured at the local terminal during ground faults may not represent a native zero-sequence contribution from the Type IV wind turbine converter. Instead, it can be associated with the grounded-wye side of the delta–grounded-wye transformer that connects the IBR to the protected line. When this component is added equally to the three phase currents, the phase-segregated protection may incorrectly identify healthy phases as faulted.

To evaluate this effect, the zero-sequence component is removed from the phase currents measured at the local terminal before applying the phase differential protection. The zero-sequence removal is performed as:

$$\begin{bmatrix} \bar{I}'_A \\ \bar{I}'_B \\ \bar{I}'_C \end{bmatrix} = \frac{1}{3} \begin{bmatrix} 2 & -1 & -1 \\ -1 & 2 & -1 \\ -1 & -1 & 2 \end{bmatrix} \begin{bmatrix} \bar{I}_A \\ \bar{I}_B \\ \bar{I}_C \end{bmatrix}, \tag{3.11}$$

where $\bar{I}'_A$, $\bar{I}'_B$, and $\bar{I}'_C$ are the phase currents after zero-sequence removal. This operation is equivalent to:

$$\bar{I}'_\phi = \bar{I}_\phi - \bar{I}_0, \quad \phi \in \{A, B, C\}. \tag{3.12}$$

This procedure is applied only to the phase elements in order to improve phase selection. It does not eliminate the need for a zero-sequence element. The 87LG element can still be used to detect ground faults. The objective of (3.11) is to prevent the transformer-related zero-sequence component from contaminating the phase quantities used by 87LA, 87LB, and 87LC.

Figure 3.4 illustrates the physical origin of this current by showing the IBR, the grid-side transformer, its grounded-wye connection, the protected line, and the zero-sequence current path during a ground fault.

This explanation is important because removing zero-sequence current from only one ter-

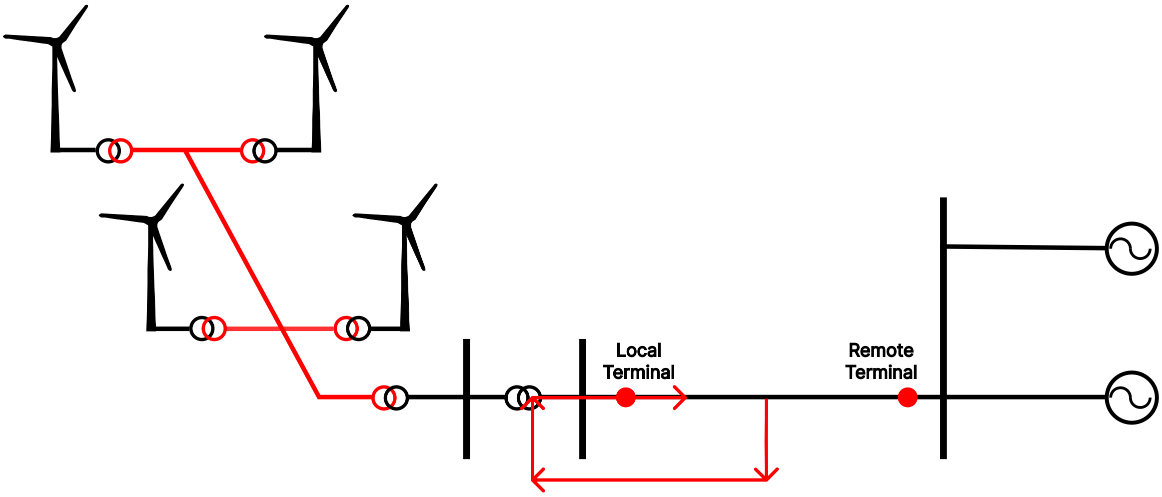

Figure 3.4. Zero-sequence current path associated with the grounded transformer at the local terminal.

minal could appear inconsistent with the differential principle if the origin of this current is not clarified. In this dissertation, the procedure is justified because the zero-sequence component observed at the local terminal is associated with the transformer grounding path and affects the phase identification performed by the local phase elements.

3.7 ALPHA-PLANE DIFFERENTIAL PROTECTION

The alpha plane is a complex plane used to represent the relationship between terminal currents in a line differential protection scheme. Instead of plotting the operating current against the restraint current, the alpha-plane method evaluates a complex ratio between the remote and local currents.

For a two-terminal line, the alpha-plane variable is defined as:

$$\Gamma_\alpha = \frac{\bar{I}_R}{\bar{I}_L} = \Gamma_{\alpha,re} + j\Gamma_{\alpha,im}, \tag{3.13}$$

where Γ_α is the alpha-plane complex variable, $\Gamma_{\alpha,re}$ is its real part, and $\Gamma_{\alpha,im}$ is its imaginary part. The currents $\bar{I}_L$ and $\bar{I}_R$ must be synchronized and expressed according to the same reference direction.

Under normal load condition or external faults, the currents at both terminals are approximately opposite because one current enters the line and the other leaves the line. Therefore:

$$\bar{I}_R \approx -\bar{I}_L \quad \Rightarrow \quad \Gamma_\alpha \approx -1 + j0. \tag{3.14}$$

Thus, the point $(-1, 0)$ in the alpha plane represents the expected region for normal operation and external faults. For internal faults, both terminals tend to feed the fault, and the current ratio moves away from the restraint region. Depending on the fault location, source strength, load current, and fault resistance, the trajectory may move toward different regions of the plane.

Figure 3.5 illustrates the typical regions of the alpha plane. The restraint region is located around the point $(-1, 0)$, where normal load and external faults are expected. The operation region is outside the restraint characteristic. Additional regions may be associated with internal faults involving outfeed, where the current at one terminal may continue to flow out of the protected zone due to high load or high fault resistance.

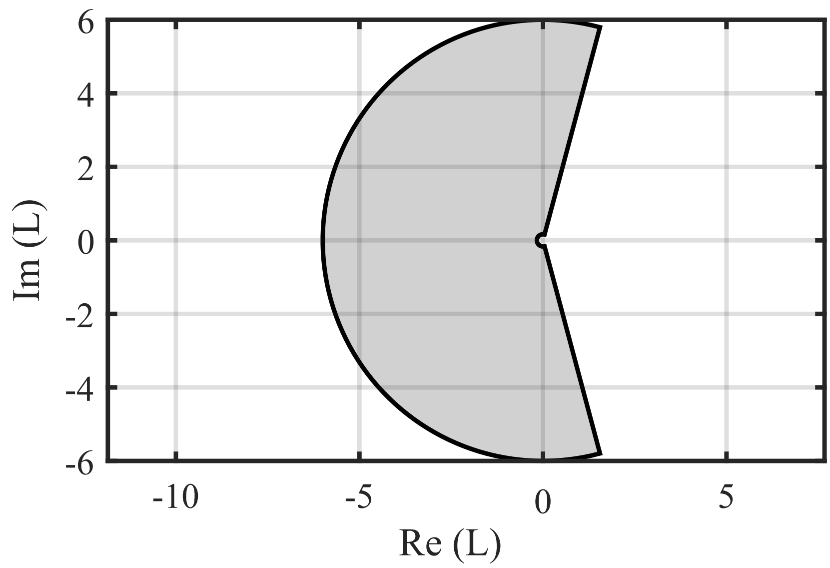

Figure 3.5. Typical regions of the alpha plane for line differential protection.

A simple circular restraint characteristic may be used around the point $(-1, 0)$. However, line differential protection often uses a modified or "rainbow" characteristic to improve the balance between sensitivity and security. This characteristic is defined by parameters such as external radius, internal radius, and angular opening. The objective is to restrain the relay for external faults, load flow, CT errors, and communication delays, while allowing operation for internal faults.

The trip decision can be written generically as:

$$\Gamma_\alpha \notin \mathcal{R}_\alpha \quad \Rightarrow \quad \text{TRIP}, \tag{3.15}$$

where $\mathcal{R}_\alpha$ represents the restraint region of the alpha-plane characteristic. If the point is inside the restraint region, the relay does not trip. If the point moves outside the restraint region and satisfies the additional security conditions, the relay issues a trip command.

3.8 PHASE AND SEQUENCE ELEMENTS IN THE ALPHA PLANE

The alpha-plane ratio can be calculated for phase currents and for sequence currents. The phase elements are:

$$\Gamma_{87LA} = \frac{\bar{I}_{A,R}}{\bar{I}_{A,L}}, \tag{3.16}$$

$$\Gamma_{87LB} = \frac{\bar{I}_{B,R}}{\bar{I}_{B,L}}, \tag{3.17}$$

$$\Gamma_{87LC} = \frac{\bar{I}_{C,R}}{\bar{I}_{C,L}}. \tag{3.18}$$

The negative-sequence and zero-sequence elements are:

$$\Gamma_{87LQ} = \frac{\bar{I}_{2,R}}{\bar{I}_{2,L}}, \tag{3.19}$$

$$\Gamma_{87LG} = \frac{\bar{I}_{0,R}}{\bar{I}_{0,L}}. \tag{3.20}$$

The phase elements are useful for identifying the faulted phases. The sequence elements improve sensitivity for unbalanced faults, especially when the phase elements are affected by load current, fault resistance, or weak source conditions. However, in IBR-connected systems, the negative-sequence current may be very low depending on the converter control. Therefore, the 87LQ response must be interpreted carefully. In the studied Type IV wind turbine model, the negative-sequence current contribution is limited, which can produce unstable trajectories in the negative-sequence alpha-plane element.

The zero-sequence element is relevant for ground faults. However, its behavior depends strongly on transformer grounding and zero-sequence current paths. For this reason, the interpretation of 87LG must be correlated with the system topology, especially the transformer connection at the local terminal.

3.9 CURRENT MAPPING STRATEGY

The Current Mapping Strategy is a formulation previously proposed in the literature to improve the performance of alpha-plane line differential protection. In this dissertation, the CMS is not presented as an original method proposed by the author. Instead, it is adopted from previous work and evaluated in a new application context: a transmission line connected to a Type IV wind turbine.

The CMS modifies the current representation before plotting the operating point in the alpha plane. Instead of using the direct ratio between local and remote currents, the method defines equivalent mapped currents. The objective is to obtain a more controlled trajectory in the alpha plane and to allow the adjustment of sensitivity and security through specific parameters.

Starting from the conventional differential current:

$$\bar{I}_{dif} = \bar{I}_L + \bar{I}_R = I_{dif,re} + jI_{dif,im}, \tag{3.21}$$

and the restraint current:

$$I_{res} = \left|\bar{I}_L\right| + \left|\bar{I}_R\right|, \tag{3.22}$$

the CMS defines two equivalent currents, $\bar{I}_M$ and $\bar{I}_N$, such that:

$$\bar{I}_{dif,eq} = \bar{I}_M + \bar{I}_N, \tag{3.23}$$

$$\bar{I}_{res,eq} = \eta_1 \bar{I}_M - \eta_2 \bar{I}_N, \tag{3.24}$$

where $\bar{I}_{dif,eq}$ and $\bar{I}_{res,eq}$ are the equivalent differential and restraint currents of the CMS, respectively, and η_1 and η_2 are adjustment factors.

The equivalence between the conventional currents and the mapped currents is obtained by imposing:

$$\bar{I}_{dif,eq} = \bar{I}_{dif}, \tag{3.25}$$

$$\bar{I}_{res,eq} = I_{res}. \tag{3.26}$$

Solving the resulting system, the mapped currents are obtained as:

$$\bar{I}_M = \frac{1}{\eta_1 + \eta_2} \left(\eta_2 \bar{I}_{dif} + I_{res} \right), \tag{3.27}$$

$$\bar{I}_N = \frac{1}{\eta_1 + \eta_2} \left(\eta_1 \bar{I}_{dif} - I_{res} \right). \tag{3.28}$$

Finally, the CMS alpha-plane variable is calculated as:

$$\Gamma_{CMS} = \frac{\bar{I}_M}{\bar{I}_N} = \Gamma_{CMS,re} + j\Gamma_{CMS,im}. \tag{3.29}$$

where $\Gamma_{CMS,re}$ and $\Gamma_{CMS,im}$ are the real and imaginary parts of the CMS operating point.

Figure 3.6 illustrates the CMS concept. The measured currents are first used to calculate $\bar{I}_{dif}$ and I_{res}. Then, the mapped currents $\bar{I}_M$ and $\bar{I}_N$ are obtained using (3.27) and (3.28). The ratio Γ_{CMS} is then plotted in the alpha plane.

3.10 FAULT SETTLEMENT REGION AND OPERATION CHARACTERISTIC

The CMS uses two important regions in the alpha plane: the Fault Settlement Region (FSR) and the Operation Characteristic (OC). The FSR represents the region where the mapped

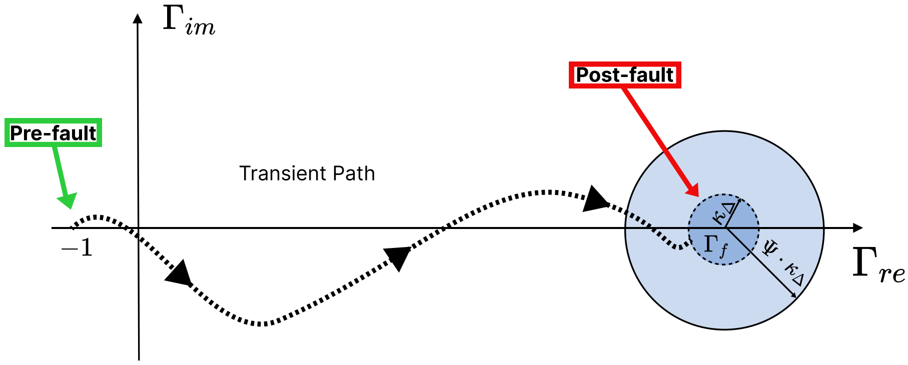

Figure 3.6. Current Mapping Strategy applied to line differential protection.

operating point is expected to settle during an internal fault. The OC is the tripping region associated with the CMS. Both regions can be adjusted according to the desired sensitivity and security.

The main CMS parameters are Γ_f, k_Δ, and Ψ. The parameter Γ_f is associated with the location of the fault settlement region in the alpha plane. The parameter k_Δ is associated with the distance or offset between the pre-fault point and the fault settlement region. The parameter Ψ is used to define the size of the operation characteristic. In general, larger operation regions tend to increase sensitivity and speed, while smaller regions tend to increase security.

In this dissertation, two CMS settings are evaluated. They are referred to as CMS-1 and CMS-2. The first setting is adjusted with emphasis on sensitivity, while the second setting is adjusted with emphasis on security. Table 3.1 presents the numerical values used in the simulations.

Table 3.1. CMS settings used in this dissertation.

Setting	Γ_f	k_Δ	Ψ	Main emphasis
CMS-1	10	0.2	25	Sensitivity
CMS-2	2	0.4	5	Security

3.11 APPLICATION TO LINES CONNECTED TO TYPE IV WIND TURBINES

The protection methods described in this chapter are applied in this dissertation to a transmission line connected to a Type IV wind turbine. This application differs from conventional line protection because the IBR-side current is controlled by the power electronic converter. During faults, the converter limits the current magnitude to protect its semiconductor devices and internal components. Therefore, the local current contribution may be much lower than that of a conventional synchronous generator.

This current limitation affects the alpha-plane trajectory. In a conventional system, the current contribution from both terminals is mostly determined by the equivalent source impedances and the fault location. In an IBR-connected system, the current contribution from the wind turbine side also depends on the converter control, current limiter, PLL dynamics, and the adopted active/reactive current priority. As a result, the operating point may not move as expected when using the conventional alpha-plane method.

The CMS is evaluated in this dissertation because it provides an alternative representation of the differential quantities. By mapping the original currents into $\bar{I}_M$ and $\bar{I}_N$, the CMS can improve the separation between faulted and non-faulted conditions in the alpha plane. This is particularly relevant when the IBR current is low, controlled, or affected by sequence-component behavior.

For ground faults, the zero-sequence component must also be considered. In the analyzed system, the delta–grounded-wye transformer provides a zero-sequence path through its grounded-wye connection. This zero-sequence current can affect the phase currents used by 87LA, 87LB, and 87LC. Therefore, the phase elements are evaluated both with and without zero-sequence removal at the local terminal. This comparison is necessary to determine whether the zero-sequence component causes incorrect phase identification.

The complete protection analysis in this dissertation follows the sequence:

1. Measure local and remote phase currents;
2. Estimate synchronized phasors;
3. Apply current normalization when required;
4. Calculate symmetrical components;
5. Remove the zero-sequence component from local-terminal phase currents for the selected cases;
6. Calculate alpha-plane phase and sequence quantities;

7. Calculate CMS-1 and CMS-2 quantities;

8. Compare the protection response for each fault type, resistance, and location.

This procedure allows the dissertation to correlate the converter-controlled current response with the behavior of the protection algorithms. The results must therefore be interpreted not only by observing whether the relay trips, but also by explaining why the trajectory moves in a certain direction, why some phases are identified, and how the sequence components influence the protection response.

3.12 CHAPTER SUMMARY

This chapter presented the theoretical basis of the protection methods used in this dissertation. The differential protection principle was introduced through the definition of operating and restraint currents. The main characteristics of line differential protection were then discussed, including communication, synchronization, and sequence components.

The alpha-plane method was presented as a complex-plane representation of the relationship between local and remote currents. In this representation, normal operation and external faults tend to remain close to the point $(-1, 0)$, while internal faults move the operating point toward the tripping region. Phase and sequence elements were also defined, including 87LA, 87LB, 87LC, 87LQ, and 87LG.

The Current Mapping Strategy was then introduced as a previously proposed method that maps the original differential quantities into equivalent currents. The CMS allows the definition of adjustable regions in the alpha plane and is evaluated in this dissertation as an alternative to improve the protection of lines connected to Type IV wind turbines.

Finally, the chapter explained why zero-sequence removal is evaluated at the local terminal. The procedure is justified by the grounded transformer connection, which can introduce a zero-sequence component into the phase currents and affect faulted-phase identification. This theoretical foundation supports the simulation analysis presented in the results chapter.

CHAPTER 4

TYPE IV WIND TURBINE MODEL

4.1 INTRODUCTION

This chapter presents the Type IV wind turbine model used in this dissertation. The objective is to describe the main components of the full-converter wind turbine and to explain how the electrical and control structures influence the current injected into the grid during faults. This description is important because the behavior of an inverter-based resource (IBR) during short-circuit conditions is not determined only by passive impedances, as in conventional synchronous machines. Instead, it depends on the converter topology, current controllers, phase-locked loop (PLL), DC-link dynamics, current limiters, and protection mechanisms associated with the semiconductor devices.

The wind turbine considered in this work follows the Type IV topology, also known as a full-converter wind turbine. In this configuration, the generator is fully decoupled from the grid through a back-to-back power electronic converter. The generator-side converter, also called machine-side converter (MSC), converts the variable-frequency AC voltage generated by the machine into DC voltage. The DC-link capacitor stores energy and provides the interface between the machine-side and grid-side converters. The grid-side converter (GSC) then converts the DC voltage into AC voltage synchronized with the grid. This structure allows the turbine to operate at variable speed while injecting controlled currents into the transmission system.

Figure 4.1 shows the general structure of the Type IV wind turbine model. The main components are the aerodynamic rotor, the permanent magnet synchronous machine, the machine-side converter, the DC-link, the chopper circuit, the grid-side converter, the output filter, the step-up transformer, and the grid.

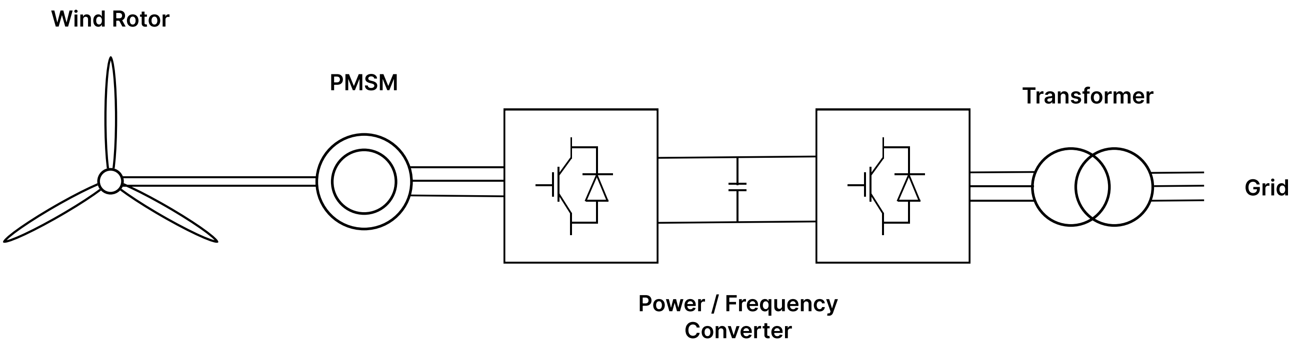

Figure 4.1. General configuration of the Type IV wind turbine model.

The Type IV topology was selected because all the electrical power transferred from the generator to the grid passes through the converter. Therefore, the grid-side current is mainly determined by the converter control strategy and by its current limitation. This characteristic is particularly relevant for protection studies, since the fault current contribution of the IBR can be significantly different from that of a synchronous generator. During faults, the converter may limit the current to protect its semiconductor devices, which affects the magnitude, phase angle, and sequence components observed by the differential protection.

4.2 MODEL ORIGIN AND IMPLEMENTATION SCOPE

The model used in this dissertation was developed from a combination of an existing EMTP-based Type IV wind turbine model and modifications implemented for this work. The DC-AC side of the model was based on an existing implementation, while the AC-DC side and part of the control adaptation were implemented and modified during the development of this dissertation. This distinction is important because the objective of the chapter is not only to present the final model, but also to identify the parts of the implementation that were adapted or developed by the author.

In this dissertation, the model is used as a reportable electromagnetic transient representation of a Type IV wind turbine connected to a transmission system. The focus is not the aerodynamic performance of the turbine, but the electrical response of the converter-interfaced source during line faults. Therefore, the wind speed and pitch angle are kept constant in the analyzed cases. This assumption is adopted because the objective of the simulations is to evaluate the interaction between the IBR current injection and the differential protection algorithms, not to study the influence of wind variability on mechanical power extraction.

The model is represented as a grid-following IBR. In this type of control, the grid-side converter synchronizes its injected current with the grid voltage through a PLL. Therefore, the converter follows the voltage angle imposed by the grid instead of establishing the grid voltage and frequency. This is different from grid-forming control, in which the converter behaves as a controlled voltage source and actively establishes voltage magnitude and frequency. Since the analyzed model is grid-following, its behavior during voltage sags and faults is strongly influenced by PLL dynamics and current limitation.

4.3 AERODYNAMIC POWER MODEL

The mechanical power extracted from the wind is defined by:

$$P_w = \frac{1}{2}\rho A v_w^3 C_p(\lambda, \beta), \tag{4.1}$$

where P_w is the mechanical power available at the turbine shaft, ρ is the air density, A is the swept area of the rotor blades, v_w is the wind speed, and C_p is the power coefficient. The swept area is given by:

$$A = \pi R_{blade}^2, \tag{4.2}$$

where R_{blade} is the rotor blade radius. The air density is commonly assumed as:

$$\rho = 1.225 \text{ kg/m}^3, \tag{4.3}$$

for standard atmospheric conditions. If a different value is adopted in the EMTP model, it must be explicitly reported in the parameter table.

The tip-speed ratio is defined as:

$$\lambda = \frac{\omega_m R_{blade}}{v_w}, \tag{4.4}$$

where λ is the tip-speed ratio and ω_m is the mechanical angular speed of the rotor.

The auxiliary variable λ' used in the C_p formulation is defined as:

$$\lambda' = \frac{1}{\lambda + 0.08\beta} - \frac{0.035}{\beta^3 + 1}, \tag{4.5}$$

where β is the pitch angle of the blades. In this formulation, λ' is not a second tip-speed ratio. It is an auxiliary variable used to calculate the power coefficient.

The power coefficient used in the model is expressed as:

$$C_p = c_1 \left(c_2\lambda' - c_3\beta - c_4\beta^{\chi} - c_5\right) e^{-c_6\lambda'} + c_7. \tag{4.6}$$

The coefficients adopted in the implemented model are summarized in Table 4.1. These constants are explicitly presented because they define the aerodynamic characteristic used by the turbine model.

Table 4.1. Power coefficient parameters used in the wind turbine model.

Parameter	Value	Description
c_1	0.5	Power coefficient scale factor
c_2	116	Tip-speed coefficient
c_3	0.4	Pitch angle coefficient
c_4	0	Additional pitch coefficient
c_5	5	Constant term
c_6	21	Exponential coefficient
c_7	0	Additional correction term
χ	1	Pitch exponent used in the implemented expression

Figure 4.2 shows the response of C_p as a function of the tip-speed ratio. According to the curve used in the model, the maximum power coefficient is approximately $C_{p,max} = 0.49$ for a nominal tip-speed ratio close to $\lambda_{nom} = 8.18$. Therefore, the maximum power point tracking strategy is designed to keep the operating point of the turbine close to this region.

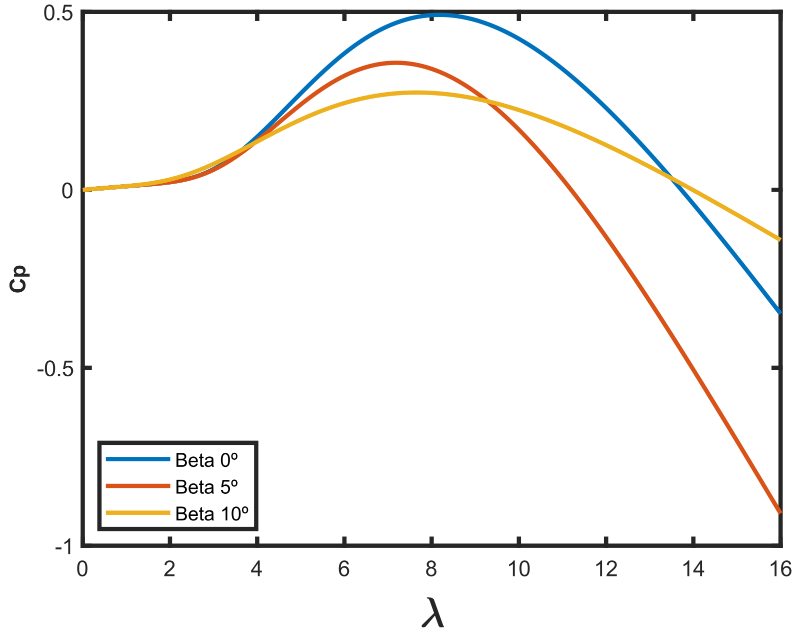

Figure 4.2. Power coefficient curve used in the Type IV wind turbine model.

The mechanical torque applied to the generator shaft is calculated as:

$$T_m = \frac{P_w}{\omega_m}, \tag{4.7}$$

where T_m is the mechanical torque. In practical simulations, a minimum value of ω_m must be considered to avoid numerical division problems when the rotor speed is close to zero.

4.4 MAXIMUM POWER POINT TRACKING

The objective of the maximum power point tracking (MPPT) algorithm is to extract the maximum available wind power for a given wind speed. Since the maximum value of C_p occurs near $\lambda_{nom} = 8.18$, the turbine control seeks to maintain the rotor speed compatible with this optimal tip-speed ratio.

For constant wind speed and constant pitch angle, the optimal mechanical power can be expressed as a function of the rotor speed:

$$P_{opt} = K_{opt}\omega_m^3, \tag{4.8}$$

where K_{opt} is a constant obtained from the turbine aerodynamic parameters. The corresponding optimal torque is:

$$T_{opt} = K_T \omega_m^2, \quad (4.9)$$

where K_T is the optimal torque coefficient. In a PMSG-based Type IV turbine, the electromagnetic torque is mainly controlled through the q-axis current of the machine-side converter. Therefore, the MPPT block produces a current reference proportional to the optimal torque:

$$i_{q,MSC}^{*} = \text{sat}\left(K_{MPPT}\omega_m^2\right), \quad (4.10)$$

where $i_{q,MSC}^{*}$ is the q-axis current reference for the machine-side converter, K_{MPPT} is the MPPT gain, and sat(·) represents the saturation block used to keep the reference within admissible limits.

In the implemented model, the wind speed and pitch angle are not varied. Therefore, the MPPT block does not aim to evaluate wind variability, but to provide a consistent torque/current reference for the generator-side control. This assumption is adequate for this dissertation because the main focus is the protection response during electrical faults.

Figure 4.3 shows the MPPT characteristic used in the model.

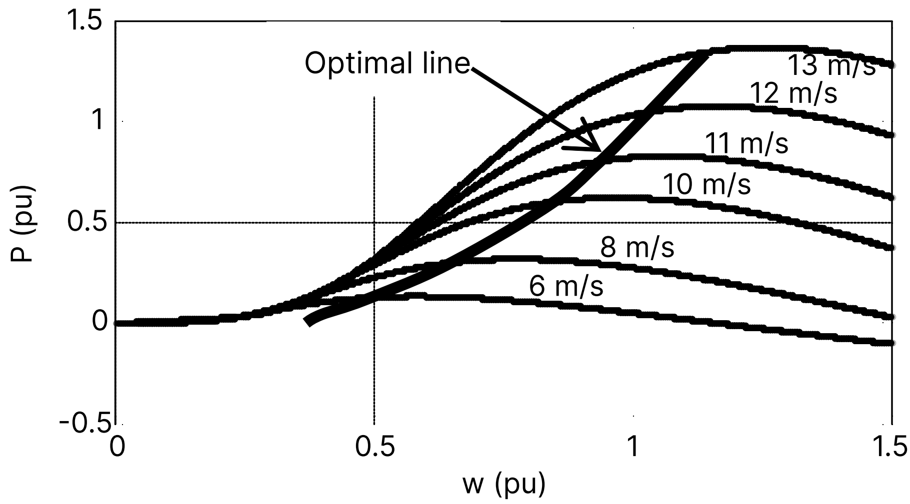

Figure 4.3. MPPT characteristic used to generate the machine-side current reference.

Figure 4.4 shows the MPPT circuit implemented in the model.

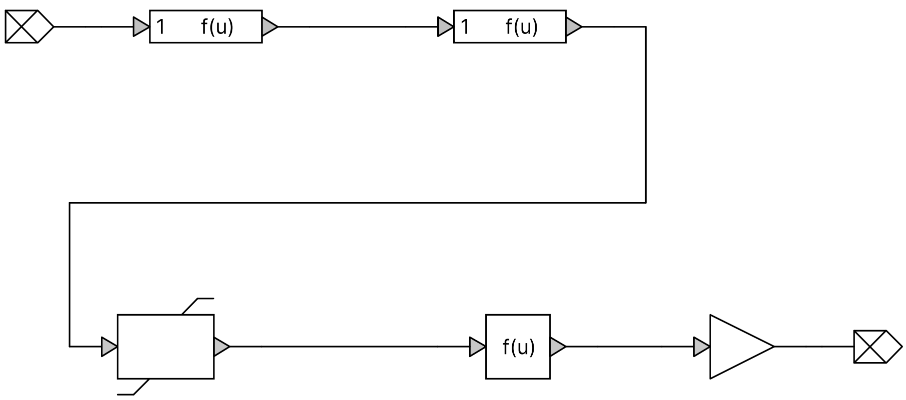

Figure 4.4. MPPT implementation used in the Type IV wind turbine model.

4.5 PERMANENT MAGNET SYNCHRONOUS GENERATOR

The generator used in the Type IV wind turbine model is represented as a permanent magnet synchronous machine. In this type of machine, the rotor magnetic field is produced by permanent magnets, while the stator contains three-phase windings. As the rotor rotates, a sinusoidal magnetic flux is produced and a three-phase AC voltage is induced in the stator windings. The frequency and amplitude of the generated voltage are proportional to the rotor speed.

In the synchronous dq reference frame, the PMSG can be represented by:

$$v_d = R_s i_d + L_d \frac{di_d}{dt} - \omega_e L_q i_q, \tag{4.11}$$

$$v_q = R_s i_q + L_q \frac{di_q}{dt} + \omega_e L_d i_d + \omega_e \psi_f, \tag{4.12}$$

where v_d and v_q are the stator voltage components, i_d and i_q are the stator current components, R_s is the stator resistance, L_d and L_q are the direct- and quadrature-axis inductances, ω_e is the electrical angular speed, and ψ_f is the permanent magnet flux linkage.

The electromagnetic torque is:

$$T_e = \frac{3}{2} p \left[\psi_f i_q + \left(L_d - L_q\right) i_d i_q\right], \tag{4.13}$$

where p is the number of pole pairs. If a surface-mounted PMSG is considered, $L_d \approx L_q$

and the reluctance torque term becomes small. In this case, the torque is mainly controlled by the q-axis current.

The mechanical dynamics are given by:

$$J\frac{d\omega_m}{dt} = T_m - T_e - B\omega_m, \tag{4.14}$$

where J is the equivalent inertia and B is the viscous friction coefficient. In this dissertation, the mechanical dynamics are kept approximately constant during the analyzed fault windows because the protection response occurs in a short time interval compared with the mechanical dynamics of the turbine.

4.6 MACHINE-SIDE CONVERTER

The machine-side converter is responsible for controlling the generator current and extracting power from the wind turbine according to the MPPT strategy. It is implemented as a three-phase IGBT bridge connected to the generator terminals, as shown in Figure 4.5.

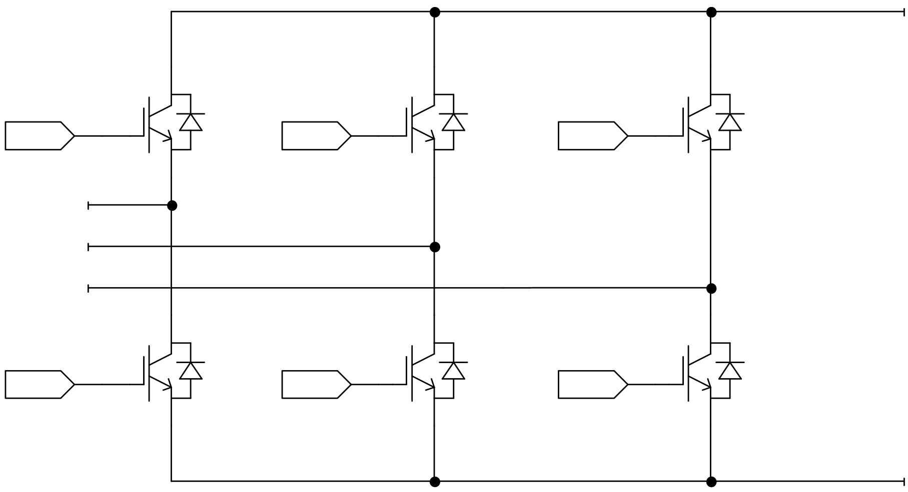

Figure 4.5. Machine-side AC-DC converter implemented with IGBTs.

The converter is controlled in the dq reference frame. Therefore, the three-phase generator currents are transformed from the abc frame to the rotating $dq0$ frame. This transformation reduces the complexity of the control problem because sinusoidal quantities in the three-phase frame become approximately constant quantities in the synchronous reference frame.

For a generic three-phase variable x, the Park transformation is:

$$\begin{bmatrix} x_d \\ x_q \\ x_0 \end{bmatrix} = \frac{2}{3} \begin{bmatrix} \cos(\theta) & \cos\left(\theta - \frac{2\pi}{3}\right) & \cos\left(\theta + \frac{2\pi}{3}\right) \\ -\sin(\theta) & -\sin\left(\theta - \frac{2\pi}{3}\right) & -\sin\left(\theta + \frac{2\pi}{3}\right) \\ \frac{1}{2} & \frac{1}{2} & \frac{1}{2} \end{bmatrix} \begin{bmatrix} x_a \\ x_b \\ x_c \end{bmatrix}. \tag{4.15}$$

The inverse transformation is:

$$\begin{bmatrix} x_a \\ x_b \\ x_c \end{bmatrix} = \begin{bmatrix} \cos(\theta) & -\sin(\theta) & 1 \\ \cos\left(\theta - \frac{2\pi}{3}\right) & -\sin\left(\theta - \frac{2\pi}{3}\right) & 1 \\ \cos\left(\theta + \frac{2\pi}{3}\right) & -\sin\left(\theta + \frac{2\pi}{3}\right) & 1 \end{bmatrix} \begin{bmatrix} x_d \\ x_q \\ x_0 \end{bmatrix}. \tag{4.16}$$

Figure 4.6 shows the transformation block used in the machine-side converter control.

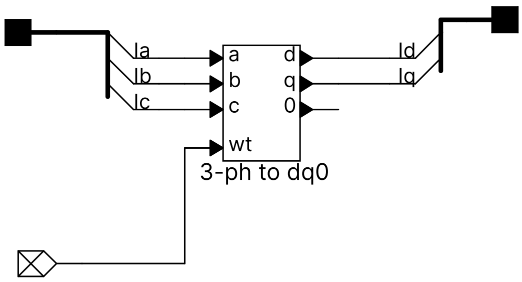

Figure 4.6. ABC to DQ0 transformation block used in the machine-side converter.

The detailed transformation circuit is shown in Figure 4.7.

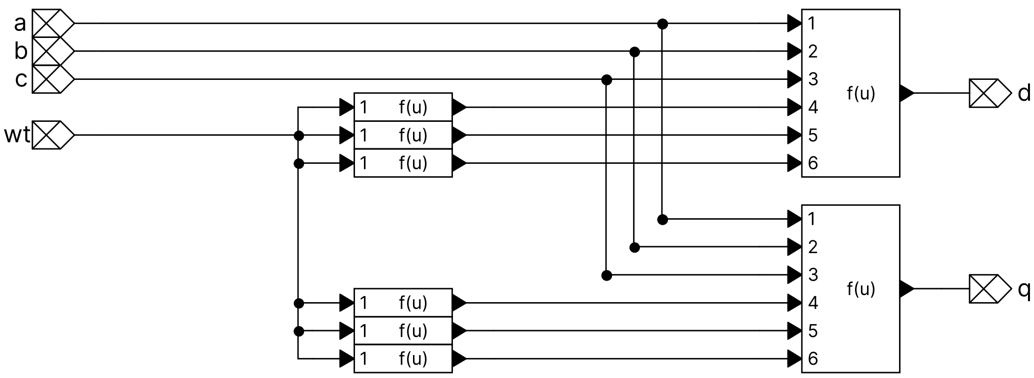

Figure 4.7. Detailed implementation of the ABC to DQ0 transformation.

4.6.1 Machine-Side Inner Current Control

The machine-side converter uses inner current control loops to regulate the d- and q-axis currents. The d-axis current is commonly controlled to a value close to zero in PMSG applications, while the q-axis current is associated with electromagnetic torque and active power extraction.

The current errors are defined as:

$$e_{d,MSC} = i^*_{d,MSC} - i_{d,MSC}, \tag{4.17}$$

$$e_{q,MSC} = i^*_{q,MSC} - i_{q,MSC}. \tag{4.18}$$

The PI controllers are:

$$u_{d,MSC} = K_{p,MSC} e_{d,MSC} + K_{i,MSC} \int e_{d,MSC} dt, \tag{4.19}$$

$$u_{q,MSC} = K_{p,MSC} e_{q,MSC} + K_{i,MSC} \int e_{q,MSC} dt. \tag{4.20}$$

The values adopted in the implemented model are:

$$K_{p,MSC} = 0.3496, \qquad K_{i,MSC} = 0.439. \tag{4.21}$$

The implemented d-axis voltage reference also includes coupling and resistive terms. In the model, these terms are represented by constants associated with the rotor speed and the measured currents:

$$v^*_{d,MSC} = u_{d,MSC} - k_{\omega,MSC} \omega_m i_{q,MSC} - k_{R,MSC} i_{d,MSC}, \tag{4.22}$$

where the implemented constants are:

$$k_{\omega,MSC} = 0.6, \qquad k_{R,MSC} = 0.002. \tag{4.23}$$

The q-axis reference follows an analogous control structure, using the q-axis current reference generated by the MPPT block. The output of the d- and q-axis current controllers is transformed back to the *abc* frame and used to generate the PWM pulses for the IGBTs of the machine-side converter.

Figure 4.8 shows the implemented inner control loop for the d-axis current.

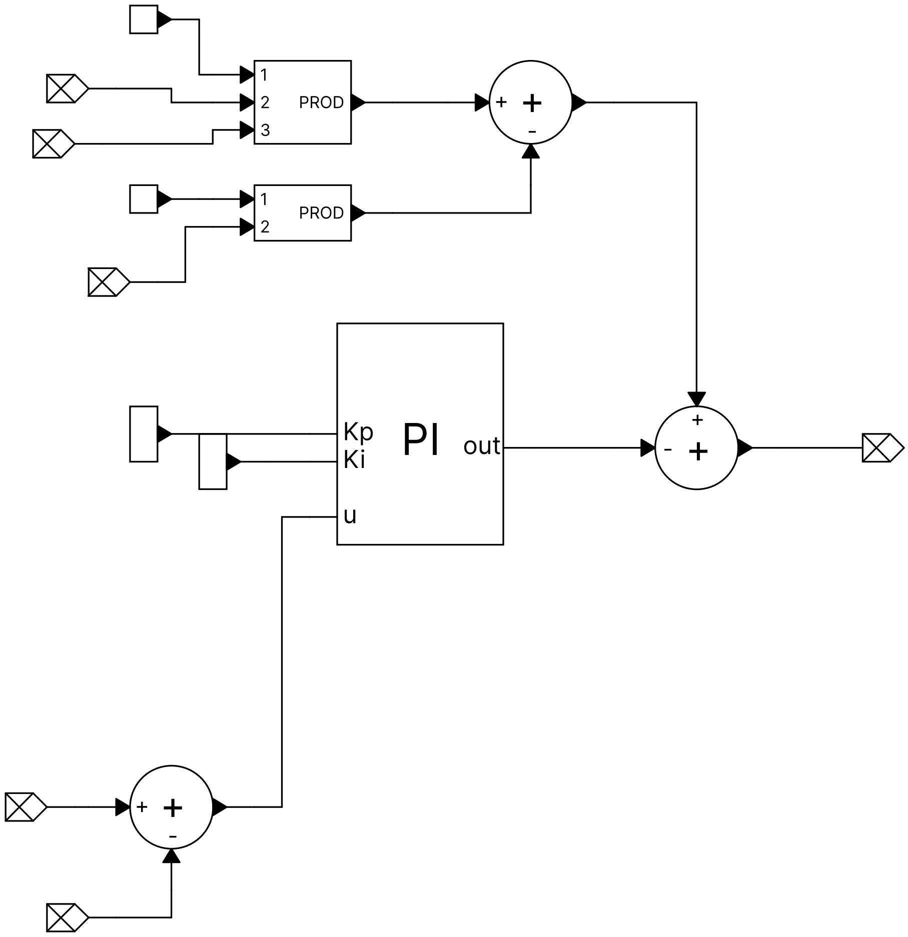

Figure 4.8. Machine-side inner control loop for the *d*-axis current.

4.7 DC-LINK AND CHOPPER CIRCUIT

The DC-link connects the machine-side converter to the grid-side converter. It is represented by a capacitor that smooths the DC voltage and temporarily stores energy. The DC-link voltage is one of the most important internal variables of the Type IV wind turbine because it reflects the power balance between the generator-side and grid-side converters.

The energy stored in the DC-link capacitor is:

$$E_{dc} = \frac{1}{2} C_{dc} V_{dc}^2, \tag{4.24}$$

where C_{dc} is the DC-link capacitance and V_{dc} is the DC-link voltage. The DC-link dynamic behavior can be represented by:

$$C_{dc}V_{dc}\frac{dV_{dc}}{dt} = P_{MSC} - P_{GSC} - P_{ch}, \tag{4.25}$$

where P_{MSC} is the power received from the machine-side converter, P_{GSC} is the power delivered to the grid-side converter, and P_{ch} is the power dissipated in the chopper resistor.

During faults, the grid voltage may decrease. When this occurs, the grid-side converter may not be able to transfer the same amount of active power to the grid. If the machine-side converter continues to inject power into the DC-link, V_{dc} may increase. To prevent overvoltage, the chopper circuit is activated.

The chopper circuit consists of an IGBT and a resistor connected to the DC-link, as shown in Figure 4.9. When V_{dc} exceeds an upper threshold, the chopper switch is activated and part of the energy is dissipated in the resistor. This protects the DC-link capacitor and the semiconductor devices.

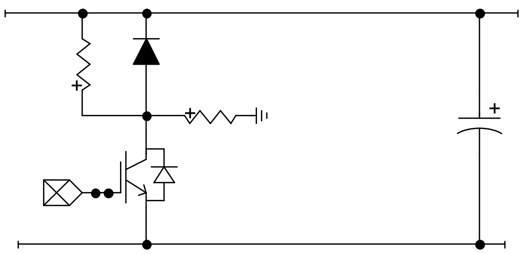

Figure 4.9. Chopper circuit connected to the DC-link capacitor.

The chopper logic can be represented as:

$$S_{ch} = \begin{cases} 1, & V_{dc} \geq V_{dc,max}, \\ 0, & V_{dc} \leq V_{dc,min}, \end{cases} \tag{4.26}$$

where S_{ch} is the chopper switching signal, $V_{dc,max}$ is the upper activation threshold, and $V_{dc,min}$ is the lower deactivation threshold. The use of two thresholds creates a hysteresis band and avoids excessive switching.

The dissipated power is:

$$P_{ch} = S_{ch}\frac{V_{dc}^2}{R_{ch}}, \tag{4.27}$$

where R_{ch} is the chopper resistance.

Figure 4.10 shows the chopper function implemented in the model.

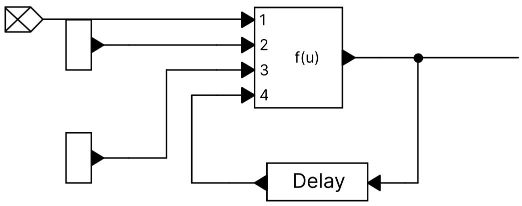

Figure 4.10. Chopper activation logic used in the DC-link protection.

4.8 GRID-SIDE CONVERTER

The grid-side converter converts the DC-link voltage into AC voltage synchronized with the grid. It is implemented as a three-phase IGBT bridge, as shown in Figure 4.11. Its main functions are to regulate the DC-link voltage, control the active and reactive current injected into the grid, and maintain the converter current within safe limits.

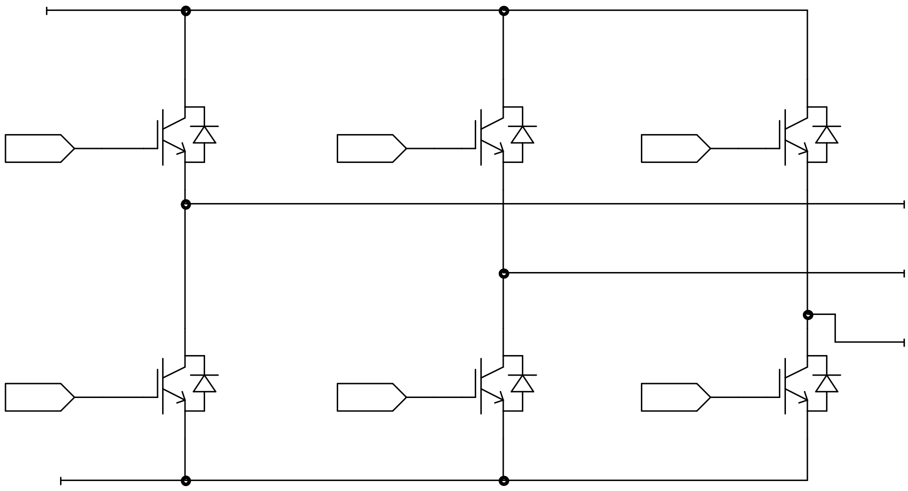

Figure 4.11. Grid-side DC-AC converter implemented with IGBTs.

The grid-side converter is controlled in a synchronous reference frame aligned with the grid voltage. In this structure, the PLL estimates the grid voltage angle θ_{PLL}. This angle is then used to transform the grid voltages and currents from the *abc* frame to the $dq0$ frame.

The instantaneous active and reactive powers in the dq frame are:

$$P = \frac{3}{2}\left(v_d i_d + v_q i_q\right), \tag{4.28}$$

$$Q = \frac{3}{2}\left(v_q i_d - v_d i_q\right), \tag{4.29}$$

where P is the active power, Q is the reactive power, v_d and v_q are the grid voltage components, and i_d and i_q are the grid current components.

When the PLL aligns the d-axis with the grid voltage vector, $v_q \approx 0$. In this condition:

$$P \approx \frac{3}{2} v_d i_d, \tag{4.30}$$

Therefore, the d-axis current mainly controls active power and DC-link voltage, while the q-axis current mainly controls reactive power. The sign of Q may change depending on the adopted convention for current direction and Park transformation.

4.9 PHASE-LOCKED LOOP

The PLL is a fundamental component of the grid-following converter. Its function is to estimate the phase angle and frequency of the grid voltage. This angle is used in the Park transformations and therefore directly affects the control of active and reactive currents.

In the implemented model, the PLL receives the three-phase grid voltages v_a, v_b, and v_c. These voltages are transformed to the $dq0$ frame using the estimated angle θ_{PLL}. The objective of the PLL is to force the q-axis voltage component to zero. When this condition is satisfied, the d-axis is aligned with the grid voltage vector.

The transformation used by the PLL is:

$$\begin{bmatrix} v_{d,PLL} \\ v_{q,PLL} \\ v_{0,PLL} \end{bmatrix} = T_{dq0}(\theta_{PLL}) \begin{bmatrix} v_a \\ v_b \\ v_c \end{bmatrix}, \tag{4.31}$$

where $T_{dq0}(\theta_{PLL})$ is the Park transformation matrix evaluated with the estimated PLL angle.

The PLL error is defined as:

$$e_{PLL} = v^*_{q,PLL} - v_{q,PLL}. \tag{4.32}$$

For voltage-vector alignment, the reference is:

$$v^*_{q,PLL} = 0. \tag{4.33}$$

Thus:

$$e_{PLL} = -v_{q,PLL}. \tag{4.34}$$

The PLL frequency is generated by a PI controller:

$$\Delta\omega_{PLL} = K_{p,PLL} e_{PLL} + K_{i,PLL} \int e_{PLL} dt, \tag{4.35}$$

$$\omega_{PLL} = \omega_0 + \Delta\omega_{PLL}, \tag{4.36}$$

where ω_0 is the nominal angular frequency of the grid. For a 60 Hz system:

$$\omega_0 = 2\pi 60 \text{ rad/s}. \tag{4.37}$$

The estimated angle is then obtained by integration:

$$\theta_{PLL} = \int \omega_{PLL} dt. \tag{4.38}$$

At steady state, the PLL reaches:

$$v_{q,PLL} \approx 0, \qquad v_{d,PLL} \approx |V|, \tag{4.39}$$

where $|V|$ is the magnitude of the positive-sequence grid voltage vector.

The PLL is particularly important during faults. When a voltage sag or an unbalanced fault occurs, the measured grid voltage can contain negative-sequence components, oscillations, and transient distortions. A conventional synchronous reference frame PLL may then experience oscillations in the estimated angle. Since this angle is used in the current controllers, the PLL response can influence the current injected by the IBR during the fault. Therefore, the PLL is one of the reasons why the fault response of a Type IV wind turbine differs from the response of a synchronous generator.

4.10 GRID-SIDE OUTER CONTROL LOOPS

The grid-side converter uses outer control loops to generate the current references for the inner current controllers. The first outer loop regulates the DC-link voltage. The second loop controls reactive power or AC voltage support, depending on the selected control mode.

The DC-link voltage error is:

$$e_{Vdc} = V_{dc}^{*} - V_{dc}, \tag{4.40}$$

where V_{dc}^{*} is the DC-link voltage reference. The d-axis current reference is obtained through a PI controller:

$$i_{d,GSC}^{*} = K_{p,Vdc} e_{Vdc} + K_{i,Vdc} \int e_{Vdc} dt. \tag{4.41}$$

The implemented gains are:

$$K_{p,Vdc} = 1.2, \qquad K_{i,Vdc} = 24.4. \tag{4.42}$$

Figure 4.12 shows the outer DC-link voltage control loop.

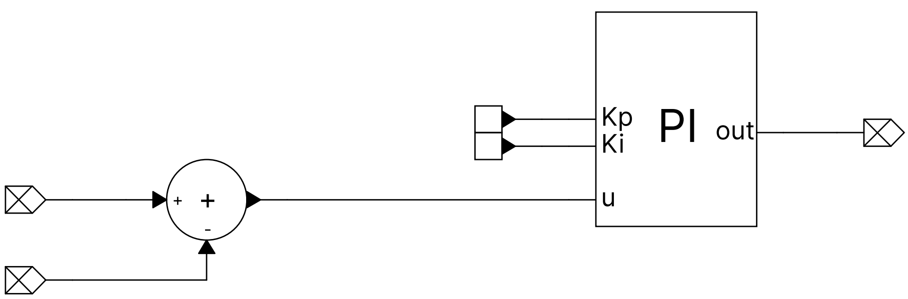

Figure 4.12. Outer DC-link voltage control loop of the grid-side converter.

The reactive power control loop compares the measured reactive power with a reference value:

$$e_Q = Q^* - Q. \tag{4.43}$$

The q-axis current reference is then generated as:

$$i^*_{q,GSC} = K_{p,Q} e_Q + K_{i,Q} \int e_Q dt. \tag{4.44}$$

where $K_{p,Q}$ and $K_{i,Q}$ are the proportional and integral gains of the reactive power controller. In the implemented model, the reactive current reference follows the adopted reactive power control structure, while the current magnitude is limited by the grid-side converter current limiter described in the next section.

4.11 CURRENT LIMITER

The converter current must be limited to protect the IGBTs and other power electronic components. This is a fundamental difference between Type IV wind turbines and synchronous generators. While synchronous generators can inject high short-circuit currents for a short time, converter-based sources are constrained by the maximum admissible current of their semiconductor devices.

The current magnitude reference is:

$$I_{ref} = \sqrt{\left(i^*_{d,GSC}\right)^2 + \left(i^*_{q,GSC}\right)^2}. \tag{4.45}$$

The current limiter imposes:

$$I_{ref} \le I_{max}. \tag{4.46}$$

If the calculated current reference exceeds I_{max}, the controller scales the references according to:

$$i^*_{d,GSC,lim} = i^*_{d,GSC} \frac{I_{max}}{I_{ref}}, \tag{4.47}$$

$$i^*_{q,GSC,lim} = i^*_{q,GSC}\frac{I_{max}}{I_{ref}}. \tag{4.48}$$

The exact priority between active and reactive current depends on the implemented control strategy. Some grid codes require reactive current priority during voltage sags, while other implementations may prioritize active current or apply proportional limiting. In this dissertation, the current limiter is important because it explains why the IBR does not inject a high short-circuit current during line faults.

4.12 GRID-SIDE INNER CURRENT CONTROL

After the current references are generated by the outer loops and limited by the current limiter, the grid-side converter applies inner current control in the synchronous reference frame.

The current errors are:

$$e_{d,GSC} = i^*_{d,GSC} - i_{d,GSC}, \tag{4.49}$$

$$e_{q,GSC} = i^*_{q,GSC} - i_{q,GSC}. \tag{4.50}$$

The PI controllers generate the control signals:

$$u_{d,GSC} = K_{p,GSC}e_{d,GSC} + K_{i,GSC}\int e_{d,GSC}dt, \tag{4.51}$$

$$u_{q,GSC} = K_{p,GSC}e_{q,GSC} + K_{i,GSC}\int e_{q,GSC}dt. \tag{4.52}$$

The implemented gains are:

$$K_{p,GSC} = 0.286, \qquad K_{i,GSC} = 11.333. \tag{4.53}$$

The voltage references are calculated with decoupling terms:

$$v^*_{d,GSC} = v_d + u_{d,GSC} - \omega_{PLL} L_f i_{q,GSC} + R_f i_{d,GSC}, \tag{4.54}$$

$$v^*_{q,GSC} = v_q + u_{q,GSC} + \omega_{PLL} L_f i_{d,GSC} + R_f i_{q,GSC}, \tag{4.55}$$

where R_f and L_f are the filter resistance and inductance between the converter and the grid. The signs of the decoupling terms may vary depending on the current direction convention and the Park transformation adopted in the model. The signs of these terms are kept consistent with the current direction convention and the Park transformation adopted in the implemented EMTP model.

The voltage references are transformed back to the *abc* frame and applied to the PWM block, which generates the IGBT gate pulses.

Figure 4.13 shows the implemented grid-side inner current control loop.

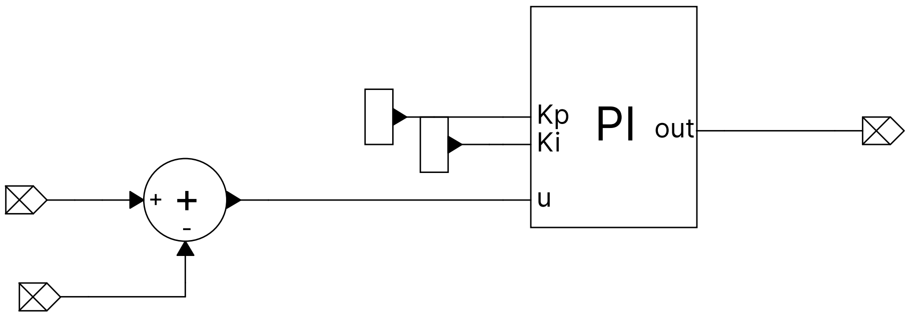

Figure 4.13. Grid-side inner current control loops for the *d*- and *q*-axis components.

The complete outer and inner current control structure is shown in Figure 4.14.

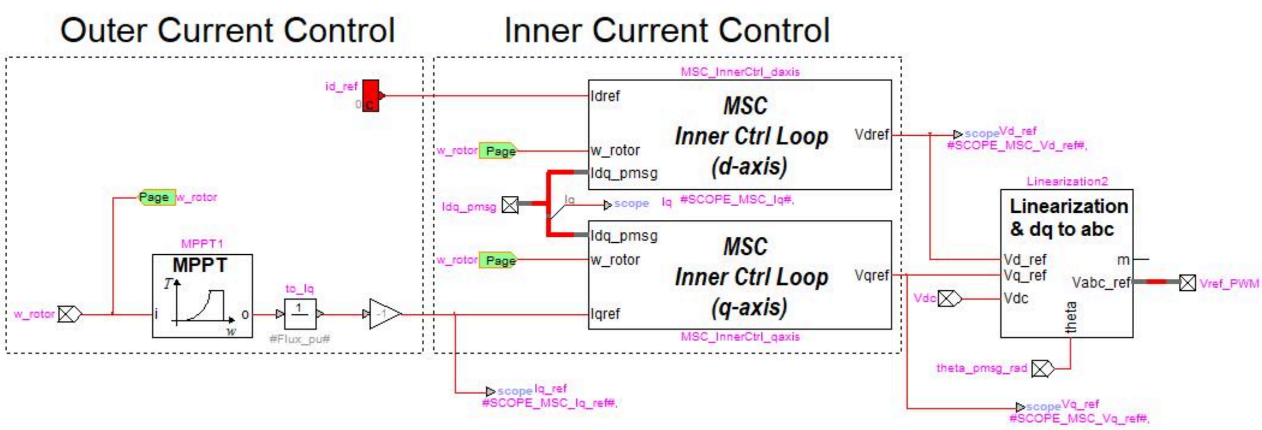

Figure 4.14. Complete outer and inner current control block of the grid-side converter.

4.13 PWM AND IGBT SWITCHING

The voltage references generated by the current controllers are converted into gate signals for the IGBTs. The PWM block compares the voltage reference signals with a high-frequency carrier waveform and generates the switching pulses for each converter leg.

For a two-level voltage source converter, each phase leg contains two IGBTs. Therefore, the three-phase bridge uses six IGBTs. The upper and lower switches of each leg must operate complementarily to avoid short-circuiting the DC-link. In practical converters, dead time is inserted between the switching commands to prevent simultaneous conduction of both devices in the same leg.

The converter output voltage is determined by the switching states and by the DC-link voltage. Therefore, the DC-link voltage dynamics and the PWM pulses are directly connected. During faults, when the current limiter and the chopper act, the voltage references and switching behavior are modified to protect the converter.

4.14 FILTER, TRANSFORMER, AND GRID CONNECTION

The grid-side converter is connected to the grid through an output filter and a step-up transformer. The filter reduces the high-frequency components produced by PWM switching and improves the quality of the injected current. Depending on the model, the filter may be represented as an L filter or an LCL filter. The filter parameters adopted in the implemented EMTP model are listed in Table 4.2.

The transformer provides voltage adaptation between the converter level and the transmission system. It also affects the zero-sequence network. This aspect is particularly important for the protection analysis developed in this dissertation. If the transformer has a grounded-wye connection on one side, zero-sequence currents can circulate during ground faults. Therefore, the transformer connection must be explicitly reported.

In the analyzed system, the transformer is connected as delta–grounded-wye in the direction from the IBR to the remaining system. The Type IV wind turbine and the grid-side converter are connected to the delta side, which blocks a native zero-sequence contribution from the converter side. The protected transmission line and the line differential protection terminals are connected on the grounded-wye side. Therefore, during ground faults on the protected line, the grounded-wye side provides a zero-sequence current path that can appear in the local-terminal phase currents used by the differential protection algorithm.

4.15 MODEL BEHAVIOR DURING FAULTS

During normal operation, the Type IV wind turbine injects controlled active and reactive currents into the grid. The active current is mainly associated with DC-link voltage regulation, while the reactive current is associated with the reactive power reference or voltage support. The PLL synchronizes the current injection with the grid voltage.

During faults, the voltage at the point of common coupling can decrease. The grid-side converter reacts by modifying its current references. However, the total current cannot exceed the converter current limit. Therefore, the IBR does not behave as a conventional synchronous generator. Its fault current is limited and controlled.

This behavior affects the differential protection analysis in three main ways. First, the magnitude of the current injected by the IBR can be much lower than the current injected by a conventional source. Second, in the analyzed cases, the positive-sequence current at the IBR-side terminal remains close to 1 pu in the post-fault interval, while the converter current remains limited by the control and protection loops. Third, the negative-sequence current may be low or absent if the converter does not intentionally inject negative-sequence current. These characteristics explain why the protection response must be analyzed carefully.

In ground faults, the delta–grounded-wye transformer connection can introduce zero-sequence current paths on the grounded-wye side of the protected line. The zero-sequence component measured at the IBR-side terminal may therefore be associated with the transformer grounding instead of being a native contribution from the converter. This is one of the reasons why this dissertation evaluates the removal of the zero-sequence component from the IBR-side phase currents before applying the phase-segregated differential protection.

4.16 MODEL PARAMETERS

Table 4.2 summarizes the main parameters adopted for the Type IV wind turbine model. The mechanical and converter parameters that were not explicitly available in the original description were assumed as representative values for a full-converter wind turbine model and kept constant in all simulated cases.

Table 4.2. Main parameters of the Type IV wind turbine model.

Parameter	Value	Description
ρ	1.225 kg/m^3	Air density
$C_{p,max}$	0.49	Maximum power coefficient
λ_{nom}	8.18	Nominal tip-speed ratio
R_{blade}	40 m	Rotor blade radius
v_w	12 m/s	Wind speed used in the simulations
β	0°	Pitch angle used in the simulations
C_{dc}	0.01 F	DC-link capacitance
V_{dc}^*	1.0 pu	DC-link voltage reference
$V_{dc,max}$	1.10 pu	Chopper activation threshold
$V_{dc,min}$	1.05 pu	Chopper deactivation threshold
R_{ch}	10 Ω	Chopper resistance
I_{max}	1.2 pu	Converter current limit
R_f	0.01 pu	Filter resistance
L_f	0.15 pu	Filter inductance
$K_{p,MSC}$	0.3496	Machine-side current PI proportional gain
$K_{i,MSC}$	0.439	Machine-side current PI integral gain
$K_{\omega,MSC}$	0.6	Machine-side coupling constant
$K_{R,MSC}$	0.002	Machine-side resistive constant
$K_{p,Vdc}$	1.2	DC-link voltage PI proportional gain
$K_{i,Vdc}$	24.4	DC-link voltage PI integral gain
$K_{p,GSC}$	0.286	Grid-side current PI proportional gain
$K_{i,GSC}$	11.333	Grid-side current PI integral gain
$K_{p,PLL}$	60	PLL proportional gain
$K_{i,PLL}$	1400	PLL integral gain

4.17 CHAPTER SUMMARY

This chapter described the Type IV wind turbine model used in this dissertation. The model is based on a full-converter topology in which the generator is decoupled from the grid by a back-to-back converter. The aerodynamic model, MPPT strategy, PMSG representation, machine-side converter, DC-link, chopper circuit, grid-side converter, PLL, current limiter, and control loops were described.

The chapter also emphasized that the model is a grid-following IBR. Therefore, the grid-side converter depends on the PLL to synchronize with the grid voltage. During faults, the PLL, current limiter, and DC-link control influence the current injected into the grid. This behavior is essential for the protection analysis because the IBR does not inject fault currents in the same way as a synchronous generator.

Finally, the chapter explained why the transformer connection and zero-sequence current path must be clearly reported. In the analyzed system, ground faults can produce zero-sequence current through the grounded-wye side of the delta–grounded-wye transformer, affecting the phase currents observed by the protection algorithm. This justifies the detailed analysis of the interaction between the Type IV wind turbine model and the differential protection schemes evaluated in the following chapter.

CHAPTER 5

RESULTS AND DISCUSSIONS

5.1 INTRODUCTION

This chapter presents the simulation results obtained for the transmission line connected to the Type IV wind turbine-based IBR. The protection performance is evaluated using conventional alpha-plane differential protection and the Current Mapping Strategy (CMS). The analyzed cases include phase-A-to-ground (AG), phase-A-and-B-to-ground (ABG), and three-phase (ABC) faults, considering different fault resistances and fault locations. The IBR-side zero-sequence removal is evaluated only for ground-fault cases, since the ABC fault does not involve a ground-return path.

Before presenting the individual fault cases, it is important to clarify the role of the local transformer in the zero-sequence current path. The transformer is connected as delta–grounded-wye in the direction from the IBR to the remaining system. The Type IV wind turbine is connected to the delta side, while the studied line and the differential protection terminals are connected to the grounded-wye side. During ground faults on the protected line, the zero-sequence component is not produced as a native contribution of the full-converter IBR in the same way as in a conventional synchronous generator. Instead, the zero-sequence current associated with the fault can return through the grounded-wye side of the transformer and appear in the local-terminal phase measurements.

This component is added equally to the three phase currents and can contaminate the phase-segregated quantities used by the alpha-plane and CMS protection schemes. Therefore, the ground-fault cases are evaluated without and with IBR-side zero-sequence removal. In the sequence-current figures, the local-terminal positive-sequence current remains close to the IBR current limit, approximately 1 pu, in the analyzed post-fault intervals. Thus, the main issue investigated in the ground-fault cases is not a collapse of the positive-sequence component, but the influence of the transformer-related zero-sequence component on the phase elements of the differential protection.

5.2 SYSTEM

The simulated system consists of a 230 kV, 80 km transmission line connected to a Type IV wind turbine-based IBR at the local terminal and to a Thévenin equivalent at the remote terminal. The local transformer is connected as delta–grounded-wye in the direction from the IBR to the remaining system; therefore, the IBR is connected to the delta side and the studied line is connected to the grounded-wye side.

Table 5.1 summarizes the transmission-line parameters and the equivalent source data used in the EMTP simulations.

Table 5.1. EMTP model data.

Transmission Line	Source S1	Source S2
Length: 80 km	$\hat{V}_1 = 1.02\angle 0°$ pu	$\hat{V}_1 = 0.98\angle 20°$ pu
$Z_{L,0} = 0.532 + j1.541\ \Omega/\text{km}$	$Z_0 = 1.014 + j18.754\ \Omega$	$Z_0 = 1.127 + j20.838\ \Omega$
$Y_{L,0} = j2.293\ \mu\mho/\text{km}$	$Z_1 = 0.871 + j25.661\ \Omega$	$Z_1 = 0.968 + j28.513\ \Omega$
$Z_{L,1} = 0.098 + j0.510\ \Omega/\text{km}$		
$Y_{L,1} = j3.252\ \mu\mho/\text{km}$		

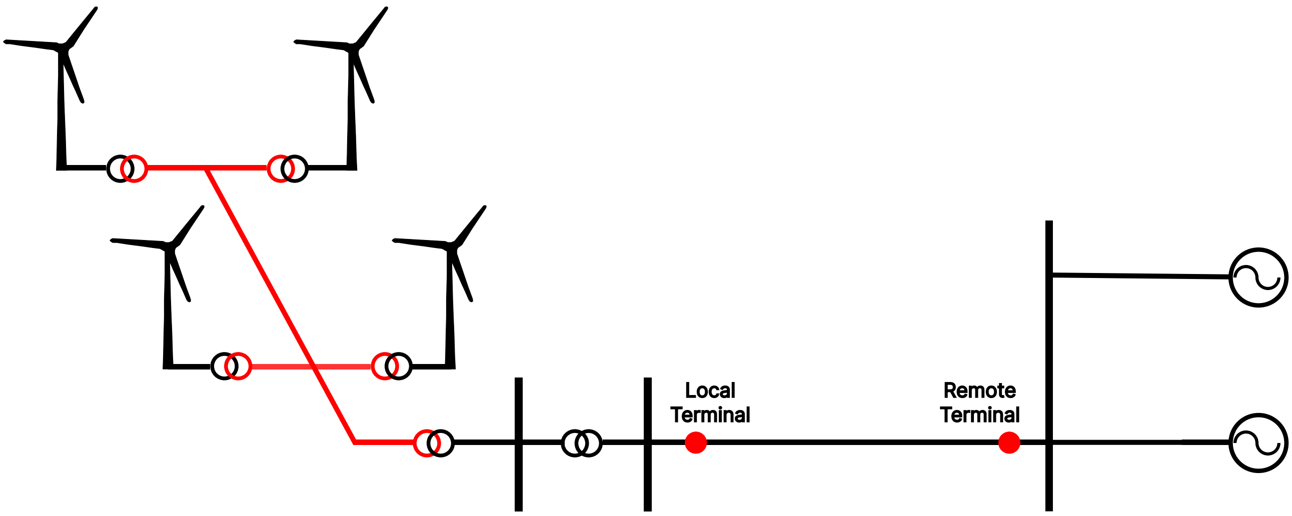

Figure 5.1. Simulated system.

The transformer connection is a key element in the interpretation of the results. Since the IBR is connected to the delta side of the transformer and the protected line is connected to the grounded-wye side, the converter itself does not act as a conventional zero-sequence source. However, during ground faults on the protected line, zero-sequence current can circulate through the grounded-wye side of the transformer and appear in the local-terminal phase currents used by the protection algorithm. This component can contaminate the phase-segregated quantities and may cause non-faulted phases to be identified as faulted. For this reason, the results compare cases without and with IBR-side zero-sequence removal before the phase-segregated differential protection is evaluated.

The analyzed cases are summarized in Table 5.2. The fault location of 10% is measured from the local terminal, meaning that the fault is close to the IBR-side terminal.

Table 5.2. Summary of simulated fault cases.

Case group	Fault type	Fault resistance	Fault location	IBR-side zero-sequence removal
1	AG	0 Ω	50% of the line	No
2	AG	0 Ω	50% of the line	Yes
3	AG	100 Ω	50% of the line	No
4	AG	100 Ω	50% of the line	Yes
5	AG	0 Ω	10% from the local terminal	No
6	AG	0 Ω	10% from the local terminal	Yes
7	ABG	0 Ω	50% of the line	No
8	ABG	0 Ω	50% of the line	Yes
9	ABG	100 Ω	50% of the line	No
10	ABG	100 Ω	50% of the line	Yes
11	ABC	0 Ω	50% of the line	No

Table 5.3 reports approximate post-fault sequence-current magnitudes read from the sequence-current figures in the interval after the transient settling. These values are used as a numerical reference for the discussion of the protection behavior. The local-terminal positive-sequence current remains close to the IBR current limit in the analyzed post-fault interval, while the zero-sequence component becomes dominant in several ground-fault cases because of the transformer grounding path.

Table 5.3. Approximate post-fault sequence-current magnitudes read from the sequence-current plots.

Fault case	Terminal	I_1 (A)	I_2 (A)	I_0 (A)
AG, 0 Ω, 50%	Local	176	12	507
AG, 100 Ω, 50%	Local	156	9	114
AG, 0 Ω, 10%	Local	174	15	410
ABG, 0 Ω, 50%	Local	157	7	341
ABG, 100 Ω, 50%	Local	171	4	105
ABC, 0 Ω, 50%	Local	166	1	1
AG, 0 Ω, 50%	Remote	1645	1642	1623
AG, 100 Ω, 50%	Remote	154	168	169
AG, 0 Ω, 10%	Remote	1427	1412	1407
ABG, 0 Ω, 50%	Remote	4301	3144	1162
ABG, 100 Ω, 50%	Remote	255	151	147
ABC, 0 Ω, 50%	Remote	5864	0	0

5.3 PHASE-A-TO-GROUND FAULT

5.3.1 $R = 0\ \Omega$ without IBR-side zero-sequence removal

Figure 5.2 shows that, before the fault, the current entering the system from the IBR side is mainly positive sequence. After the AG fault, the local positive-sequence current remains close to the IBR current limit, approximately 176 A in the post-fault interval, while the zero-sequence current increases to approximately 507 A. This high zero-sequence component is associated with the return path provided by the grounded-wye side of the local transformer, not with a native zero-sequence contribution from the Type IV converter.

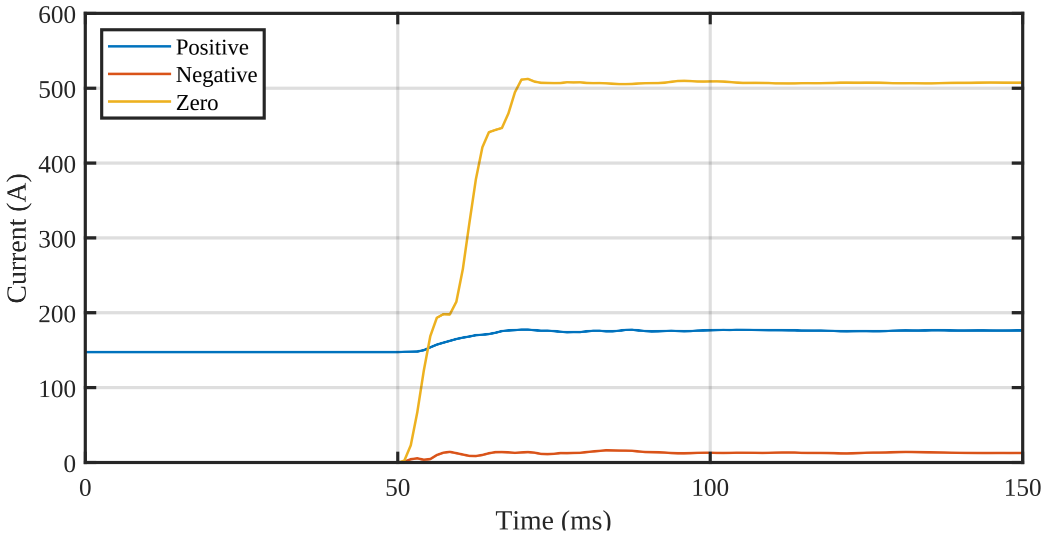

Figure 5.2. Local sequence currents.

The remote currents again are shown normal in the pre-fault scenario, where there is only positive-sequence, but after the AG fault, the sequence currents increase according to the AG fault characteristics.

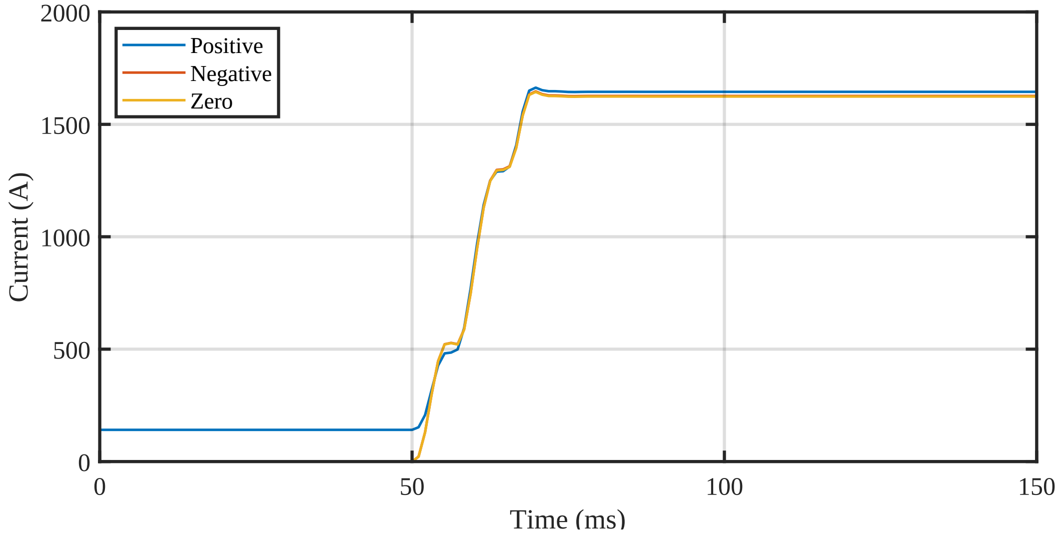

Figure 5.3. Remote sequence currents.

Due to the high zero-sequence component measured at the local terminal, the alpha-plane phase elements presented loss of phase selectivity, identifying phases A and B as faulted even though the simulated fault involved only phase A, as shown in Figure 5.4.

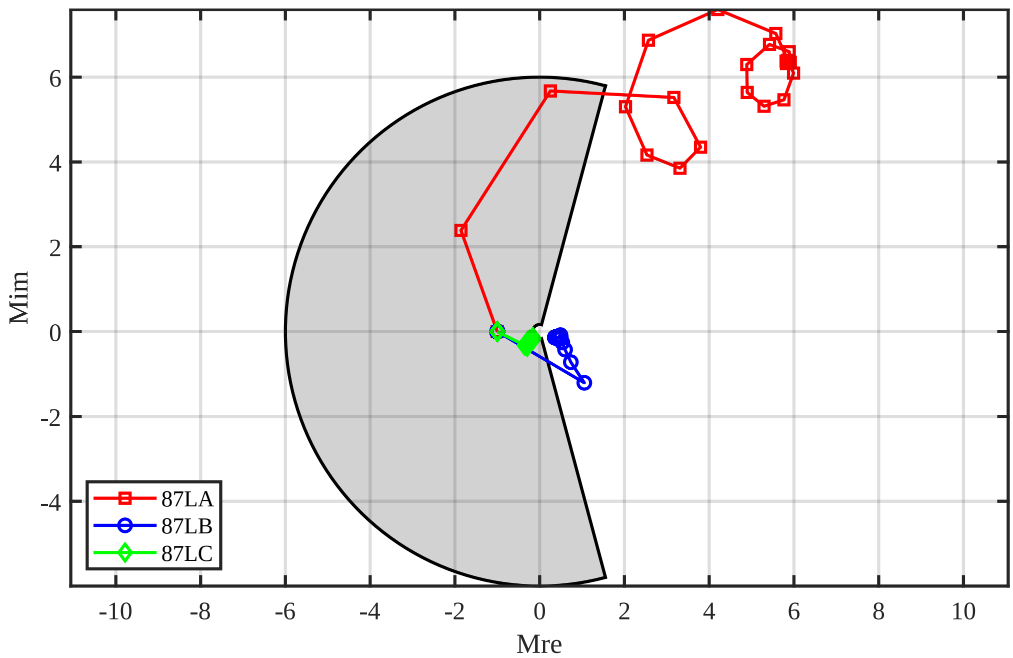

Figure 5.4. Local alpha-plane phase elements.

Similarly, the remote phase-element response also indicates an undesired operation involving phase B, as shown in Figure 5.5. This behavior is consistent with the influence of the zero-sequence component on the phase quantities used by the protection.

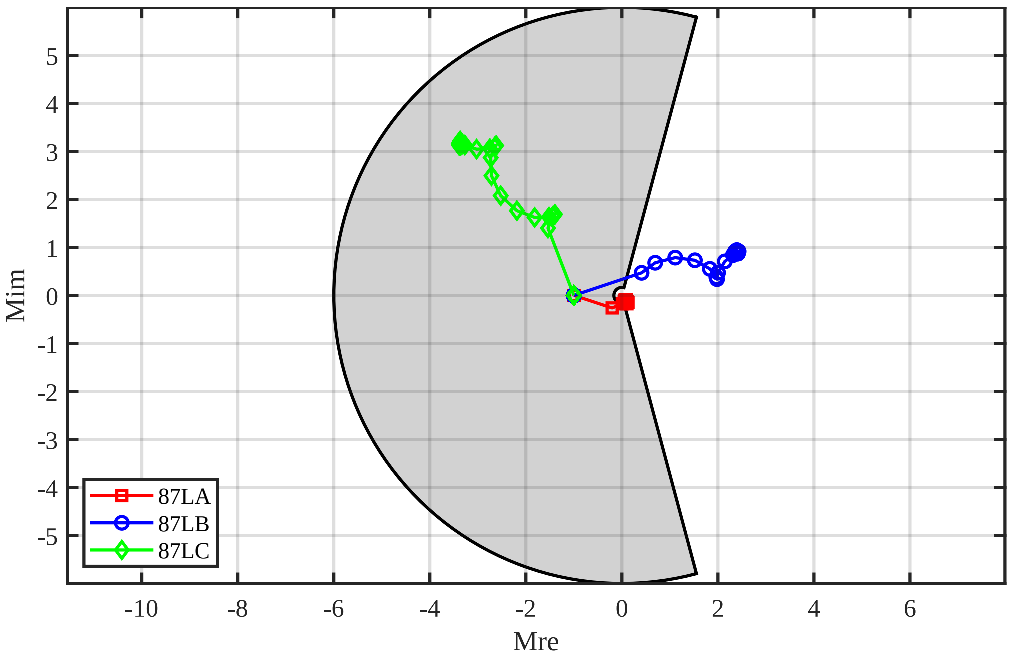

Figure 5.5. Remote alpha-plane phase elements.

Because of the high values of the zero-sequence in the IBR side of the fault contribution coming from the transformer, the three phases were detected in the AG fault for the CMS-1 protection scheme, as seen in Figure 5.6.

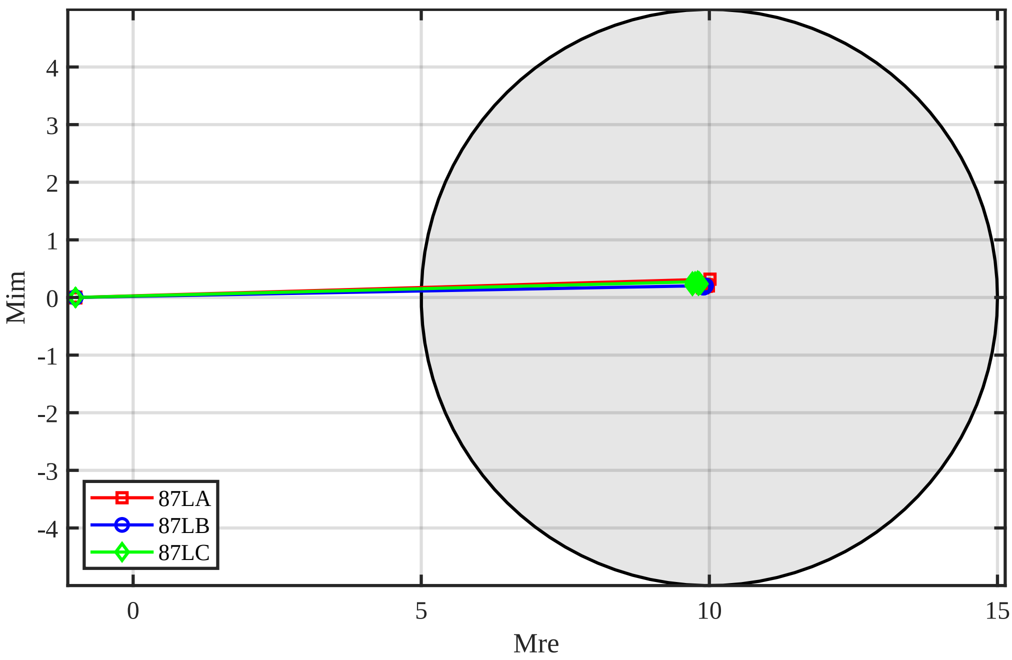

Figure 5.6. CMS-1 response.

Similarly, the CMS-2 protection algorithm has incorrectly identified the three phases for the protection scheme, because of the high values of zero-sequence previously commented in the previous texts.

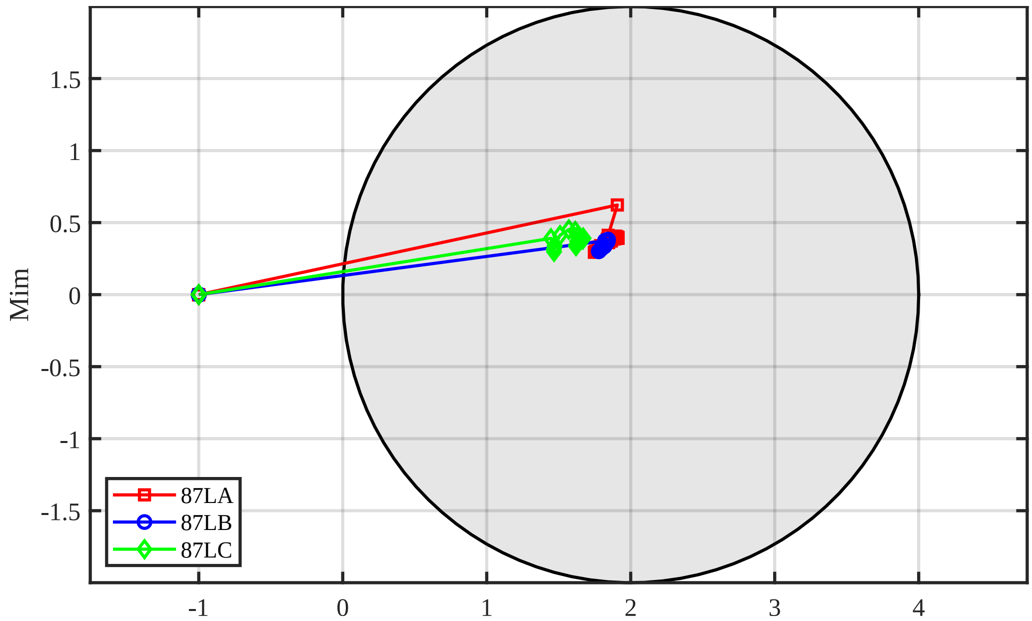

Figure 5.7. CMS-2 response.

5.3.2 $R = 0\ \Omega$ with IBR-side zero-sequence removal

Now, it is possible to see that the high zero-sequence is common observed in the IBR side of the line, and because of that, it is necessary to remove the zero-sequence of these currents in order to segregate each phase for better fault detection and enable double phase reclosing.

By removing the zero-sequence, the results show that the Local phase protection has observed the current fault detection and detected only the correct phase currents, this gives the protection the segregation of each faulted phase and the removal of the interfering zero-sequence allows to identify only the correct phases for the fault.

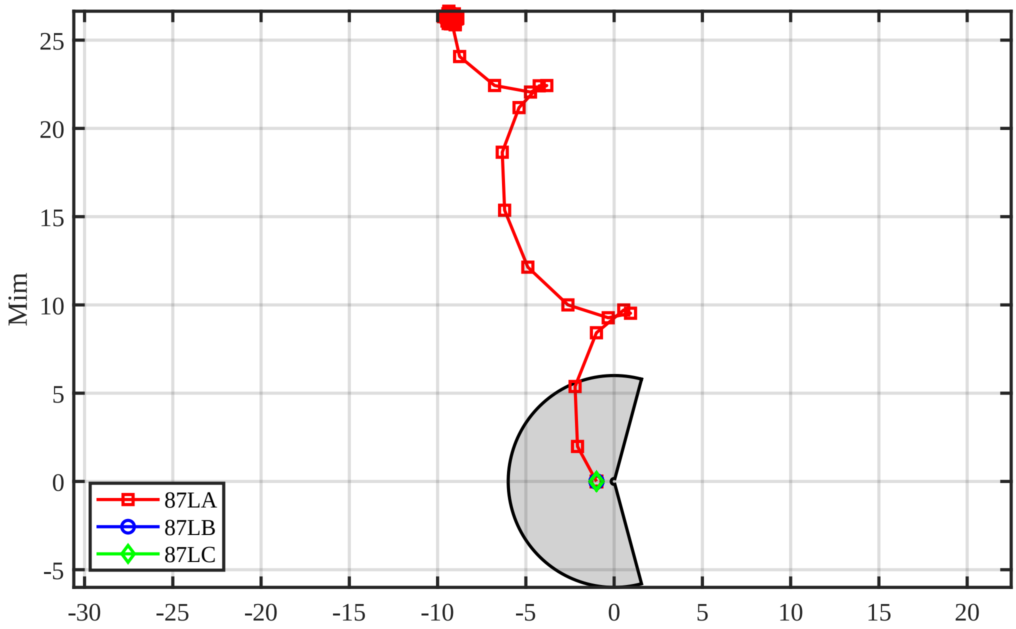

Figure 5.8. Local alpha-plane phase elements.

The remote phase elements also identified the faulted phase correctly, indicating that the phase-segregated protection operates as expected after the IBR-side zero-sequence component is removed.

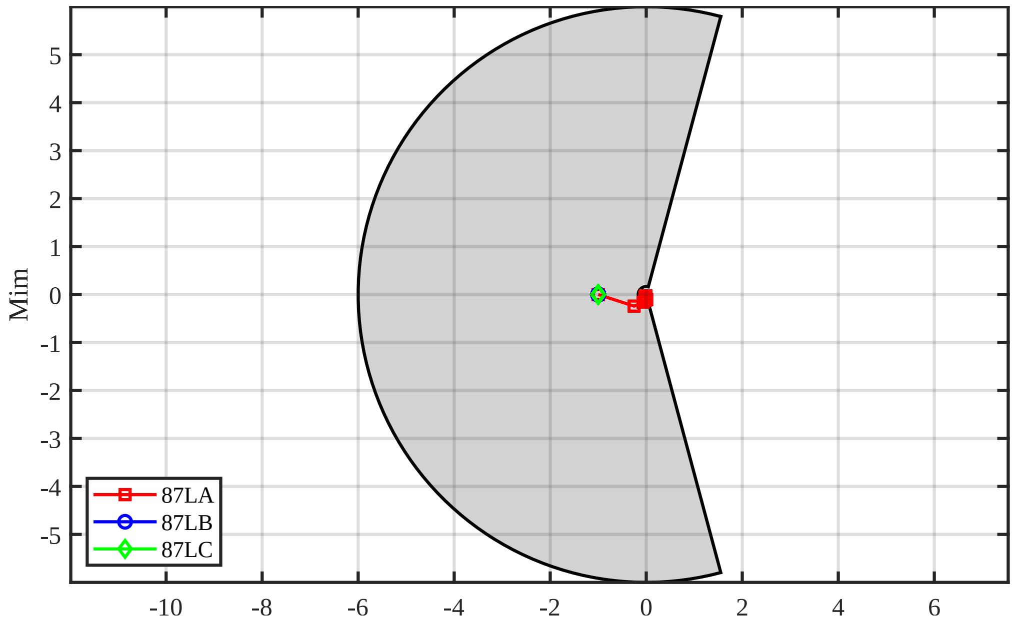

Figure 5.9. Remote alpha-plane phase elements.

In the case of the CMS-1 protection case, it is seen in Figure 5.10 that the protection has only detected the phase A, and that was the expected response of the protection, segregating only the faulted phase.

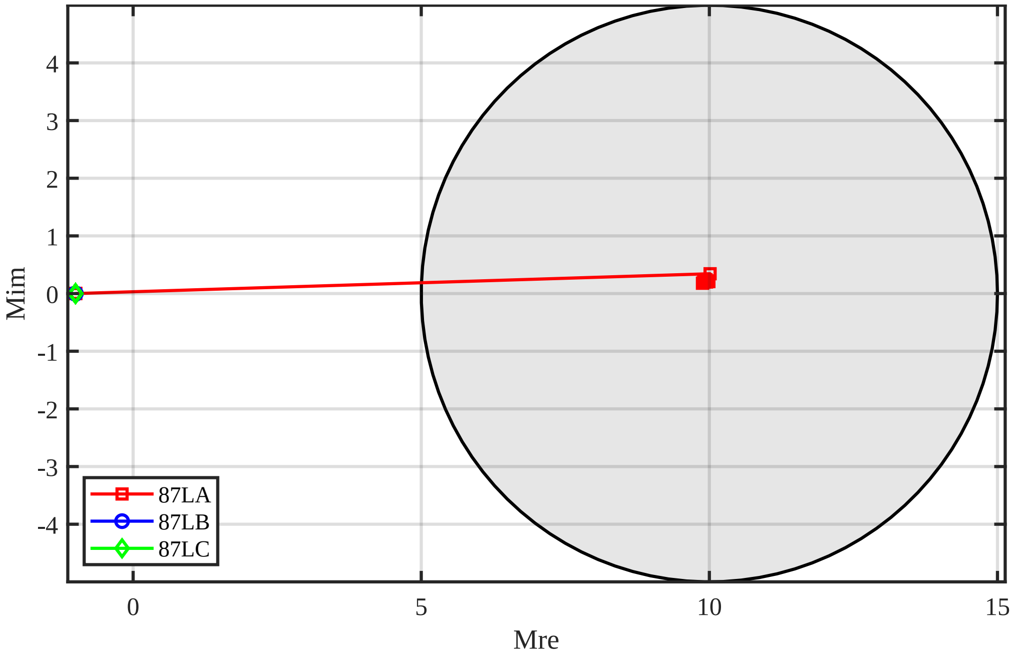

Figure 5.10. CMS-1 response.

Similarly, for the CMS-2 in the protection operated correctly by only detecting the phase A of the system, as shown in Figure 5.11, where the protection was detected because of the entrance of the activation zone.

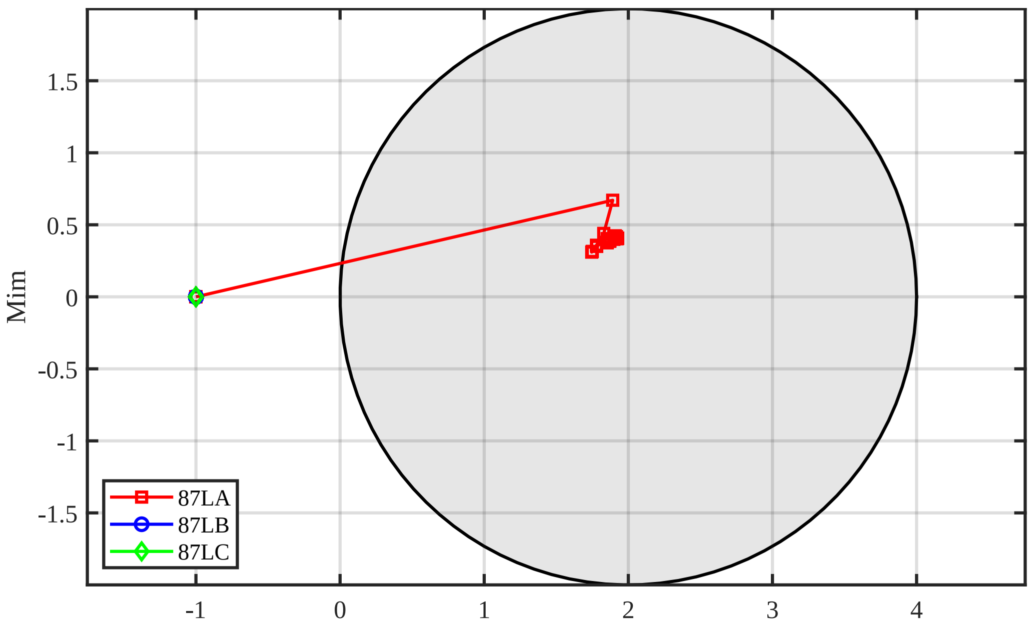

Figure 5.11. CMS-2 response.

5.3.3 $R = 100\ \Omega$ without IBR-side zero-sequence removal

Now for the same fault but adding a fault resistance, we can see that the ground-fault current magnitudes are lower because of the fault resistance.

Still the characteristic of high zero-sequence in the Local Current Terminal that came from the transformer due to the fault characteristic of the remote terminal can be observed.

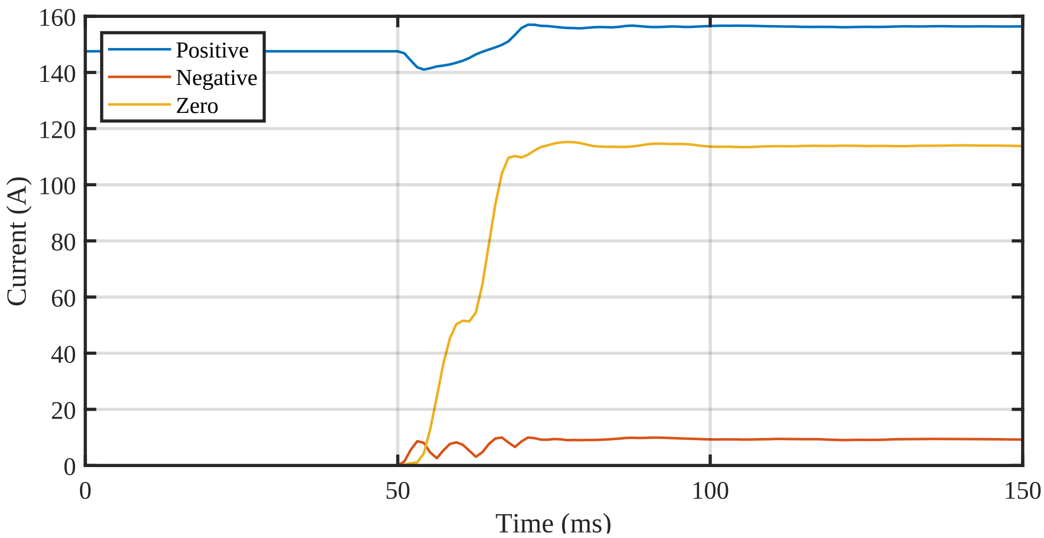

Figure 5.12. Local sequence currents.

The remote sequence currents show that the positive-sequence component remains close to 1 pu during the analyzed post-fault interval.

The zero-sequence component is still observed because the fault involves ground and includes fault resistance, while the negative-sequence component depends on the unbalance imposed by the fault and on the source contribution from the remote side of the line.

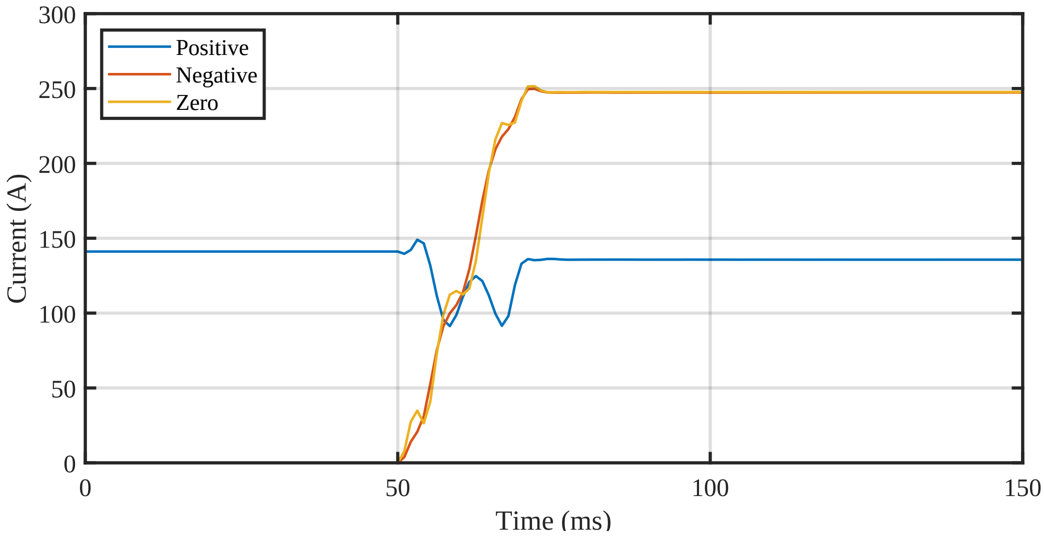

Figure 5.13. Remote sequence currents.

For the protection it is possible to see that the phase A was not tripped, this behavior is explained because of the zero-sequence observed in the local terminal explained before and the high fault resistance.

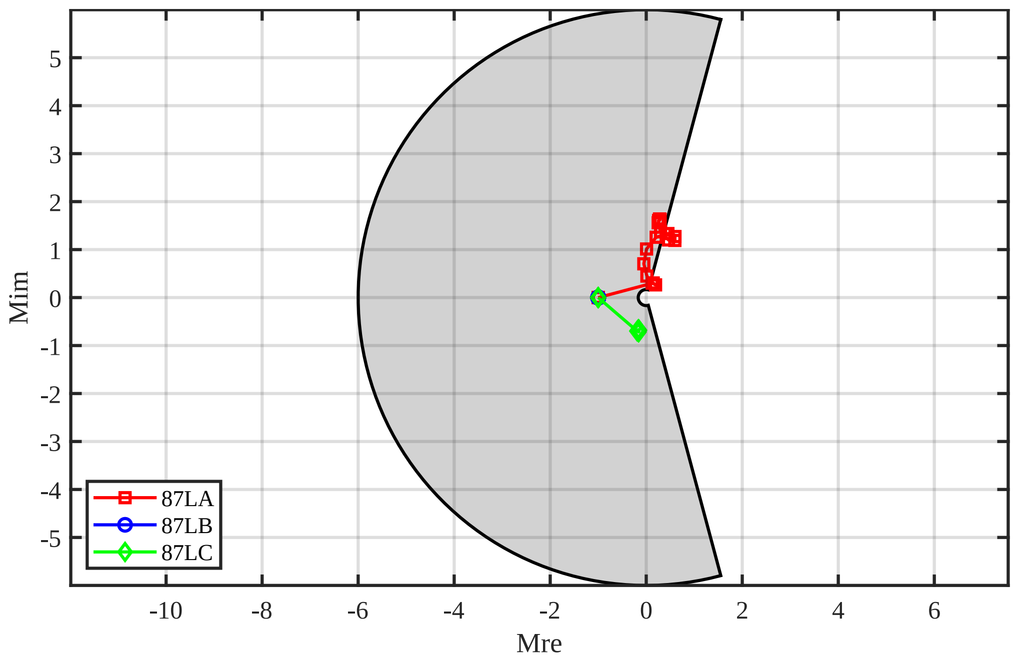

Figure 5.14. Local alpha-plane phase elements.

Similarly, in Figure 5.15, it is possible to see that no phases were tripped because of the zero-sequence components in the local terminal that came from the transformer, generating misidentification of the protection.

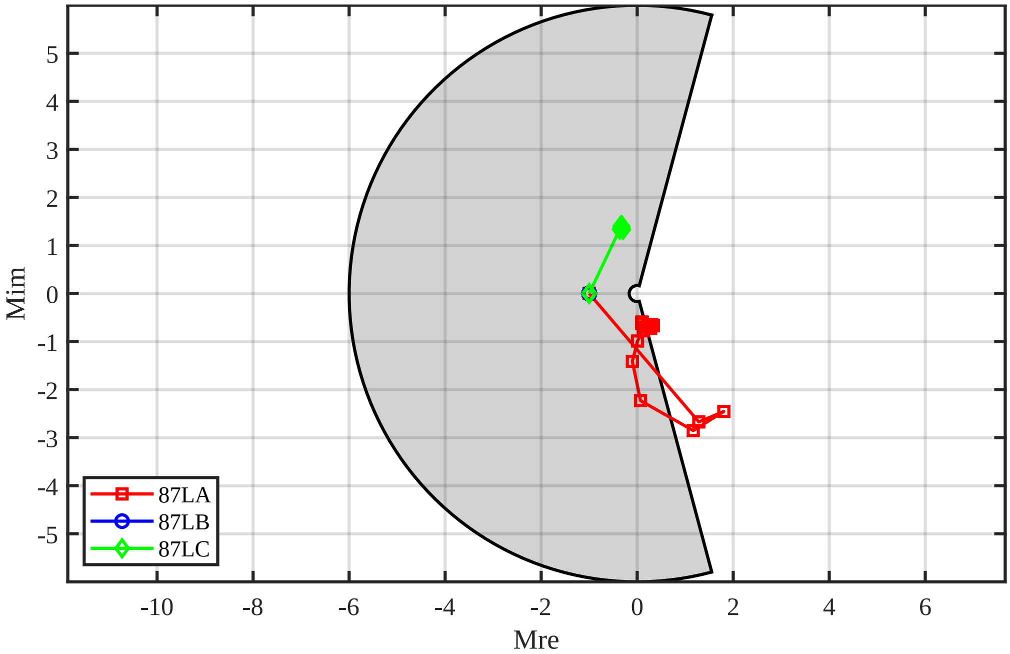

Figure 5.15. Remote alpha-plane phase elements.

And finally, the CMS-1 in Figure 5.16 shows that due to the fact of the increase of the zero-sequence current in the local terminal, the fault has been detected in two phases, and this scenario is a loss of phase selectivity.

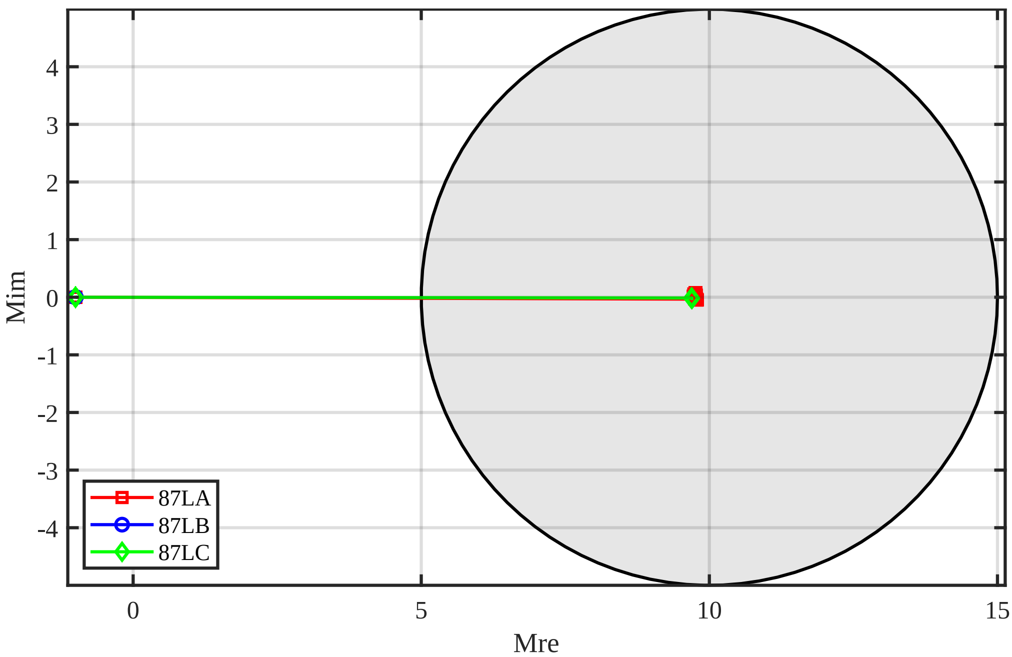

Figure 5.16. CMS-1 response.

Also in the CMS-2 scenario, the phases A and C were tripped and there was no correct protection or the B and C phases, this behavior is explained because there is a high value of zero-sequence current in the system coming from the transformer in the IBR side of the grid.

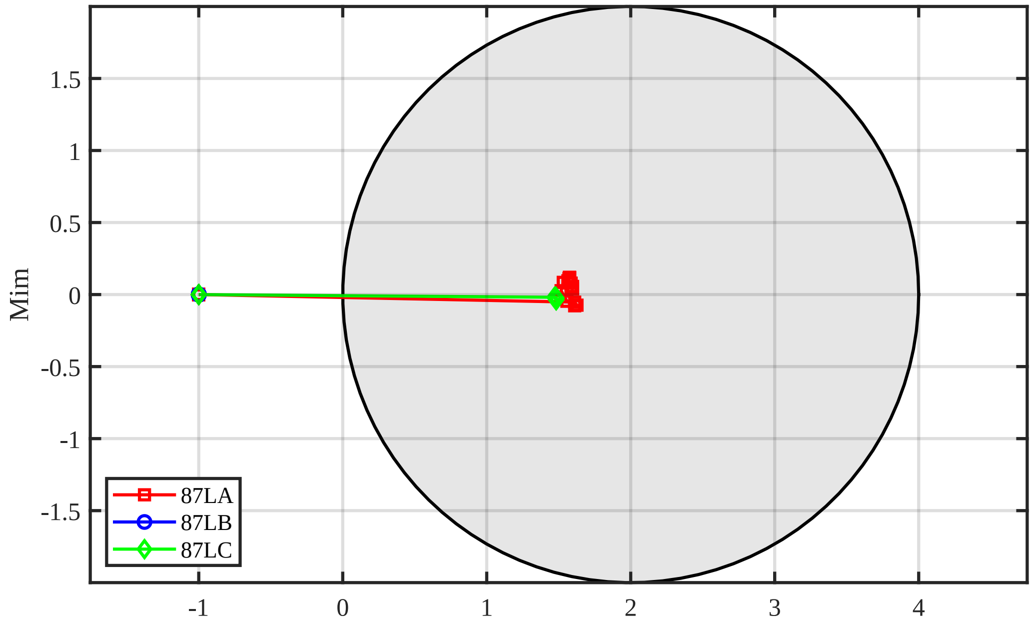

Figure 5.17. CMS-2 response.

5.3.4 $R = 100\ \Omega$ with IBR-side zero-sequence removal

It is possible to observe that the fault resistance generated a misidentification of the protection, the phase A did not trip during the fault, this behavior is explained because of the high value of fault resistance in the ground fault, as shown in Figure 5.18.

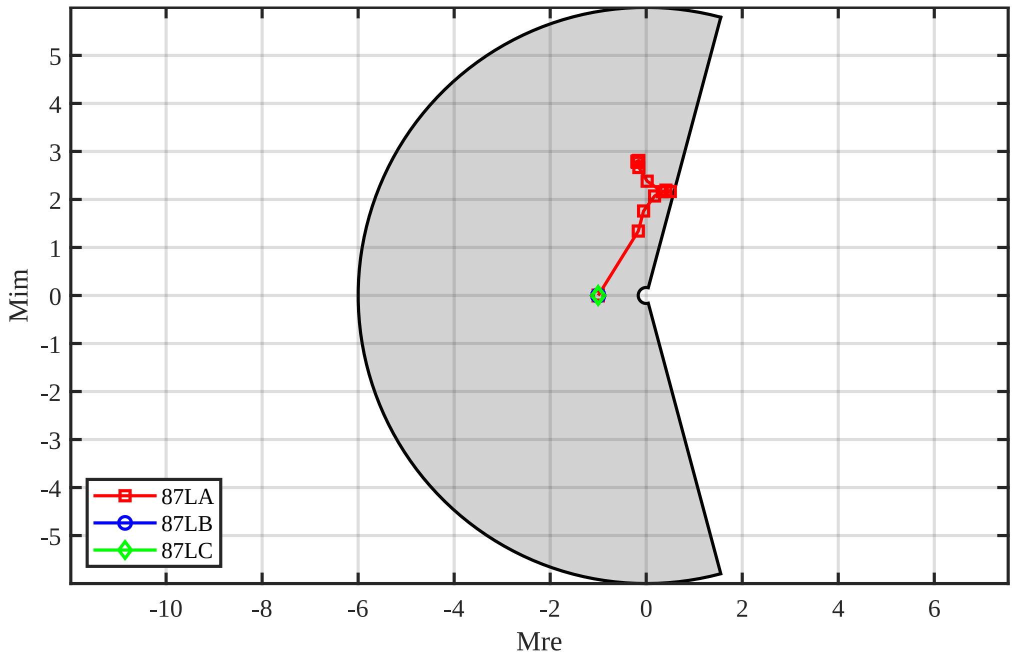

Figure 5.18. Local alpha-plane phase elements.

Similarly, in Figure 5.19, the fault did not trip in phase A because of the high value of resistance in the ground fault, but still phases B and C did not trip also, because of the removal of the zero-sequence in the IBR side of the grid.

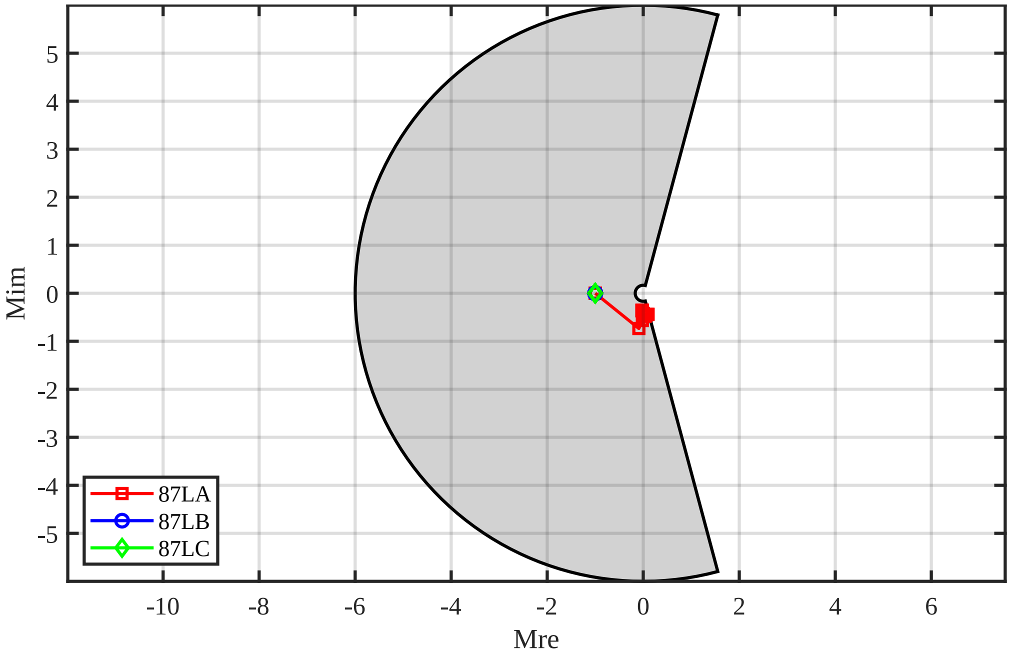

Figure 5.19. Remote alpha-plane phase elements.

In Figure 5.20, it is seen that the CMS-1 has functionally correctly because only the faulted phase has tripped, phase A, and the fault was detected correctly, segregating the correct phase.

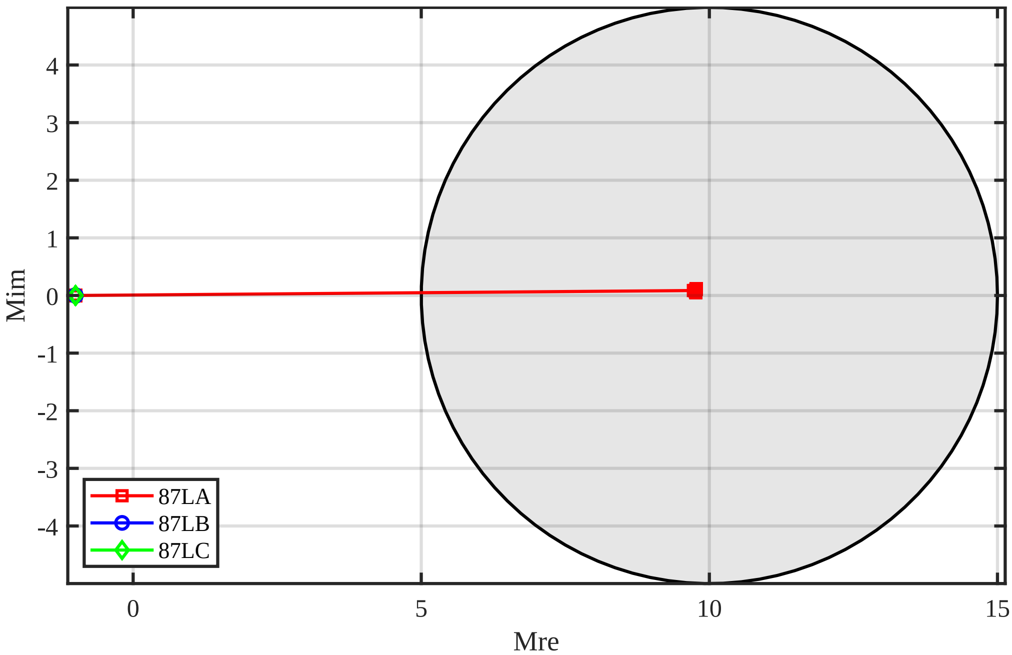

Figure 5.20. CMS-1 response.

Similarly for the CMS-2 scheme, again only the faulted phase A has detected the fault and correctly tripped for only the faulted phase, in which is phase A, showing its efficiency for cases where the zero-sequence comes through the transformer in the IBR side of the grid.

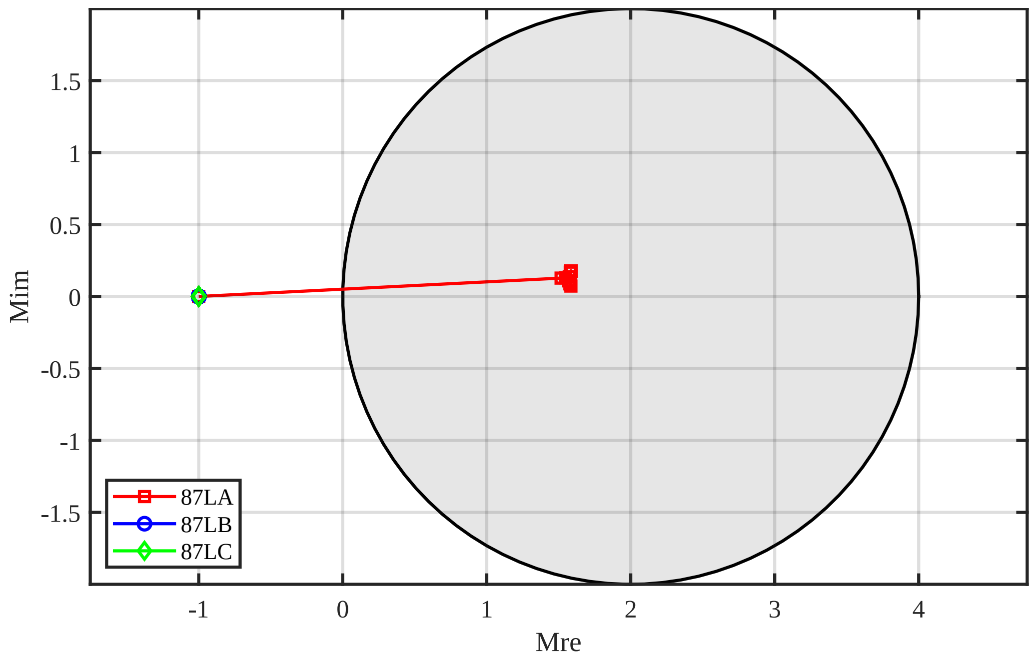

Figure 5.21. CMS-2 response.

5.3.5 $R = 0\,\Omega$ at 10% of the line from the local terminal without IBR-side zero-sequence removal

The next case considers a solid AG fault located at 10% of the line length measured from the local terminal, therefore close to the IBR-side terminal. This location is evaluated to verify how a fault near the local terminal changes the relative current contribution and the protection trajectories when compared with the midpoint fault. In this scenario, it is possible to analyze new protection scenarios, where in Figure 5.22, it is observed that the High values of the Zero Sequence are seen in the Local sequence currents.

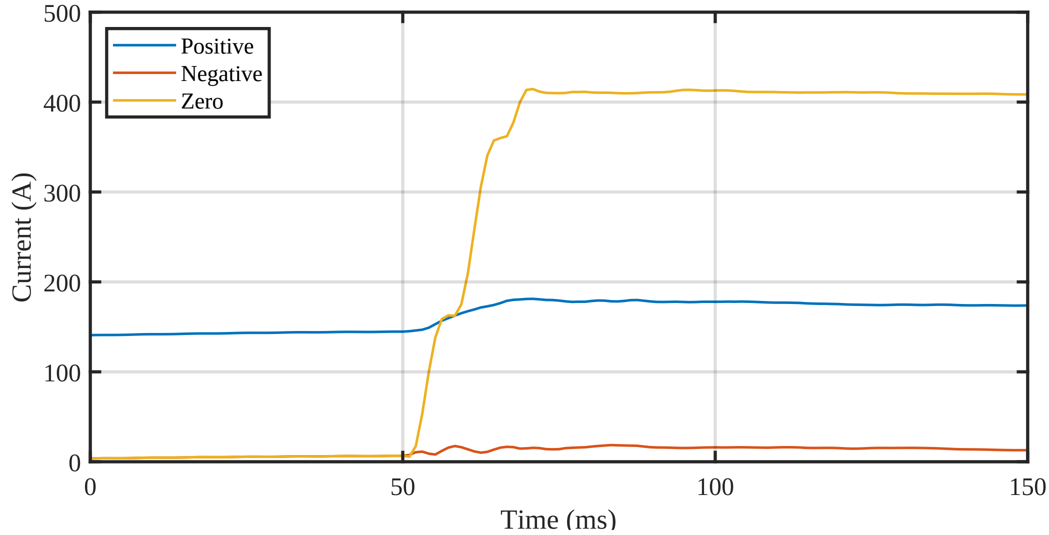

Figure 5.22. Local sequence currents.

Also in the Sequence Remote Currents shown in Figure 5.23, it is possible to see the high values of positive and zero-sequence coming from the remote side of the grid.

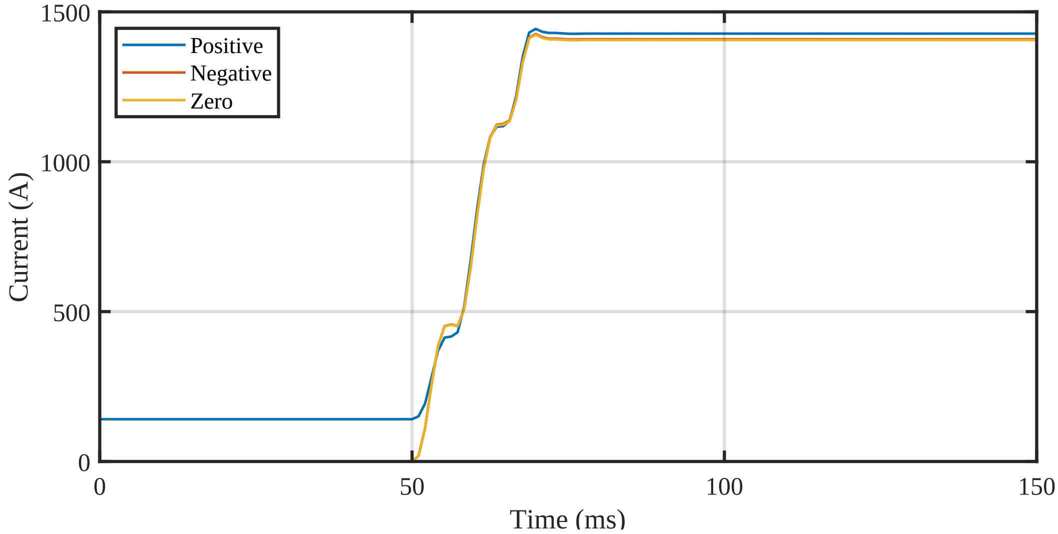

Figure 5.23. Remote sequence currents.

The Alpha-plane local Phases Protection shown in Figure 5.24 generates the identification of the A and B faults during the fault, this is not correct because of the fault only happening in the A phase, generated because of the higher values of zero-sequence when comparing with the positive-sequence from the IBR.

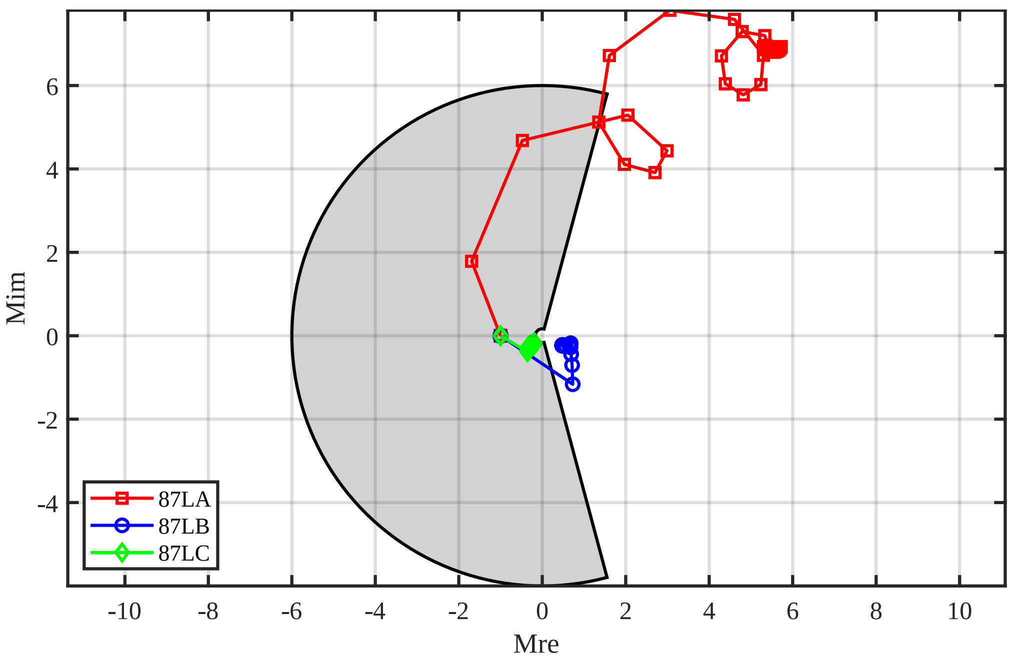

Figure 5.24. Local alpha-plane phase elements.

In Figure 5.25, the phases A and B are identified in the protection, and this behavior is explained because of the high values of the zero-sequence coming from the IBR side of the transformer.

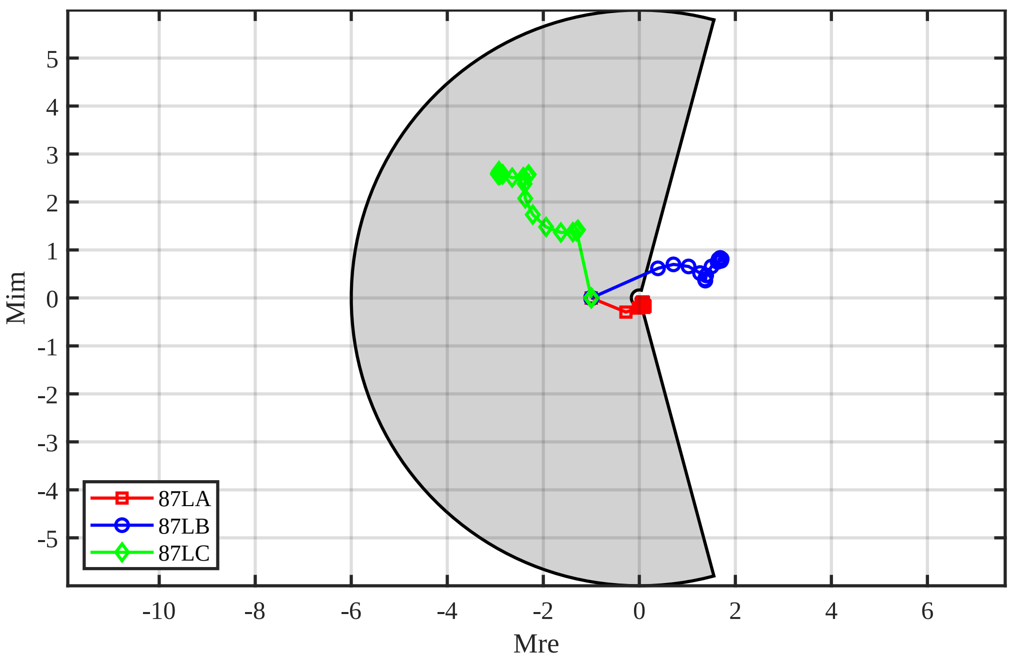

Figure 5.25. Remote alpha-plane phase elements.

Now considering the CMS-1 in Figure 5.26 for the scenario, it is possible to see that again the three phases were identified in the fault, this is again caused of the zero-sequence coming in the IBR side of the line, as explained before.

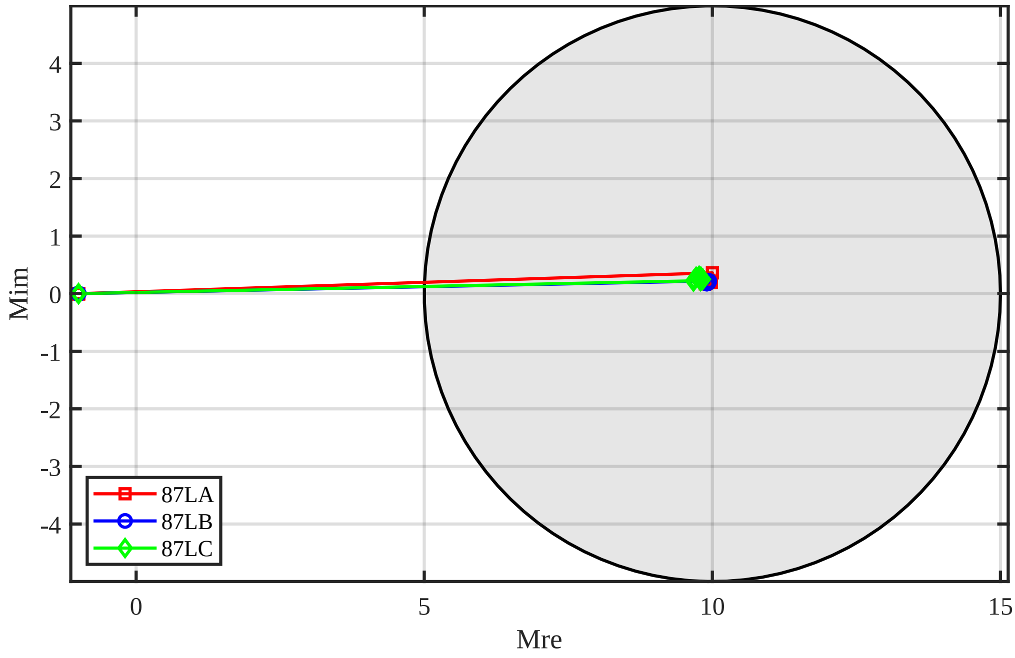

Figure 5.26. CMS-1 response.

In Figure 5.27, again all the three phases were identifies incorrectly, this again because of the high values of zero-sequence current coming from the IBR side of the grid generating this false trips of A, B and C phases in the CMS-2 algorithm protection.

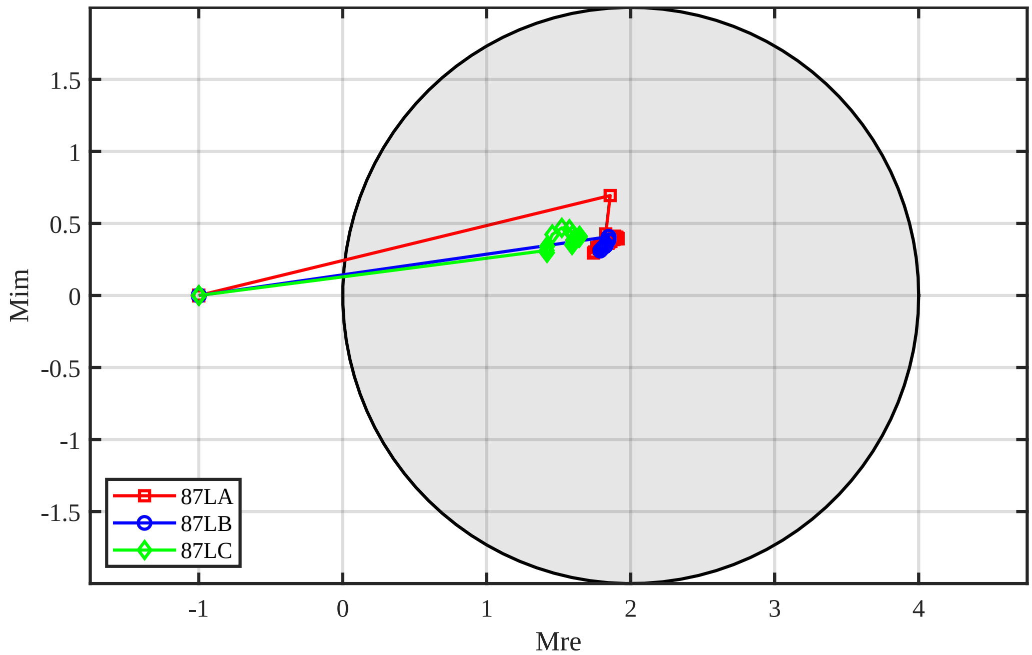

Figure 5.27. CMS-2 response.

5.3.6 $R = 0\ \Omega$ at 10% of the line from the local terminal with IBR-side zero-sequence removal

Now, by removing the zero-sequence from all the IBR currents coming from the IBR side of the grid, it is expected to improve the protection and generate only the faulted phases trips for the protection again.

The Alpha-plane local Phases Protection shown in Figure 5.28 shows that the protection has now correctly only identified the phase A for the faulted phase in this scenario, this was possible because of the removal of the zero-sequence, since its value is higher than the positive-sequence from the IBR and allowing phase protection schemes.

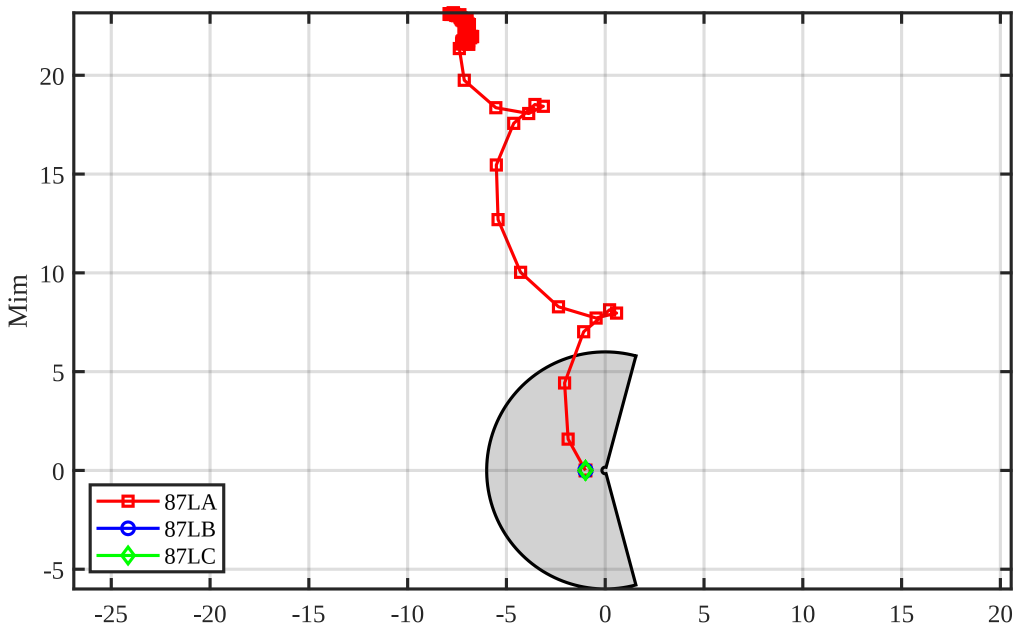

Figure 5.28. Local alpha-plane phase elements.

Again in Figure 5.29, the results show that the Alpha-plane remote Phases Protection has only identified the faulted A phase of the protection correctly after the removal of the zero-sequence from the IBR side of the grid that came through the transformer.

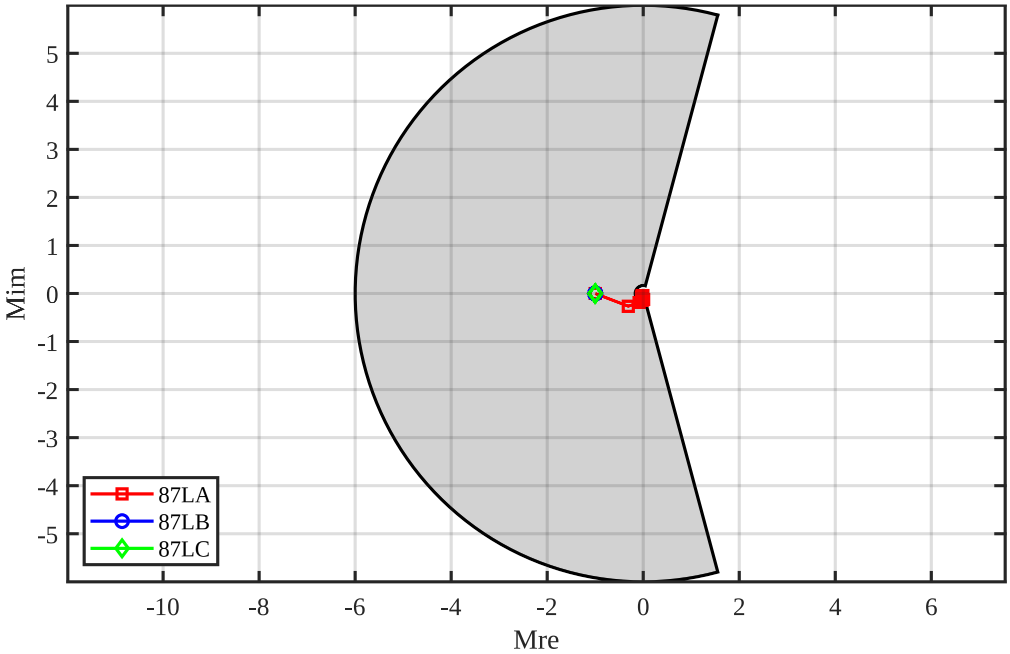

Figure 5.29. Remote alpha-plane phase elements.

Now for the CMS-1, the results show that now only the faulted phase A was identified by the protection and it worked correctly after the removal of the zero-sequence of the IBR side, by segregating the faulted phase.

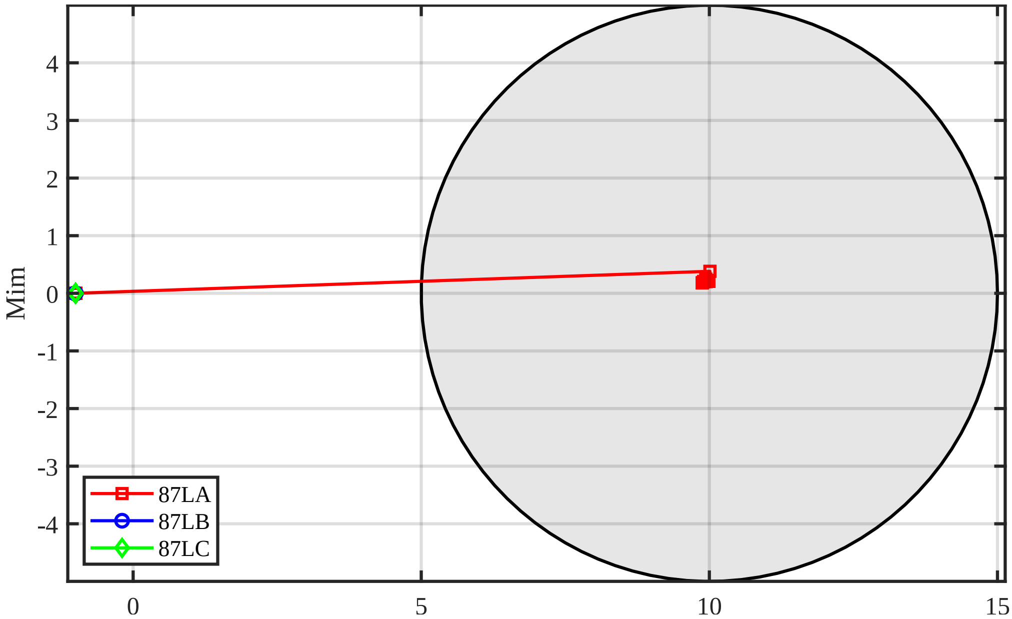

Figure 5.30. CMS-1 response.

And lastly, the CMS-2 protection scheme shown in Figure 5.31 shows that only the faulted phase A has identified the fault, and it worked properly and identified the correct phase only, by generating the correct tripping for the system protection.

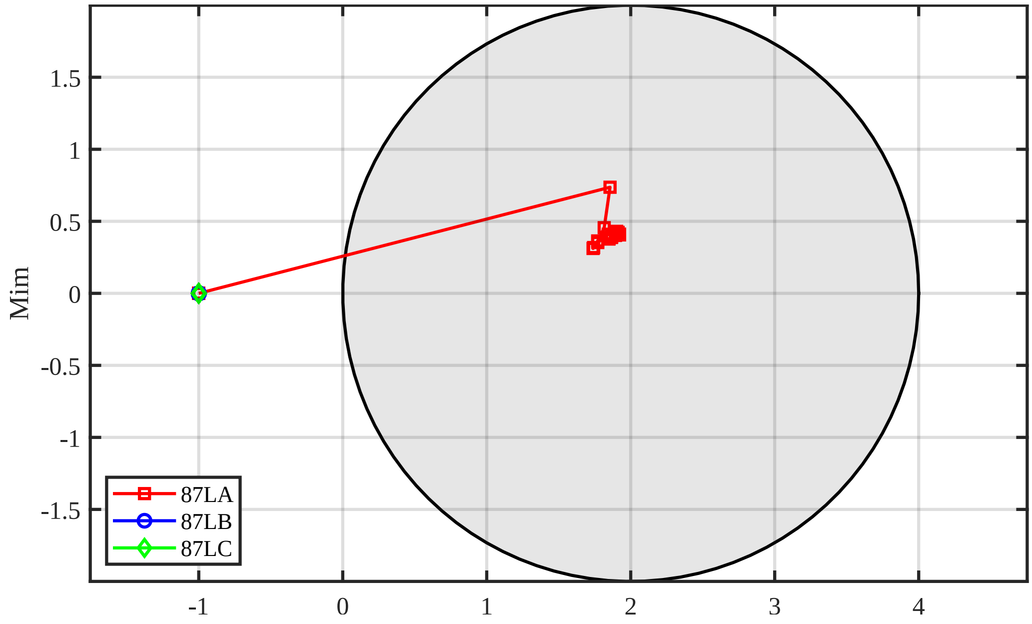

Figure 5.31. CMS-2 response.

5.4 PHASE-A-AND-B-TO-GROUND FAULT

5.4.1 $R = 0\ \Omega$ without IBR-side zero-sequence removal

Now considering the A and B fault to ground, the results show that the sequence currents are shown in Figure 5.32, where the high values of the zero-sequence can be explained by the return of the zero-sequence coming from the IBR transformer in the local terminal of the line.

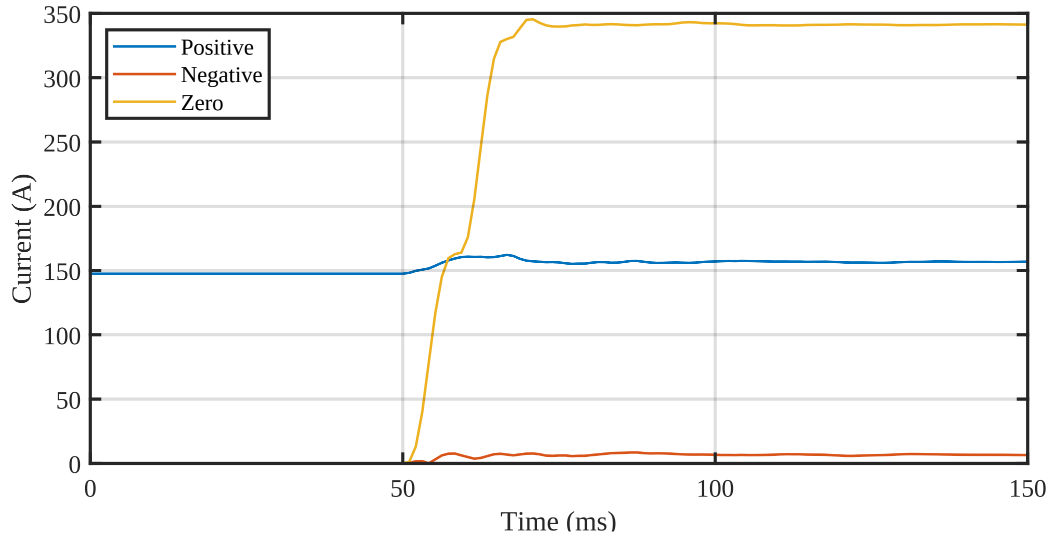

Figure 5.32. Local sequence currents.

In Figure 5.33, it is observed that there is a significant value of negative-sequence current, also a zero and positive-sequence current, due to the nature of the A and B fault to ground.

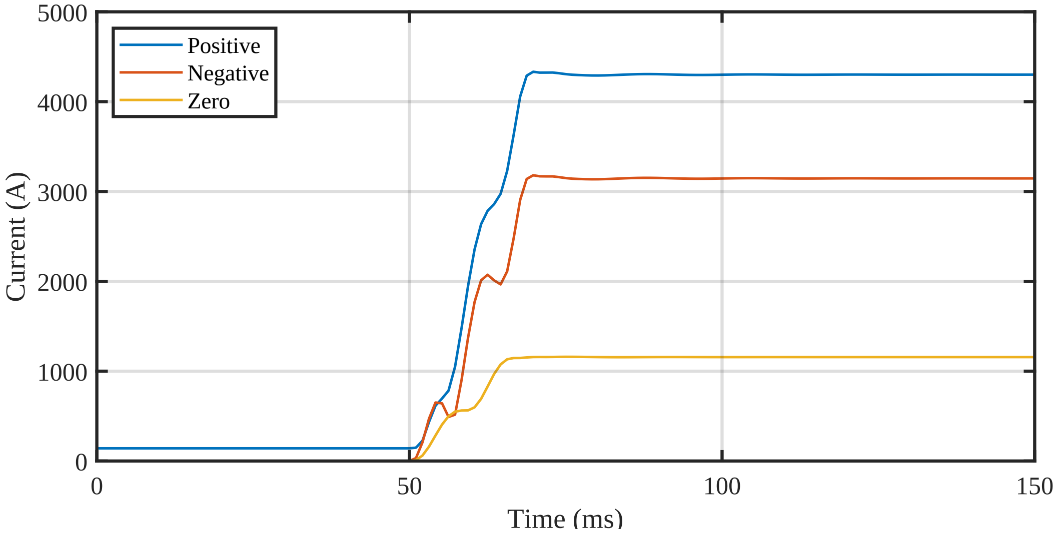

Figure 5.33. Remote sequence currents.

For the Alpha-plane local Phase protection, Figure 5.34 shows how the protection has responded, where the values of the fault A, B and C has tripped, incorrectly because of the zero-sequence in the IBR side of the line.

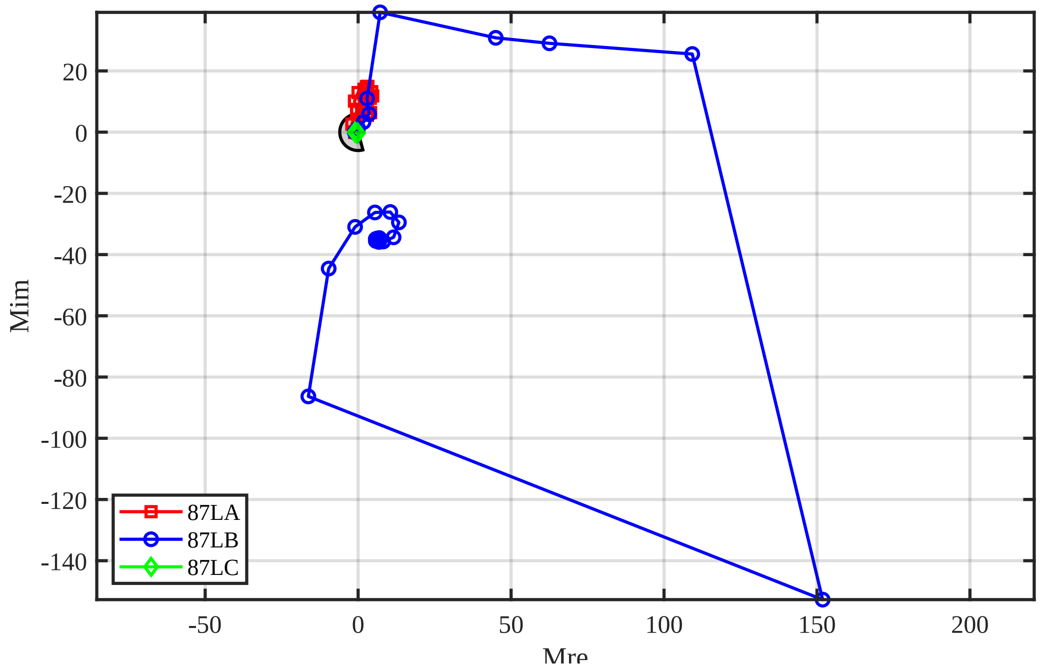

Figure 5.34. Local alpha-plane phase elements.

In Figure 5.35, it is observed that the A and B sequence currents have been detected, but the C phase did not trip, functionally working for the protection for the remote alpha plane phase protection.

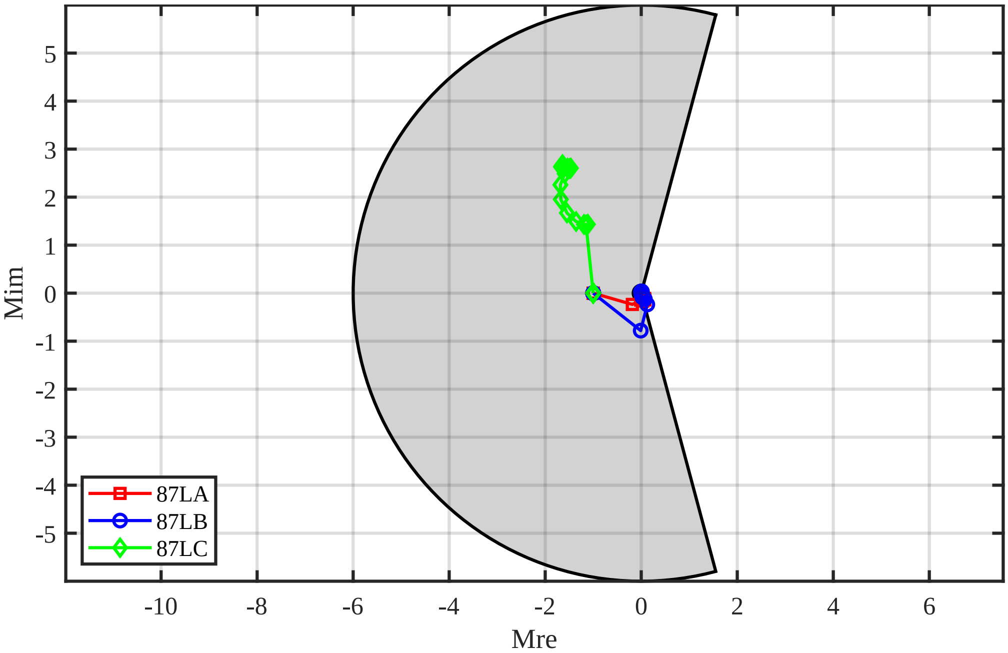

Figure 5.35. Remote alpha-plane phase elements.

For the CMS-1 protection scheme, the three phases have been tripped, being incorrectly tripped. which can be explained because of the zero-sequence is entering the local terminal and causing undesired phase operation in the three phases.

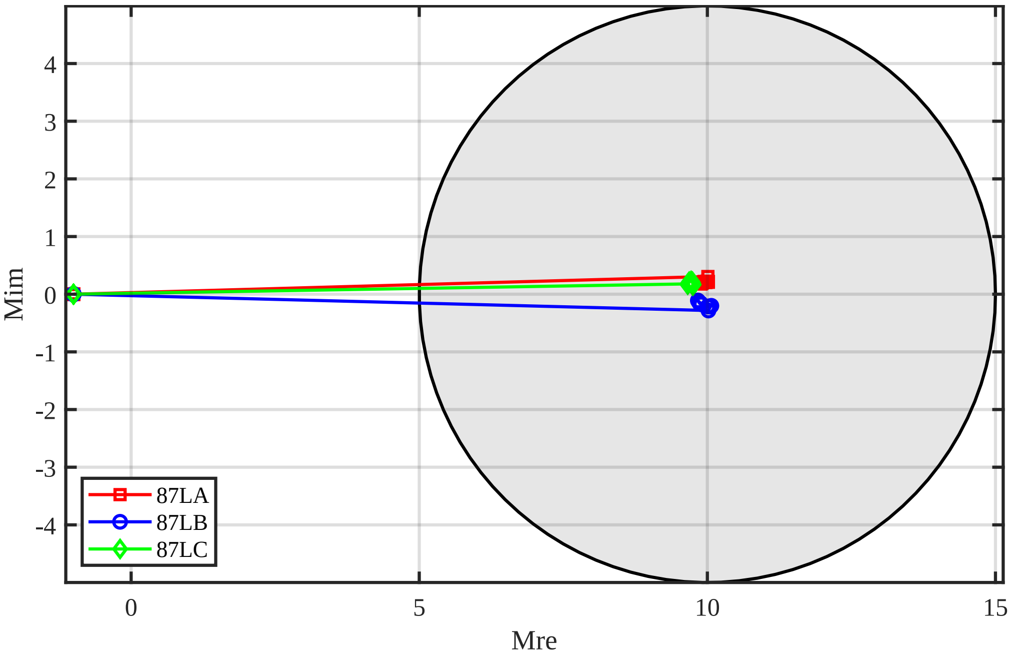

Figure 5.36. CMS-1 response.

For the CMS-2 protection scheme, the three phases were again identified, although only phases A and B were involved in the simulated fault. This response corresponds to loss of phase selectivity and is associated with the zero-sequence component measured at the local terminal through the transformer grounding path.

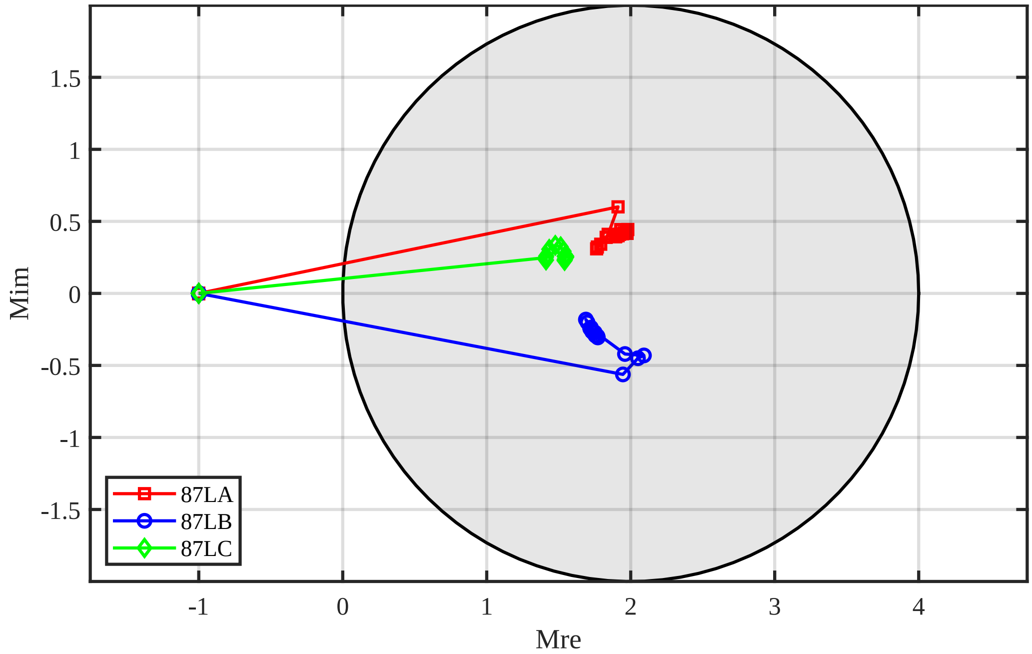

Figure 5.37. CMS-2 response.

5.4.2 $R = 0\ \Omega$ with IBR-side zero-sequence removal

Now considering the same situation but removing the zero-sequence from the IBR side of the grid, it is noted that the results of the protection will not consider the zero current components that are read in the local terminal, and this new type of reading will improve the protection activation and detection because of the segregation of each faulted phases.

Now with the Alpha-plane local Phases Protection, calculated in Figure 5.38, it is observed that the phases A and B have been correctly discovered and identified, this ies explained because of the removal of the zero-sequence currents.

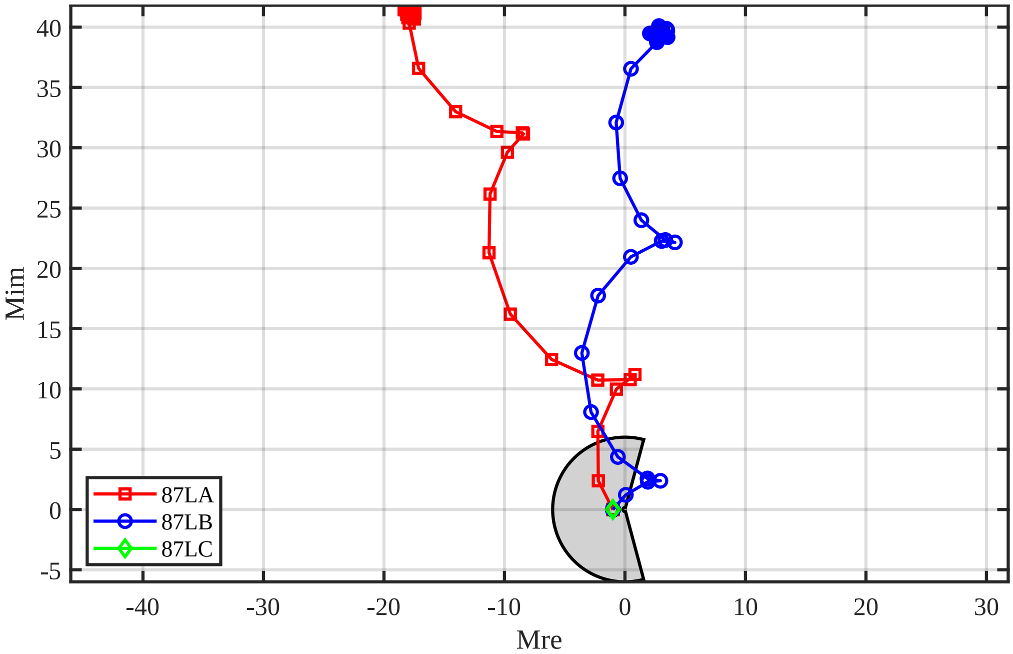

Figure 5.38. Local alpha-plane phase elements.

Similarly, now with Figure 5.39 in the Alpha-plane remote Phases Protection, the phases A and B have been correctly tripped and detected, this proper operation can be explained because of the removal of the zero-sequence from the IBR side of the grid.

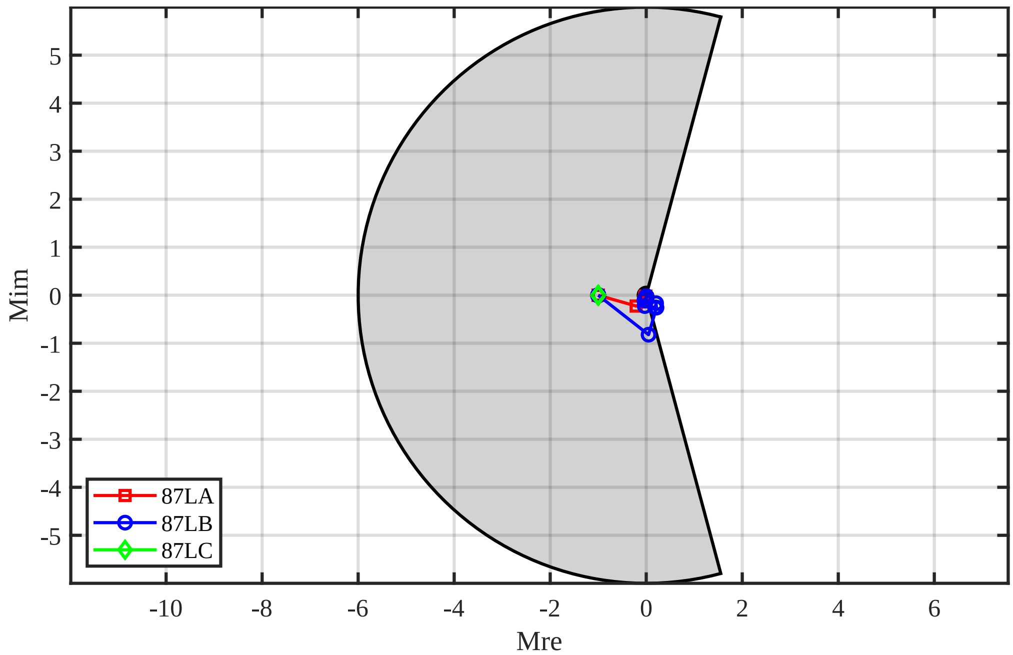

Figure 5.39. Remote alpha-plane phase elements.

Here in Figure 5.40, it is seen that the A and B phase where properly tripped and only the correct phases have been tripped. Phase C has not tripped in this scenario.

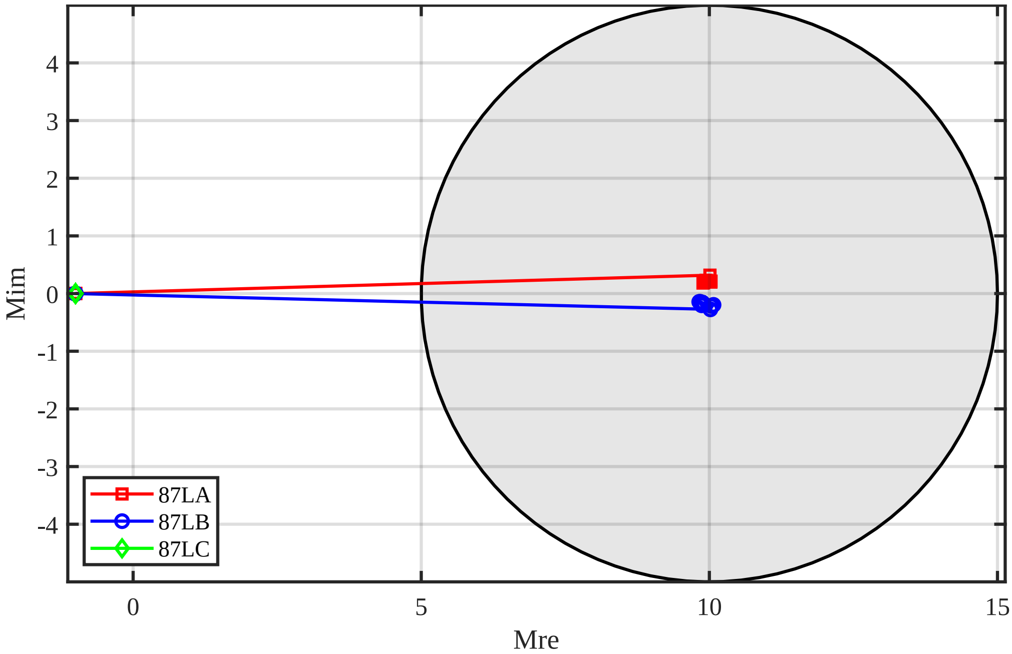

Figure 5.40. CMS-1 response.

In Figure 5.41, the Phases A and B have been correctly tripped and have entered the proper area of the CMS-2 for the tripping of the protection system in this scheme.

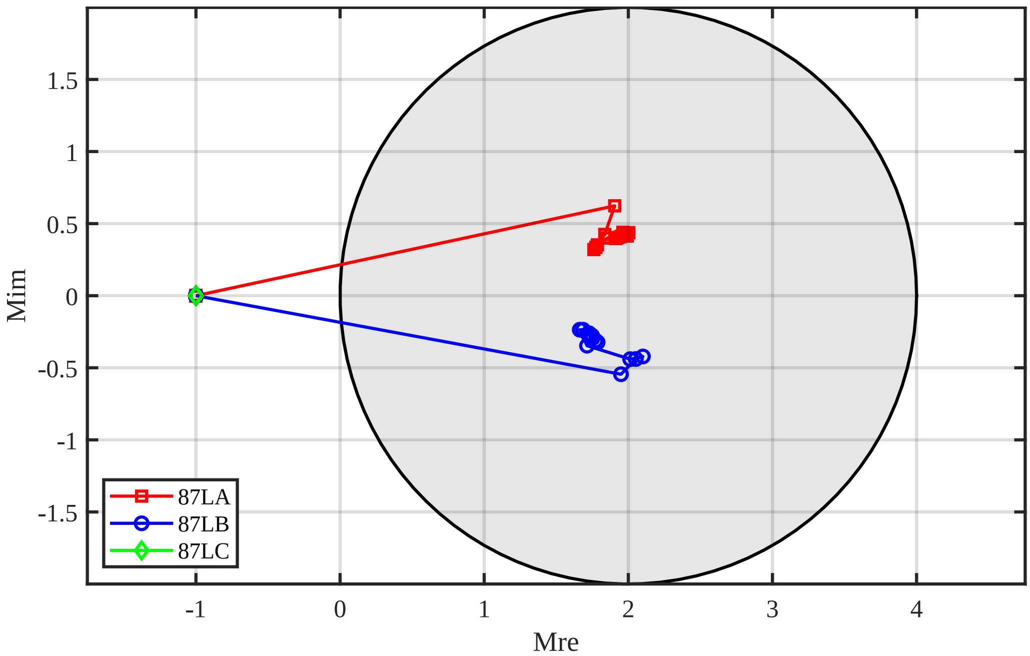

Figure 5.41. CMS-2 response.

5.4.3 $R = 100\ \Omega$ without IBR-side zero-sequence removal

Now considering the same scenario but with fault resistance, Figure 5.42 shows that the positive-sequence current remains close to 1 pu in the analyzed post-fault interval. The zero-sequence component is still present at the IBR-side terminal due to the transformer return path, although its magnitude is affected by the fault resistance.

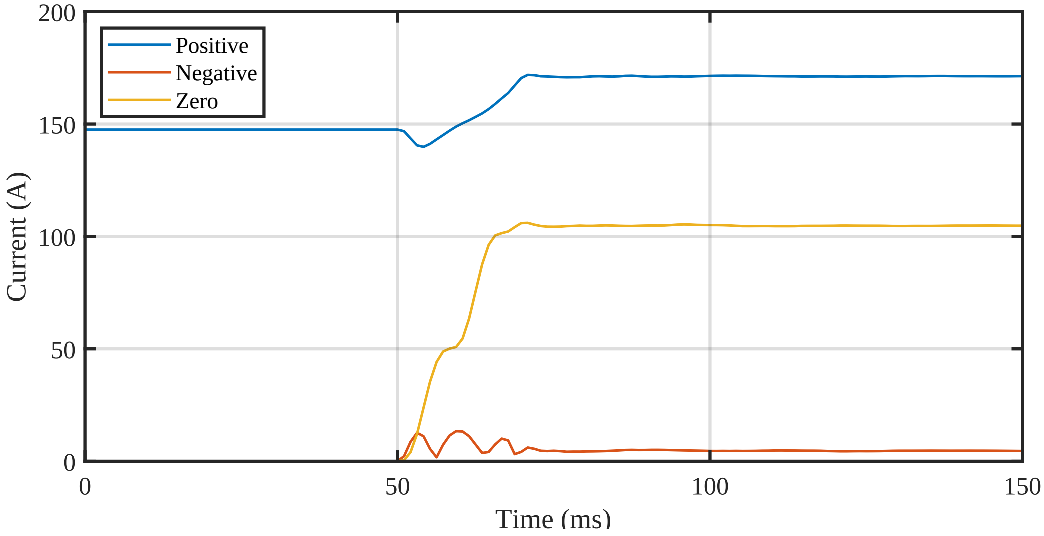

Figure 5.42. Local sequence currents.

Similarly, in Figure 5.43 where we observed the currents from the remote side of the line it is seen that the current magnitudes are lower because of the fault resistance and this scenario will be analyzed for the protection below:

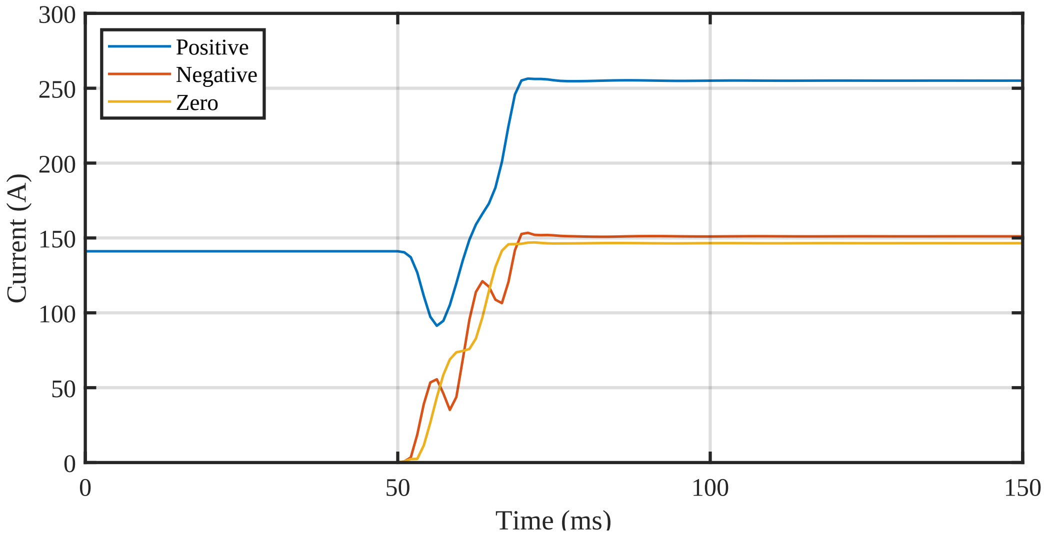

Figure 5.43. Remote sequence currents.

Because of the zero-sequence in the IBR side of the line, it is observed in Figure 5.44 that the protection has not been able to detect the B phase but only the A faulted phase, then the protection did not provide the expected phase selection in this case.

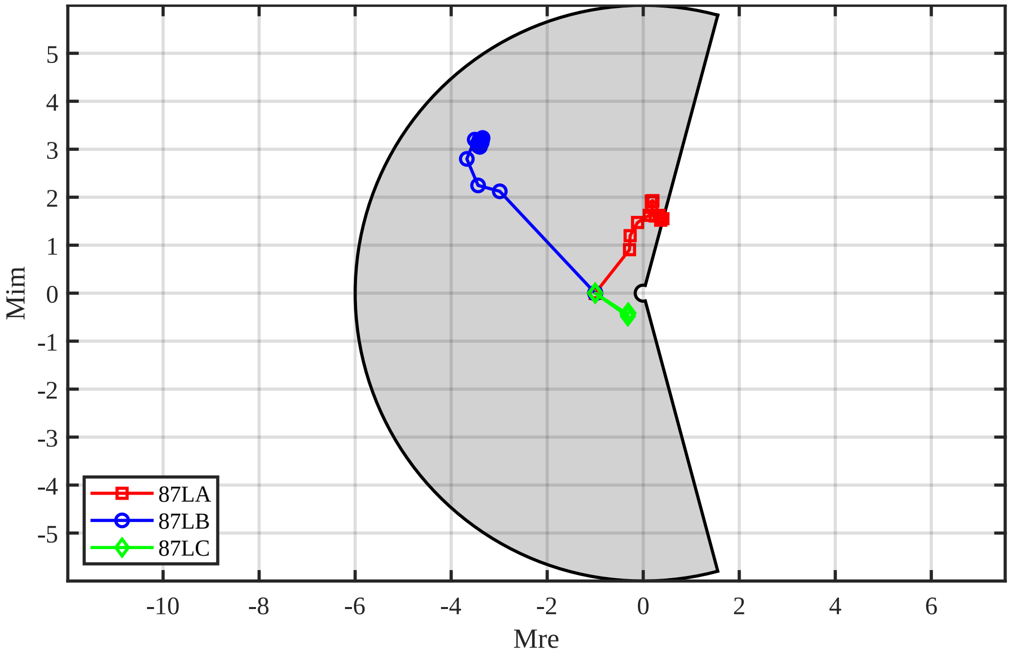

Figure 5.44. Local alpha-plane phase elements.

Similarly in Figure 5.45, the case without IBR-side zero-sequence removal has not been able to identify the correct phases, because only the A phase has been detected, this is also explained because of the zero-sequence current in the IBR side of the line.

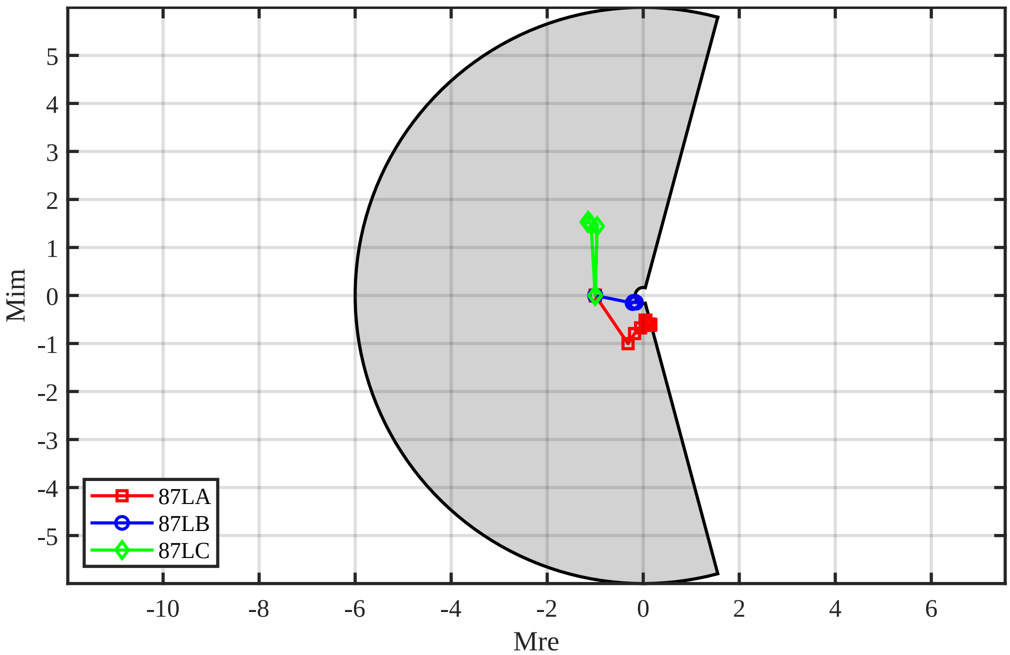

Figure 5.45. Remote alpha-plane phase elements.

For the case of the CMS-1 shown in Figure 5.46, the results show that the phases A, B and C have been incorrectly identified and this behavior is explained because of the zero-sequence that came from the IBR side of the line in the system.

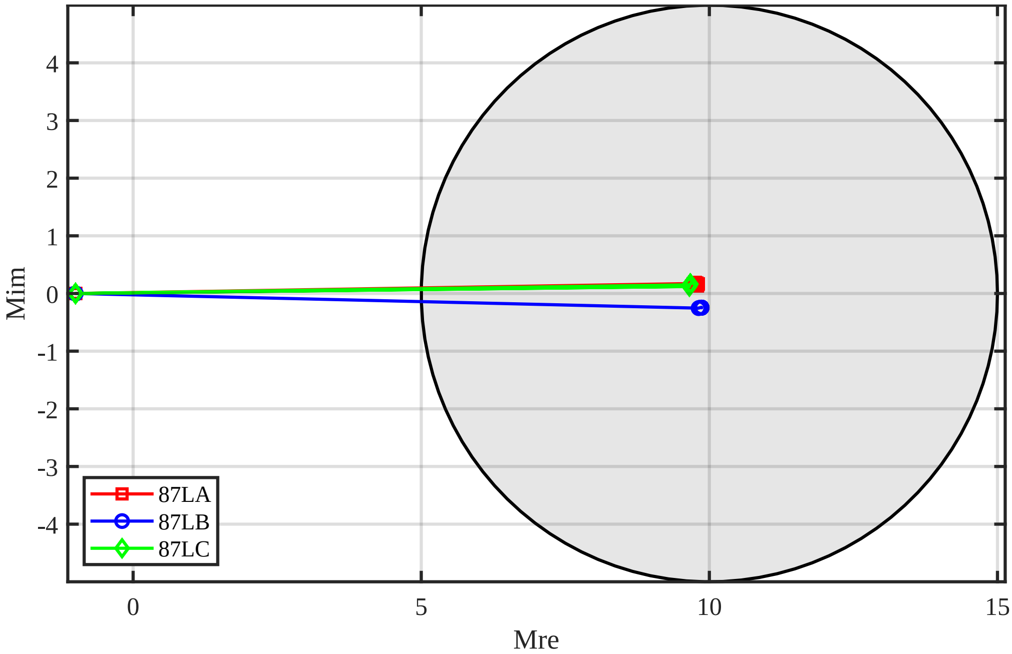

Figure 5.46. CMS-1 response.

Figure 5.47 shows that the three phases have been incorrectly detected by the protection, although the fault involves only phases A and B to ground.

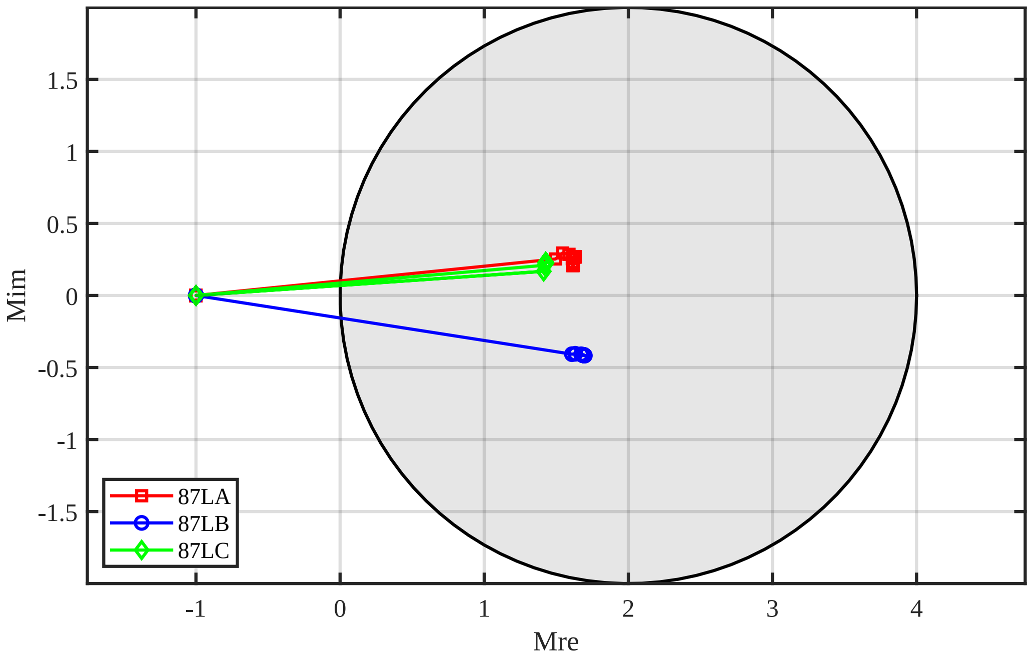

Figure 5.47. CMS-2 response.

5.4.4 $R = 100\ \Omega$ with IBR-side zero-sequence removal

Now considering the same fault after removing the IBR-side zero-sequence component from the phase currents, the protection response is evaluated without the transformer-related zero-sequence contamination in the phase elements.

In the Alpha-plane local Phases Protection, it is possible to see that the phases have not been able to identify the fault, this is likely explained because of the fault resistance.

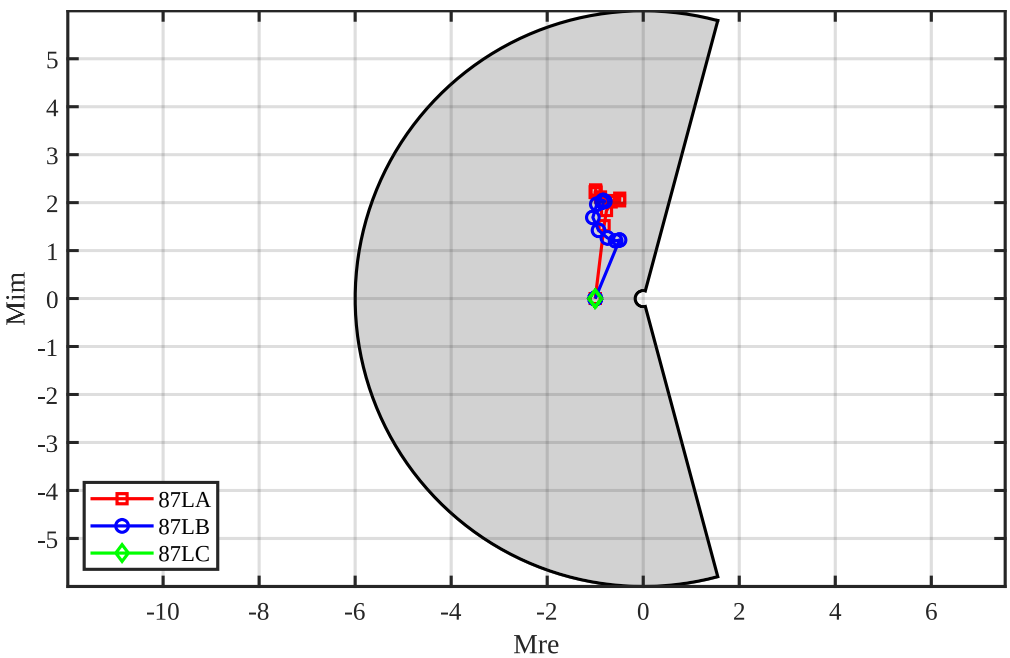

Figure 5.48. Local alpha-plane phase elements.

Similarly, in Figure 5.49, the Alpha-plane remote Phase Protection has not been able to identify the faults of the phases A and B because of the fault resistance, even after the IBR-side zero-sequence removal, the phase elements did not identify the faulted phases.

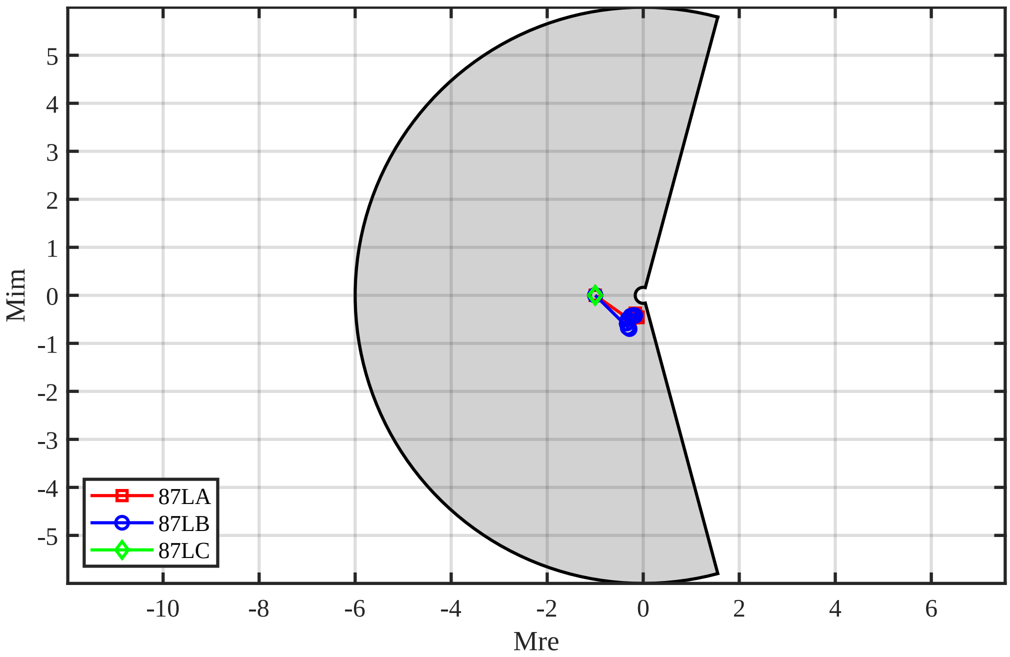

Figure 5.49. Remote alpha-plane phase elements.

Unlikely, the CMS-1 protection scheme has been identified correctly the A and B faulted phases of the fault, this is possible because of the removal of the zero-sequence currents, generating a segregated fault detection and allowing to identify the correct phases.

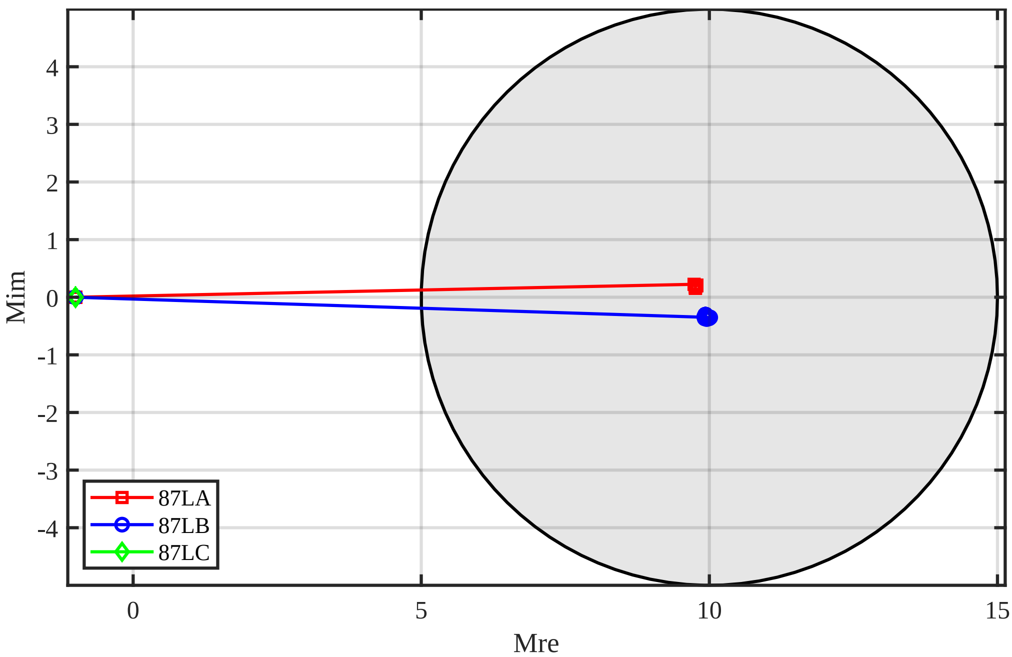

Figure 5.50. CMS-1 response.

Also with the CMS-2 only the phases A and B have been identified in the fault, this is because of the removal of the zero-sequence components of the currents from the IBR's side.

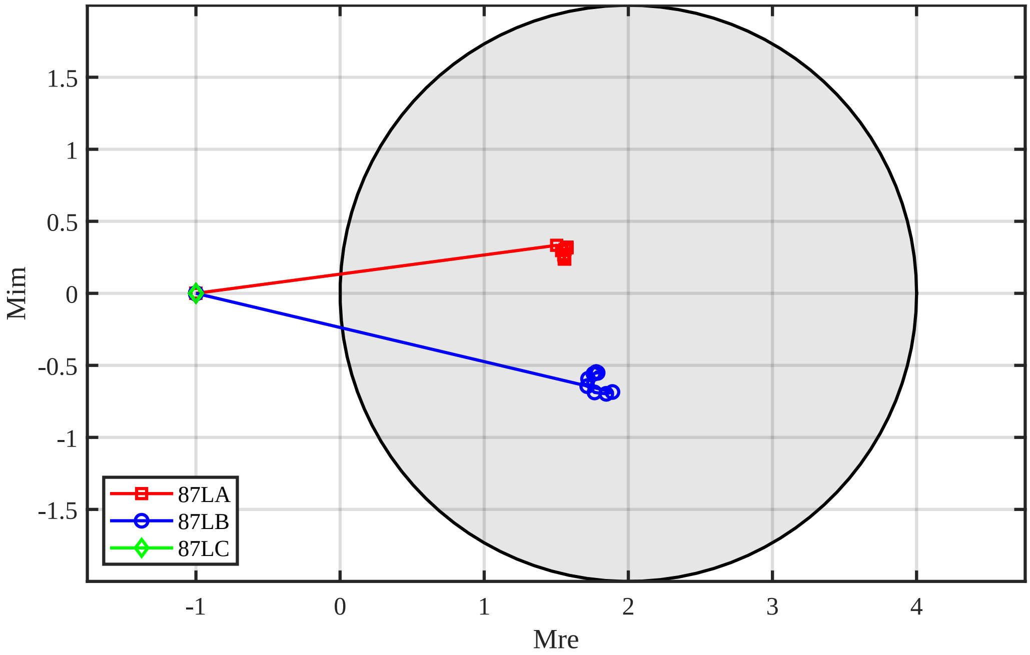

Figure 5.51. CMS-2 response.

5.5 THREE-PHASE FAULT

5.5.1 $R = 0\ \Omega$ without IBR-side zero-sequence removal

In this case of fault, there is no measure of zero-sequence currents, this is because of the nature of the A, B and C currents to the faults, this will generate values of high positive currents from the remote side of the line, but not normal values of local currents of the local currents due to the nature of the IBR when applied faults.

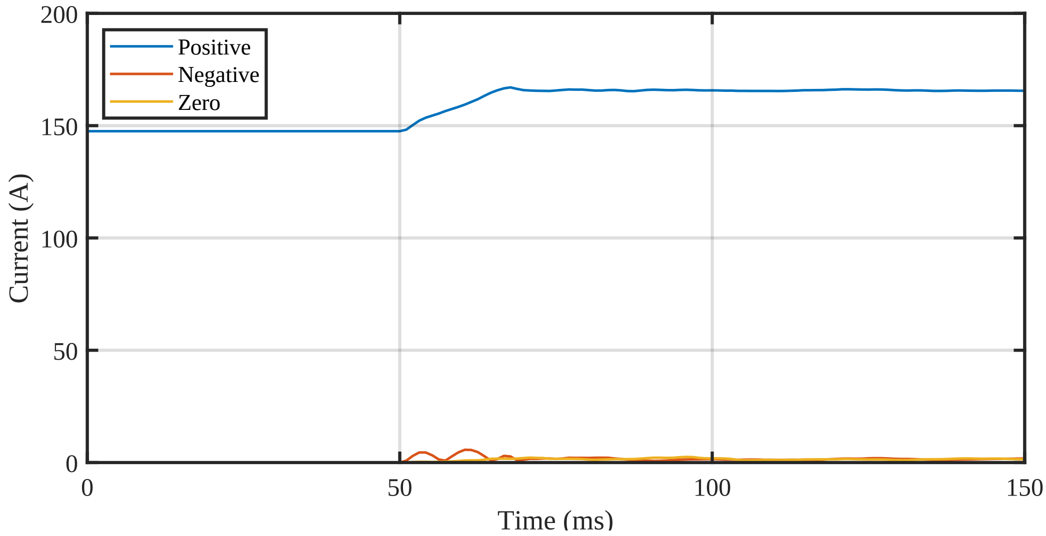

Figure 5.52. Local sequence currents.

In Figure 5.53 the results show that the high positive-sequence currents are observed in the remote side of the grid.

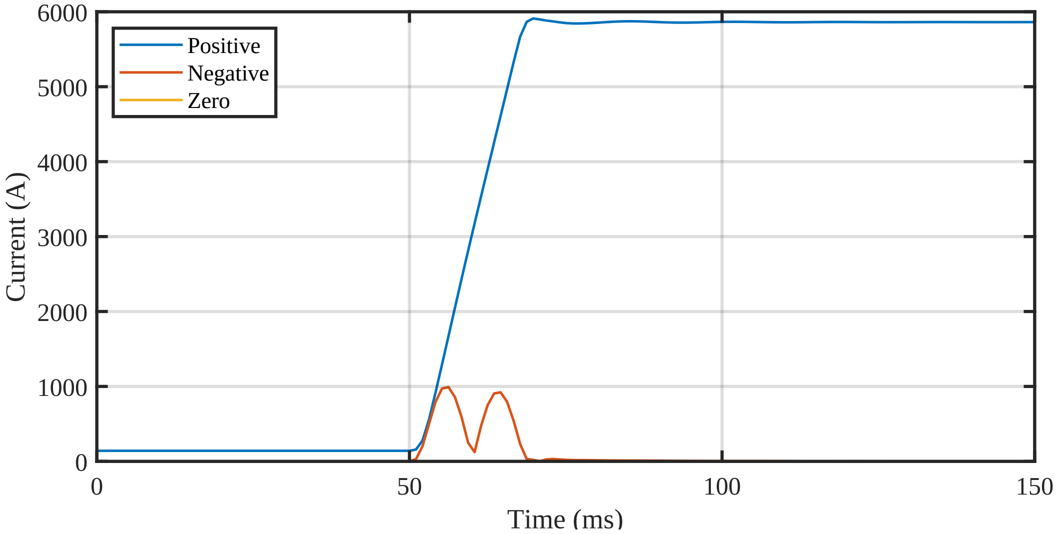

Figure 5.53. Remote sequence currents.

Figure 5.54 shows the Alpha-plane local Phase protection of the system when identifying correctly the three phases of the fault scenario.

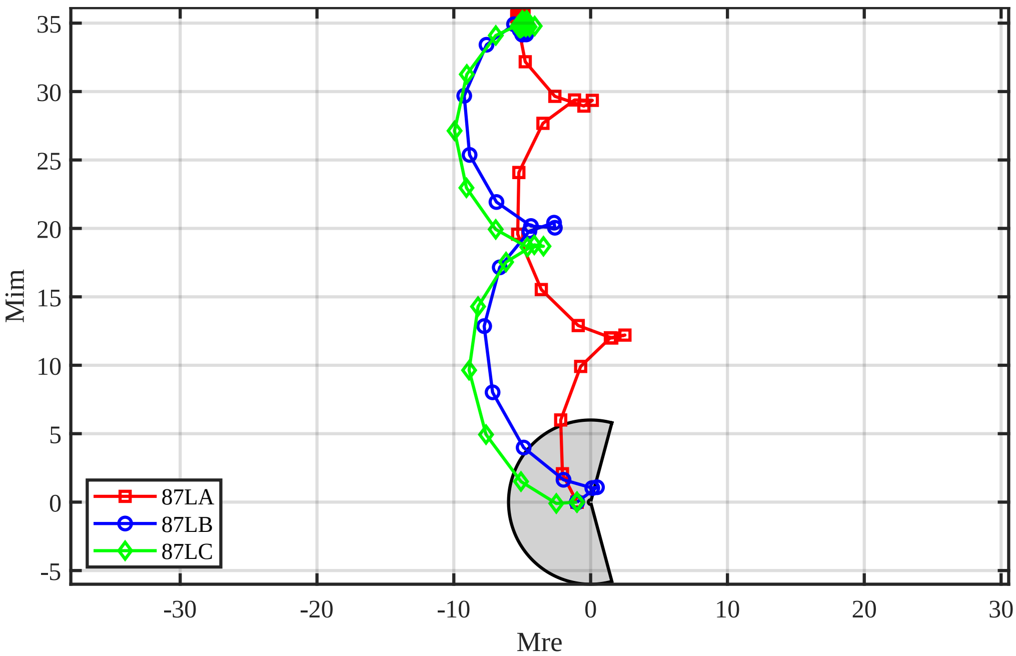

Figure 5.54. Local alpha-plane phase elements.

In a way, Figure 5.55 also shows that the fault was correctly identified by the Alpha-plane remote Phases Protection of the system with the faults explained before.

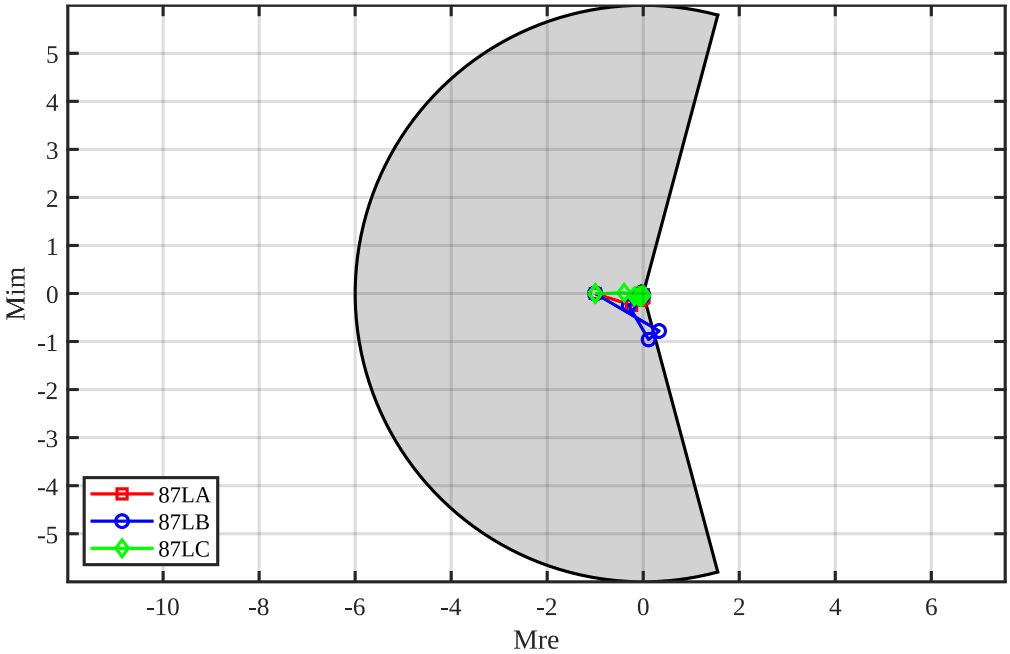

Figure 5.55. Remote alpha-plane phase elements.

The CMS-1 has also identifies the three phases of the system, this was expected because of the low values of zero-sequence coming from the IBR side of the grid.

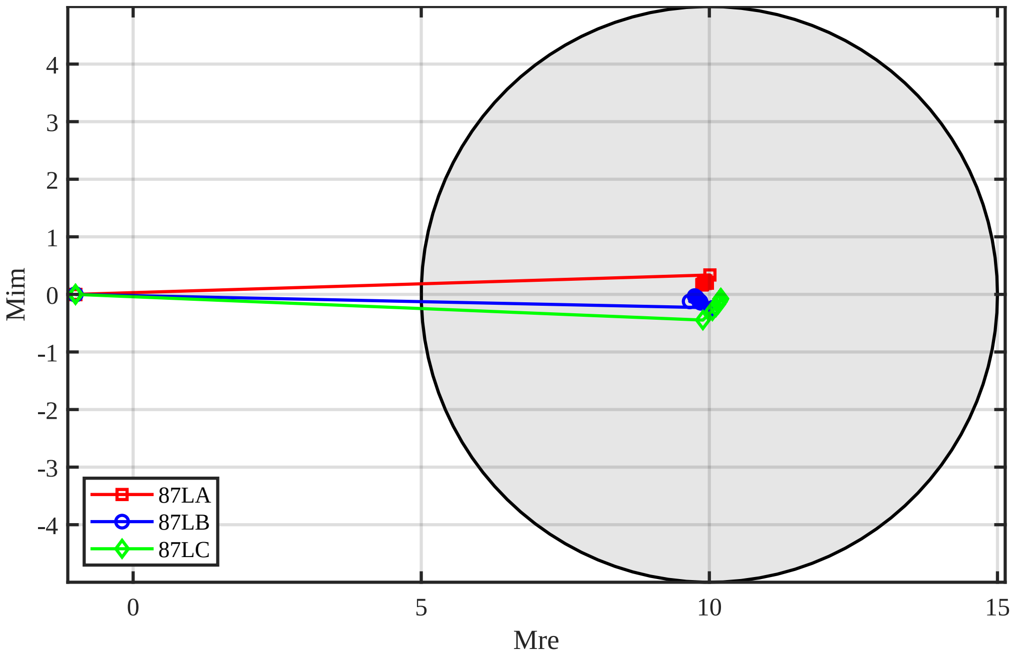

Figure 5.56. CMS-1 response.

Figure 5.57 shows the operation the three phase faults in the scenario of the three faults and how the protection behaves, this is also possible because of the low values of the zero-sequence of the fault type.

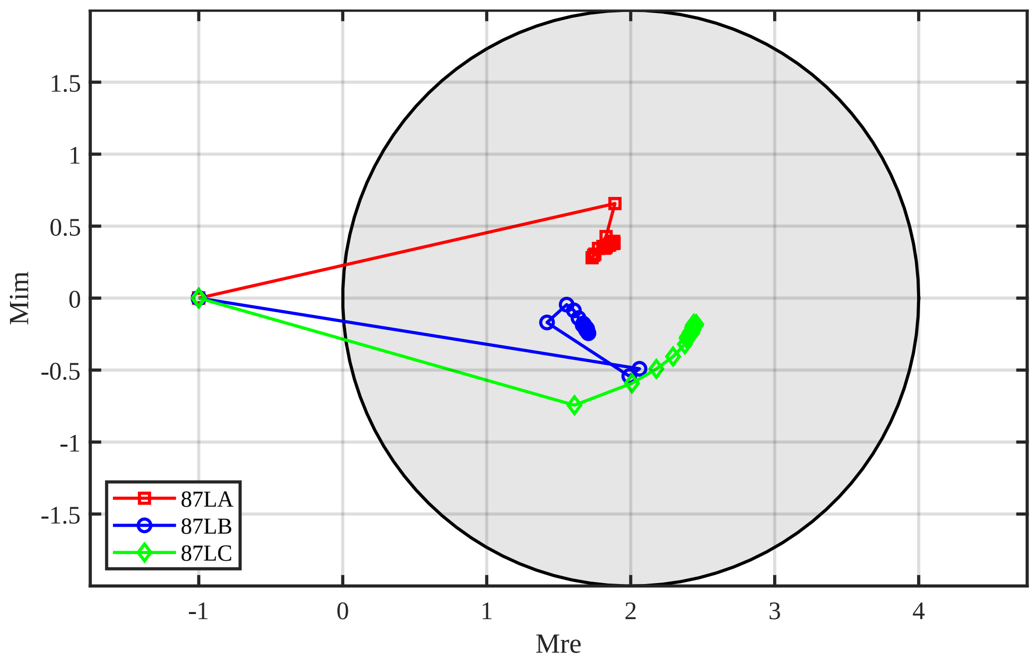

Figure 5.57. CMS-2 response.

CHAPTER 6

CONCLUSION

This dissertation evaluated the performance of line differential protection applied to a transmission line connected to a Type IV wind turbine-based inverter-based resource. The analyzed system differs from a conventional synchronous-source system because the IBR current is imposed by converter controls, current limiters, PLL dynamics, and semiconductor protection constraints. As a result, the current contribution from the IBR side remains limited during faults and does not present the same short-circuit behavior expected from a synchronous generator.

A central result of the study is the influence of the transformer connection on the phase quantities used by the protection algorithms. The local transformer is connected as delta–grounded-wye in the direction from the IBR to the remaining system. Therefore, the IBR is connected to the delta side, while the protected line and the differential protection terminals are connected to the grounded-wye side. During ground faults, the grounded-wye side provides a zero-sequence current path. This current can appear in the local-terminal phase measurements and affect the phase-segregated protection elements, even though the Type IV converter itself is not modeled as a conventional zero-sequence source.

For single-line-to-ground and double-line-to-ground faults, the local positive-sequence current remained close to the IBR current limit in the analyzed post-fault interval. However, this current is still low when compared with the typical short-circuit contribution expected from a conventional synchronous source. At the same time, the modeled Type IV wind turbine did not intentionally inject a significant negative-sequence current, while the zero-sequence component associated with the transformer grounding path became significant. Therefore, the combination of limited positive-sequence fault current, low or absent negative-sequence contribution, and elevated zero-sequence current returning through the grounded transformer can cause the phase-segregated 87L function to lose phase selectivity.

When the transformer-related zero-sequence component was directly included in the phase currents measured at the IBR-side terminal, the alpha-plane phase elements and the CMS-based phase elements could identify non-faulted phases as involved in the fault. This behavior was observed mainly in ground-fault cases, where the zero-sequence current added an equal component to the three phase currents and distorted the quantities used by the phase elements. After removing the zero-sequence component from the IBR-side phase currents, the phase-segregated protection response improved and the algorithms were able to identify the expected faulted phases in the analyzed cases. Thus, the results indicate that IBR-side zero-sequence removal is an effective procedure to mitigate the loss of phase selection caused by the transformer zero-sequence return path.

The conventional alpha-plane protection presented limitations in some scenarios involving ground faults and IBR-side zero-sequence contamination. In these cases, the operating trajectories and phase identification were affected by the combined effect of converter-limited positive-sequence current, reduced negative-sequence contribution from the IBR, and transformer-related zero-sequence current. The CMS-based methods provided an alternative representation of the differential quantities in the alpha plane and showed improved phase-selection behavior when the zero-sequence component was removed from the IBR-side currents.

The negative-sequence element requires careful interpretation in the studied system. Since the modeled Type IV wind turbine does not intentionally inject a significant negative-sequence current, the negative-sequence quantities at the IBR-side terminal may be small and may lead to unstable alpha-plane trajectories. In contrast, the zero-sequence element remains relevant for ground-fault identification because the grounded-wye transformer side provides a zero-sequence path during ground faults.

The main contribution of this dissertation is not the proposal of the CMS itself, which was previously presented in the literature, but its application and evaluation in a transmission line connected to a Type IV wind turbine-based IBR. The results show that the interaction among converter-limited current, transformer connection, sequence components, and differential protection logic must be explicitly considered when evaluating line protection for IBR-connected systems.

Future work should investigate additional transformer connections, different grounding arrangements, communication and synchronization errors, grid-forming converter controls, IBR models with intentional negative-sequence current injection, and adaptive methods capable of maintaining phase selectivity without requiring explicit zero-sequence removal from the IBR-side phase currents.

BIBLIOGRAPHY

ALI, E.; KNIGHT, A. M. An enhanced algorithm for conventional protection devices of transmission lines with dtlr. *IEEE Access*, IEEE, v. 9, p. 147295–147305, 2021. Cited 2 times in pages 19 and 22.

BAINY, R. G.; SILVA, K. M.; JOHNSON, B. K. Current mapping strategy for improving two-terminal series-compensated line current differential protection. *Electric Power Systems Research*, Elsevier, v. 196, p. 107243, 2021. Cited 4 times in pages 4, 8, 20, and 22.

BARSCH, J.; BARTOK, G.; BENMOUYA, G.; BOLADO, O.; BOYSEN, B.; BRAHMA, S.; BRETTSCHNEIDER, S.; BUKHALA, Z.; BURNWORTH, J. Fault current contributions from wind plants. *A Report to the T&D Committee, Electric Machinery Committee and Power System Relaying Committee of the IEEE PES*, 2012. Cited 2 times in pages 14 and 22.

BINI, M.; ABBOUD, R.; LIMA, P.; LOLLO, F. Challenges and solutions in the protection of transmission lines connecting nonconventional power sources. In: *48th Annual Western Protective Relay Conference*. [S.l.: s.n.], 2021. Cited 4 times in pages 6, 8, 19, and 22.

CHEN, B.; SHRESTHA, A.; ITUZARO, F. A.; FISCHER, N. Addressing protection challenges associated with type 3 and type 4 wind turbine generators. In: IEEE. *2015 68th annual conference for protective relay engineers*. [S.l.], 2015. p. 335–344. Cited 4 times in pages 6, 8, 16, and 22.

CHOWDHURY, R.; FISCHER, N. Transmission line protection for systems with inverter-based resources–part i: Problems. *IEEE Transactions on Power Delivery*, IEEE, v. 36, n. 4, p. 2416–2425, 2020. Cited 4 times in pages 6, 8, 18, and 22.

CHOWDHURY, R.; FISCHER, N. Transmission line protection for systems with inverter-based resources–part ii: Solutions. *IEEE Transactions on Power Delivery*, IEEE, v. 36, n. 4, p. 2426–2433, 2020. Cited 4 times in pages 6, 8, 18, and 22.

FANG, Y.; JIA, K.; YANG, Z.; LI, Y.; BI, T. Impact of inverter-interfaced renewable energy generators on distance protection and an improved scheme. *IEEE Transactions on Industrial Electronics*, IEEE, v. 66, n. 9, p. 7078–7088, 2018. Cited 2 times in pages 17 and 22.

GEVORGIAN, V.; SINGH, M.; MULJADI, E. Symmetrical and unsymmetrical fault currents of a wind power plant. In: IEEE. *2012 IEEE Power and Energy Society General Meeting*. [S.l.], 2012. p. 1–8. Cited 2 times in pages 14 and 22.

HOOSHYAR, A.; AZZOUZ, M. A.; EL-SAADANY, E. F. Distance protection of lines connected to induction generator-based wind farms during balanced faults. *IEEE Transactions on Sustainable Energy*, IEEE, v. 5, n. 4, p. 1193–1203, 2014. Cited 2 times in pages 14 and 22.

HOOSHYAR, A.; AZZOUZ, M. A.; EL-SAADANY, E. F. Distance protection of lines emanating from full-scale converter-interfaced renewable energy power plantsâpart i: Problem statement. *IEEE Transactions on Power Delivery*, IEEE, v. 30, n. 4, p. 1770–1780, 2014. Cited 2 times in pages 15 and 22.

HOOSHYAR, A.; AZZOUZ, M. A.; EL-SAADANY, E. F. Distance protection of lines emanating from full-scale converter-interfaced renewable energy power plantsâpart ii: Solution description and evaluation. *IEEE Transactions on Power Delivery*, IEEE, v. 30, n. 4, p. 1781–1791, 2014. Cited 2 times in pages 15 and 22.

KASZTENNY, B. Distance elements for line protection applications near unconventional sources. In: *Proc. 75th Annu. Conf. Protective Relay Engineers.* [S.l.: s.n.], 2022. p. 28–31. Cited 2 times in pages 21 and 22.

KASZTENNY, B. Line distance protection near unconventional energy sources. In: IET. *16th international conference on developments in power system protection (DPSP 2022).* [S.l.], 2022. v. 2022, p. 224–229. Cited 2 times in pages 20 and 22.

NAGPAL, M.; HENVILLE, C. Impact of power-electronic sources on transmission line ground fault protection. *IEEE Transactions on Power Delivery*, IEEE, v. 33, n. 1, p. 62–70, 2017. Cited 2 times in pages 16 and 22.

NAGPAL, M.; JENSEN, M.; HIGGINSON, M. *et al.* Protection challenges and practices for interconnecting inverter based resources to utility transmission systems. *IEEE Power Energy Soc.*, p. 1–65, 2020. Cited 4 times in pages 6, 8, 17, and 22.

RAMPOKANYO, M.; DATTARAY, P.; KAMERA, P.; BEERTEN, J.; ARONOVICH, I.; CORCORAN, D.; BOS, J.; MODI, N.; RAHIMI, I.; QUINT, R. *et al.* Impact of high penetration of inverter-based generation on system inertia of networks. *Electra*, Cigré, n. 319, 2021. Cited 2 times in pages 19 and 22.

SULLA, F. Fault behavior of wind turbines. 2012. Cited 2 times in pages 14 and 22.

VILA, D.; ALCÁZAR, E.; JUÁREZ, J.; LOZA, P.; ALTUVE, H. J. Protection system for a wind generation plant in panama: Challenges and solutions. In: IEEE. *2016 69th Annual Conference for Protective Relay Engineers (CPRE).* [S.l.], 2016. p. 1–15. Cited 2 times in pages 16 and 22.

WANG, Y.; WEN, M.; CHEN, Y. A simplified model of type-4 wind turbine for short-circuit currents simulation analysis. *IET Generation, Transmission & Distribution*, Wiley Online Library, v. 16, n. 15, p. 3036–3049, 2022. Cited 2 times in pages 20 and 22.